UNIVERSITÉ DE STRASBOURG

ÉCOLE DOCTORALE de Physique et Chimie-Physique (ED182)

Inserm BioMatériaux et BioIngénierie (UMR_S 1121),
Max Planck Institute for Polymer Research et
Institut de Physique et Chimie des Matériaux de Strasbourg (UMR 7504)

THÈSE présentée par :

Kévin ZIEGLER

soutenue le : **02 octobre 2024**

pour obtenir le grade de : **Docteur de l'université de Strasbourg**
Discipline/ Spécialité : Chimie-Physique / Sciences des Matériaux

Electropolymerization of polyphenol-related biogenic monomers to design multifunctional 2D materials

Electropolymérisation de monomères polyphénoliques pour la conception de matériaux 2D multifonctionnels

THÈSE dirigée par :

M. BALL Vincent	Professeur, Université de Strasbourg
Mme WEIL Tanja	Professeur, Max Planck Institute for Polymer Research

RAPPORTEURS :

Mme LABERTY-ROBERT Christel	Professeur, Sorbonne Université
M. MAISONHAUTE Emmanuel	Professeur, Sorbonne Université

EXAMINATEURS :

Mme SAVINOVA Elena	Professeur, Université de Strasbourg
M. PICHON Benoît	Professeur, Université de Strasbourg

Acknowledgments

I am greatly thankful to the Inserm and Max Planck Gesellschaft to welcome me as a member of these institutions. I am also very thankful to the directors of the Inserm UMRS 1121 (Strasbourg, France) and the Max Planck Institute for Polymer Research (Mainz, Germany) who allowed me to work in their institutes and laboratories.

I would like to particularly thank my PhD co-directors Pr Vincent Ball and Pr Tanja Weil for their kindness, support, advices and monitoring during the whole PhD work. I am also thankful to the other supervisors who guided me throughout these 3 years: Pr Clément Sanchez, Pr Ovidiu Ersen and Dr Christopher Synatschke. I thank Pr Tanja Weil again for the financial support from her own budget.

I am thankful to the members of the jury of this thesis who did me the honor of judging this work. Therefore, I express my gratitude to Pr Christel Laberty-Robert and Pr Emmanuel Maisonhaute (both with a professor position at Sorbonne Université, Paris, France) for accepting to be the rapporteurs of this work; but also, Pr Elena Savinova and Pr Benoît Pichon (both with a professor position at Université de Strasbourg, France) for accepting to be the examiners of this work.

I would like to warmly thank the partners and collaborators of this project, notably: Dr Cédric Boissière from the Laboratoire de Chimie de la Matière Condensée de Paris (Paris, France); Dr Tommaso Marchesi D'Alvise, the PhD students Marcel Boecker and Tilmann Herberger, and the students Julia Moser and Meret Kaliske from the Max Planck Institute for Polymer Research (Mainz, Germany); Dr Ann-Kathrin Kissmann from the Institute of Pharmaceutical Biotechnology (Ulm, Germany); and Dr Soressa Abera Chala from the Johannes Gutenberg University (Mainz, Germany). But also, to Dr Dris Ihiawakrim, Dr

Tom Ferté, Leon Prädel and Walter Scholdei for carrying out some parts of the characterization measurements.

I am thankful to all my colleagues who helped me, brought kindness and good atmosphere or became friends, notably Sadia, Valentina, Charles, Yuvna, Nivedita, Sharmin, Léon, Benjamin, Tommaso, Marcel, Jiyao, Tilmann, Julia, Kim, Meret, Venkat, Yu-Liang, Adrien, Jordana, Mélissa, Charlène and Victor; but also, all the others that I did not name but who will recognize themselves.

Finally, I am greatly thankful to my family, particularly my parents, and my friends who supported me and believed in me.

Remerciements

Je remercie énormément l'Inserm et le Max Planck Gesellschaft pour m'avoir accueilli au sein de leurs institutions. Je remercie aussi grandement les directeurs de l'Inserm UMRS 1121 (Strasbourg, France) et du Max Planck Institute for Polymer Research (Mayence, Allemagne) qui m'ont permis de travailler au sein de leurs instituts et laboratoires.

Je souhaite remercier tout particulièrement mes co-directeurs de thèse Pr Vincent Ball et Pr Tanja Weil pour leur bienveillance, soutien, supervision et leurs conseils durant ce travail. Je remercie également les autres superviseurs qui m'ont guidé tout au long de ma thèse: Pr Clément Sanchez, Pr Ovidiu Ersen et Dr Christopher Synatschke. Je remercie doublement Tanja Weil pour son soutien financier qui a permis au projet d'avoir lieu grâce à son budget.

Je remercie les membres de mon jury de thèse qui m'ont fait l'honneur de juger ce travail. Ainsi, j'exprime toute ma gratitude à Pr Christel Laberty-Robert et Pr Emmanuel Maisonhaute (professeurs à Sorbonne Université, Paris, France) pour avoir accepté d'être les rapporteurs de ma thèse; mais aussi à Pr Elena Savinova et Pr Benoît Pichon (professeurs à Université de Strasbourg, France) pour avoir accepté d'être les examinateurs de ma thèse.

Je remercie chaleureusement tous les partenaires et collaborateurs de ce projet, notamment : Dr Cédric Boissière du Laboratoire de Chimie de la Matière Condensée de Paris (Paris, France) ; Dr Tommaso Marchesi D'Alvise, les doctorants Marcel Boecker et Tilmann Herberger, et les étudiants Julia Moser et Meret Kaliske du Max Planck Institute for Polymer Research (Mayence, Allemagne) ; Dr Ann-Kathrin Kissmann du Institute of Pharmaceutical Biotechnology (Ulm, Allemagne) ; et Dr Soressa Abera Chala de

Johannes Gutenberg University (Mayence, Allemagne). Mais aussi à Dr Dris Ihiawakrim, Dr Tom Ferté, Leon Prädel et Walter Scholdei pour avoir réalisé une part des caractérisations.

Je remercie mes collègues qui m'ont aidé et soutenu, apporté de la bienveillance et une bonne ambiance ou qui sont devenus des amis, notamment Sadia, Valentina, Charles, Yuvna, Nivedita, Sharmin, Léon, Benjamin, Tommaso, Marcel, Jiyao, Tilmann, Julia, Kim, Meret, Venkat, Yu-Liang, Adrien, Jordana, Mélissa, Charlène and Victor; mais aussi tous les autres que je n'ai pas cités mais qui se reconnaîtront.

Enfin, Je remercie beaucoup ma famille, en particulier mes parents, et mes amis qui m'ont toujours soutenu et qui ont toujours eu confiance en moi.

Table of Contents

General Introduction

1.1. Place of this work and its importance

Both chemical and electrochemical routes of polymerization of monomers were intensively investigated. While chemical polymerization involves redox species, electrochemical polymerization involves electrical charges and is not possible for all monomers.[1] Electrochemical deposition emerges among low-carbon footprint processes. The method also allows the synthesis of coatings, since the deposition occurs on a substrate. Therefore, it is of particular interest for advanced technologies employing thin films.

Among the monomers studied, conductive polymers such as polyaniline, polypyrrole, and polythiophene[1-6] are the most common due to their invaluable advantages for various applications.[1]

Polyaniline is a classical conductive polymer and was among the first polymers synthesized electrochemically.[7] It has also been widely studied for electrical and optical applications, due to its good environmental stability and tunable electrical and optical properties.[8,9] The deposition of polyaniline has been reported by Eftekhari and Jafarkhani[1] and Musiani et al.[2] for instance. The substrates used were different, respectively a platinum sheet and an iron sheet. The experimental conditions were also very different, respectively an acidic solution with H_2SO_4 and an aqueous solution of KOH. Eftekhari and Jafarkhani[1] also studied the difference of the electrodeposition in absence or presence of ammonium persulfate, a chemical oxidant.

Polypyrrole is by far the most extensively studied conducting polymer.[4] That is due to its water solubility, good redox properties, and its ability to give high electrical conductivity.[4] Again, different conditions of deposition can be found in the literature. For instance, Saidman and Vela[3] described a method to electrodeposit polypyrrole on aluminum while Ryan et al.[4] reported the deposition on both platinum and gold working disk electrodes.

Despite the ability to produce thin films from various monomers and their very different properties, some conditions offer several drawbacks. Indeed, solvents are sometimes toxic for the human health or the environment. In some cases surfactants are required and they can be incorporated into the final material,[3] as well as ions present in the supporting electrolyte,[10] and some of them can be harmful. Polyaniline is harmful itself already.

Therefore, it is important to find alternatives. It is of high interest to use natural compounds to lower the carbon footprint, but also to work in mild conditions such as ambient temperatures and aqueous solutions to reduce the impact on the environment and the energy consumption.

1.2. Principle of cyclic voltammetry

Electrochemistry is a technique based on the dependence of current with potential and reactions involving electron transfers. An experiment in electrode kinetics usually consists of determining this current-potential relationship under a given set of fixed conditions, to obtain the I/E plots as a function of temperature, concentration, and so on.[11]

The experiments can be carried out either by controlling the current and measuring the potential or by controlling the potential and measuring the current. The former is referred to as a galvanostatic measurement and the latter a potentiostatic measurement. Galvanostats are much simpler than potentiostats from a matter of cost, but also of

performance. Galvanostats with controllable currents in the range of hundreds of amperes are readily available and are more convenient for industrial processes, while potentiostats became commercially available only after the late 1950s. That was particularly true in the last century but nowadays with the present-day electronic components there are fewer instrumental limitations.[11] In this work, all electrochemical measurements were performed with potentiostats and a three-electrode system.

As shown in Figure 1, the standard three-electrode system is composed of a working electrode, a reference electrode and a counter electrode (the latter is also called auxiliary electrode).[12,13] The potential of the working electrode is controlled versus the reference electrode. This reference electrode has a well-known and stable potential (against the standard hydrogen electrode).The working electrode is the place where the reaction of interest will take place. The counter electrode closes the electrical circuit and the current flows between the working electrode and the counter electrode.[14,15] In solution the current is ensured by the migration of the dissolved electrolytes. In this study, the working electrode was a glassy carbon or gold electrode and the counter electrode a platinum wire. The reference was an Ag/AgCl electrode. Therefore, all potentials given are versus Ag/AgCl.

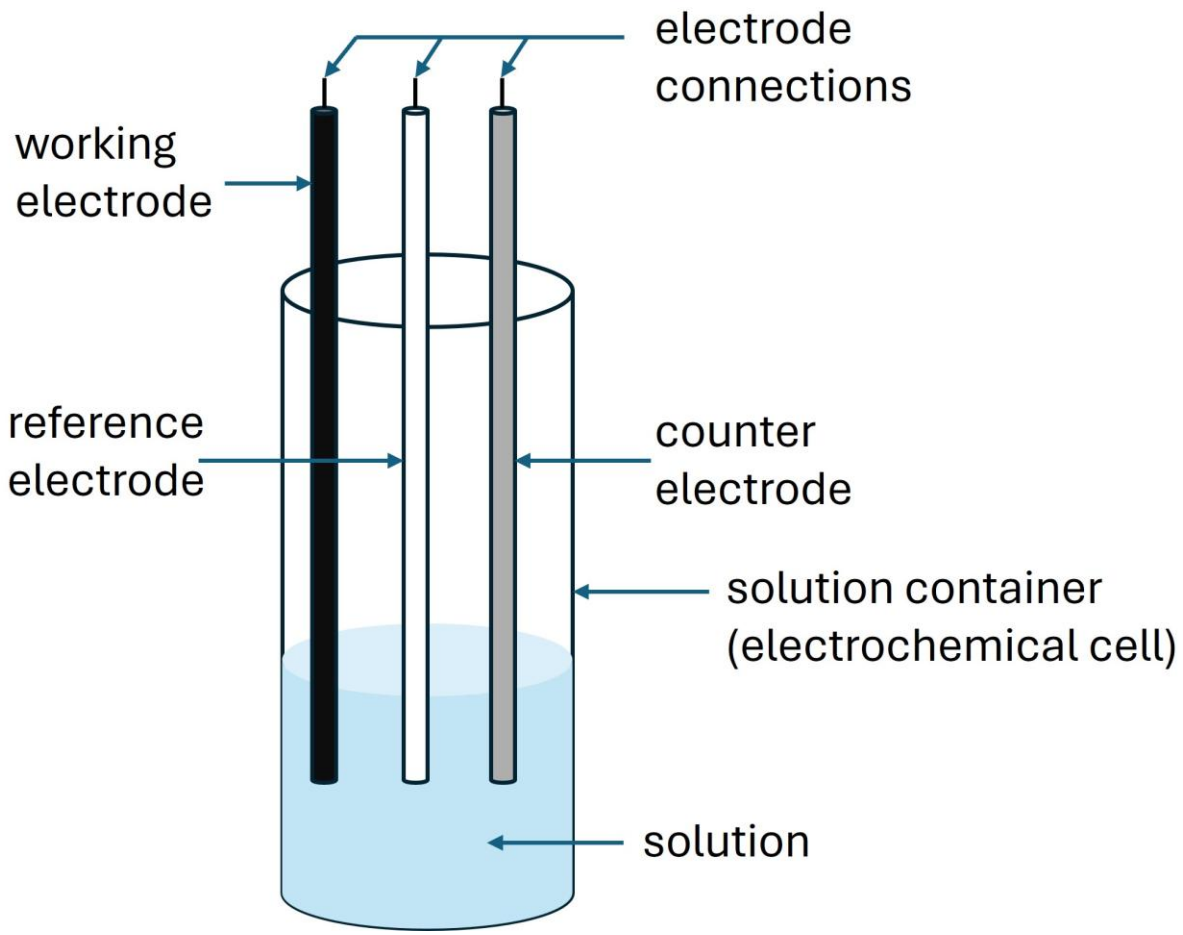

Figure 1. Schematic representation of a three-electrode electrochemical cell.

Cyclic voltammetry is often the first measurement performed in an electrochemical study of a compound, a biological material, or an electrode surface. Its versatility combined with ease of measurement has resulted in extensive use.[14] In cyclic voltammetry the potential is made to change linearly with time (this parameter is called scan rate or sweep rate) between two set values, under a determined number of cycles. Often the current during the first cycle is quite different from that in the second cycle, but after 5-10 cycles the system settles down, and the current traces the same line as a function of potential, independent of the number of cycles. It is highly reproducible and the voltammogram obtained is independent of time.[16]

1.3. Polyphenol-related molecules

Phenols, polyphenols and derivates molecules have been studied for decades and are well-known precursors to chemical, electrochemical or biochemical purposes. The presence of several hydroxyl groups allow chemical and redox reactions or also further functionalization of the obtained materials.

During the past decade, such molecules and in particular eumelanins (black/dark-brown melanin pigments)[17] have attracted increasing attention within the research community in view of their unique properties and promising applications in material sciences.[18]

To name just a few works on electrochemical studies, Voisin et al.[19] reported an investigation on the electrochemical oxidation of catechol and demonstrated that the obtained material is likely a triphenylene derivative rather than a polymeric material. Quynh et al.[20] presented a study on the electrochemical behavior of aromatic compounds (benzene, phenol, hydroquinone, catechol, 2-aminophenol and 2-chlorophenol) on gold electrodes. Saito et al.[21] reported a green synthesis of a soluble polyphenol via an oxidative polymerization of phenol in water. Iotov et al.[22] suggested a mechanistic approach to the oxidation of phenol at a platinum/gold electrode. Mosa et al.[23] reported a synthesis via a hybrid approach from the combination of electrodeposition and sol-gel methods to assemble a porous nanoelectrode based on poly(phenylene oxide) for electrochemical sensing or energy storage.

Recently, polydopamine materials, obtained through the oxidation of dopamine or related catecholamines, have been the focus of an intensive research activity.[24] Despite a wide study of the polyphenol-related molecules, there are still a lot of potential investigations to be performed to understand their complex deposition mechanism on electrodes.

These molecules and derivatives often have redox properties: they can be oxidized or reduced, but also can present a residual redox activity in the obtained material.[25] Their natural origin makes them promising candidates of precursors for electrochemical studies, such as synthesis and film deposition via cyclic voltammetry with small potential inputs and non-toxic solvents to work in accordance with the UN's 12th objective in order to reduce hazards, pollution and impacts on the environment and the human health.[26]

1.4. Dihydroxypyridines

The 2,3-dihydroxypyridine has a similar structure than catechol, but one carbon in position *ortho* (adjacent to a hydroxyl group) of the aromatic ring is replaced by a nitrogen atom (Scheme 1). This difference induces a different electron density in the aromatic ring. That might change the mechanism of the oxidative reaction in electropolymerization but also the final properties of the obtained material. One of the interests of the nitrogen-containing films is the ability to catalyze the electroreduction of CO_2, and most likely with a determined selectivity of the product.[27]

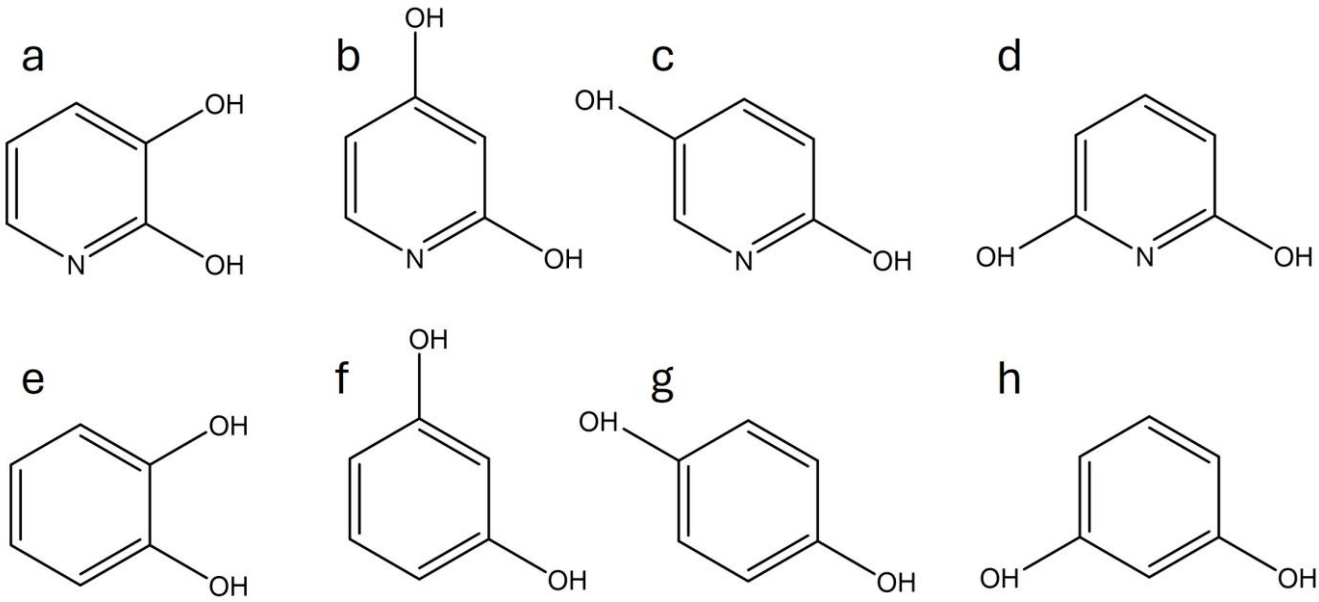

Scheme 1. Structures of the dihydroxypyridine isomers (on top) and their comparable nitrogen-free molecules (at the bottom): (a) 2,3-dihydroxypyridine, (b) 2,4-dihydroxypyridine, (c) 2,5-dihydroxypyridine, (d) 2,6-dihydroxypyridine, (e) catechol, (f) resorcinol, (g) hydroquinone and (h) resorcinol again.

To the best of our knowledge, the 2,3-dihydroxypyridine molecule has not extensively been studied and reported in the literature, either for chemical or electrochemical purposes. Soriaga et al.[28] reported the electrochemical oxidation of aromatic compounds on platinum electrodes. They included the 2,3-dihydroxypyridine in their study and the whole work is based on the influence of the adsorption orientation of these molecules. To the best of our knowledge, only the work from Varmaghani et al.[29] describes a film deposition from 2,3-dihydroxypyridine using cyclic voltammetry. However, the obtained film is not extensively characterized.

The other isomers of the dihydroxypyridines (Scheme 1) are even less found in the literature and only little data is available. For instance, even the pK_a of the 2,3-dihydroxypyridine, 2,4-dihydroxypyridine, 2,5-dihydroxypyridine and 2,6-dihydroxypyridine are only partially found in the literature.[30,31]

1.5. 1,8-dihydroxynaphthalene

1,8-dihydroxynaphthalene is a nitrogen-free melanin precursor (called allomelanin class) and is composed of 2 aromatic rings and 2 hydroxyl groups, each on a different ring (Scheme 2). This molecule can be found in fungi[32] and has been studied more than the dihydroxypyridines according to the number of papers found in the literature. The molecule is also known to have an antioxidant activity.[33]

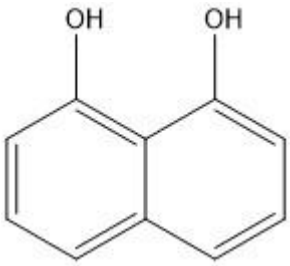

Scheme 2. Chemical structure of the 1,8-dihydroxynaphthalene.

Chemical and electrochemical studies have been performed with 1,8-dihydroxynaphthalene as a precursor; generally, to produce nanoparticles but also sometimes thin films.[34] However, to the best of our knowledge, there is no work to produce 1,8-dihydroxynaphthalene-based films by cyclic voltammetry reported in the literature.

To name only a few of the studies related to this molecule, there are several investigations on particles or precipitates such as the work reported by Mavridi-Printezi et al.[33] Manini et al.[34] reported a chemical oxidation to produce thin films.

1.6. Organization of the manuscript

This work can be separated in 3 work packages. These work packages will be described in the 3 chapters of this thesis manuscript.

First, a chapter will be dedicated to the electrodeposition of isomers of dihydroxypyridine. The study will show the differences obtained by changing the position of one of the

hydroxyl groups of the precursor, but also the influence of the scan rate on the obtained material. This part is currently close to be ready to get submitted to *Colloids and Surfaces A: Physicochemical And Engineering Aspects*.

The second chapter is dedicated to the electrodeposition of the 1,8-dihydroxynaphthalene on gold electrodes. The investigations will present the main characteristics, some promising properties and an attempt to provide a mechanism of reaction of the obtained films. This part has already been submitted to *ACS Applied Materials and Interfaces*.

The third and last chapter describes some results on the electrodeposition of 1,8-dihydroxynaphthalene films on glassy carbon. Furthermore, hybrid systems from mixtures of dihydroxypyridines and 1,8-dihydroxynaphthalene have been prepared and are also discussed in this part.

Finally, a general discussion, a general conclusion and perspectives will be given.

Main goals and purposes of this project

In a previous project, the team worked with 1,2-dihydroxybenzene and reported its electrodeposition on glassy carbon electrodes in “green chemistry” conditions. It was found that this electrodeposition leads to the formation of thin films at the surface of the glassy carbon electrode. More interestingly, the characterization made on these films showed that the films could be described as graphene oxide-like materials with a clear presence of graphitization on transmission electron microscopy images and crystallinity on electron diffraction patterns.

In our study, a first goal was to find other molecules, ideally biogenic or bioinspired molecules in “green chemistry” conditions, able to produce such materials. In order to increase this library of molecules, we started with the 2,3-dihydroxypyridine. Indeed, this molecule has the same chemical structure than the 1,2-dihydroxybenzene but has a nitrogen atom in the aromatic ring instead of one carbon atom. The idea behind this choice was to bring catalytic properties with the presence of nitrogen. After the first data obtained with the 2,3-dihydroxypyridines, we decided to enlarge the study to the different isomers of the 2,x-dihydroxypyridine: 2,4- , 2,5- and 2,6-dihydroxypyridines were studied. The difference in the chemical structure is a shift of the position of one hydroxyl group. Due to the successful film formation, characterizations were carried out on these films.

Another molecule came in the project a bit later: 1,8-dihydroxynaphthalene. It presents 2 hydroxyl groups like the 1,2-dihydroxybenzene of the former study, but they are placed on 2 aromatic rings instead of 1. The idea behind this choice was to compare the material obtained with a starting precursor already presenting a higher order in the chemical structure to the crystalline material obtained previously. Due to limitations with the glassy carbon electrodes, the study has been extended to gold electrodes as deposition

substrates. In both cases, characterizations of the formed films were carried out and another goal was then to get a comparison of the materials according to the nature of the substrate.

Chapter 1: Electrodeposition of films from dihydroxypyridines

2,3-dihydroxypyridine and the other isomers of dihydroxypyridines discussed here are the first candidates of precursors for film deposition used in our project. Their deposition was primary planned on glassy carbon electrodes, but due to limitations of the electrodes used (discussed in Chapter 3) the investigations were extended to deposition on gold electrodes too. The results obtained on gold electrodes must be treated with a cautious attention in comparison to glassy carbon since it is known that the nature of the substrate can impact the deposited material.[35]

This chapter corresponds to a manuscript dedicated for submission to *Colloids and Surfaces A: Physicochemical And Engineering Aspects*. Additional data obtained in this work but not chosen for publication are presented in section 3.5.

3.1. Introduction

Electrodeposition on electrodes from complex mixtures of molecules may lead to electrode passivation and hinder the determination of an analyte of interest.[36] However, electrodeposition performed by cyclic voltammetry or chronoamperometry, may also be considered as an advantage when using solutions of electroactive molecules because it leads to film deposition in a controlled manner. This allows deposition of oxidized-reduced molecules and their forthcoming reaction products without precipitation in solution which would occur upon solution-based oxidation in the presence of added oxidants. In this manner, polyaniline,[1,2] polypyrrole,[3,4] and polythiophene[5,6] coated electrodes have been produced for numerous applications, in particular for biosensing. Polydopamine, a eumelanin-like material can also be deposited on electrodes from dopamine solutions[37-43]

in a pH-dependent manner, the deposition being efficient only when the ethylamino group of dopamine is not fully protonated.[43] Eumelanin itself can be deposited as rough coatings through a potentiostatic method[44,45] and the isomers of dihydroxybenzene (catechol, resorcinol, and hydroquinone) display a specific behavior at amorphous carbon working electrodes[46] and at pH=5: resorcinol yields to impermeable coatings (with respect to potassium hexacyanoferrate) in a sweep potential dependent manner during deposition by CV and after a very low number of CV cycles. Hydroquinone does not lead to film deposition owing to its fully reversive oxidation-reduction wave. Catechol yields an intermediate behavior: a progressive passivation of the amorphous carbon working electrode (passivation occurs faster with slower potential sweep rates) but with the appearance of graphitic domains when the CV cycles are performed at 20 mV/s.[47] The oxidation mechanism of phenol derivatives has been investigated from a mechanistic point of view related to changes in the chemical structure, pH of the solution, and nature of the working electrode[48-53] but the structural characterization of the deposited material is highly challenging,[47] often due to low solubility of the produced films.

The addition of nitrogen atoms in the electrodeposited films should modify the electronic density of the structures incorporated in the electrodeposited films and afford some interesting applications in catalysis.[54] With the exception of pyrrole,[3,4] aniline,[1,2] and dopamine,[37-43] few nitrogen-containing precursors have been investigated for their possibility to yield conformal coatings by electrodeposition methods. Surprisingly the electrodeposition of hydroxylated pyridines has been scarcely explored: the structure and the electrochemical behavior of preadsorbed hydroxylated pyridines on Pt working electrodes have been investigated[55,56] and the electrodeposition of 2,3-dihydroxypyridine on glassy carbon electrodes has been studied as a function of the solution pH.[29] By analogy with the isomers of dihydroxybenzene,[46] leading to impressive different

electrochemical behavior on glassy carbon working electrodes, it is of the highest interest to compare the morphology, the composition, and the properties of coatings produced from isomers of dihydroxypyridines (DHP) by cyclic voltammetry (CV) and chronoamperometry (CA). This is the main aim of this study, where we systematically investigate the ability of 2,3-DHP, 2,4-DHP, 2,5-DHP, and 2,6-DHP (Scheme 3) to form films by CV on two types of substrates, namely, amorphous carbon and polycrystalline gold electrodes at pH 5 as a function of the potential sweep rate. Some complementary experiments will be performed on amorphous carbon at pH 10 and pH 5 but using CA instead of CV. The obtained data will be compared with those obtained with the isomers of dihydroxybenzene.[46] Indeed, in 2,3-DHP the two hydroxyl groups are in a relative ortho position, and this molecule should hence be compared with 1,2 dihydroxybenzene (catechol). Similarly, 2,4-DHP and 2,5-DHP should be compared with 1,3-dihydroxybenzene (resorcinol) and 2,4-dihydroxybenzene (hydroquinone) respectively. The electrochemical behavior of 2,6-DHP cannot be compared with that of resorcinol because the two OH groups in a relative meta position are separated by an N atom. It should be noted that molecules like hydroxy and dihydroxypyridines are of interest in pharmacology.[57]

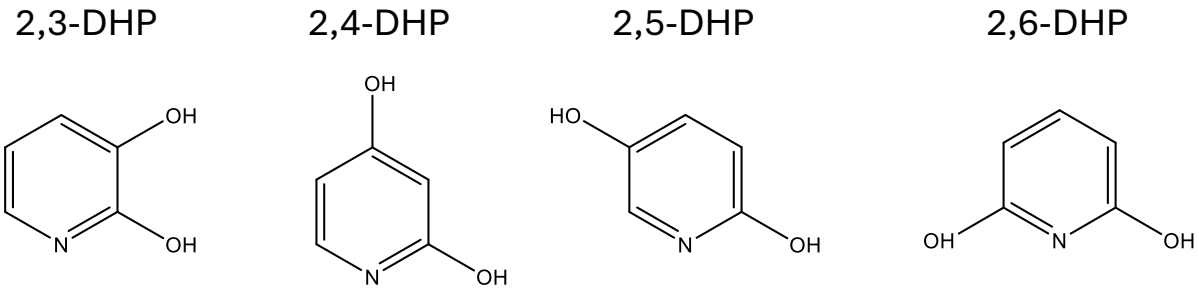

Scheme 3. Structures of the isomers of DHP used in this investigation.

3.2. Experimental section

3.2.1. Chemicals

All solutions were prepared from double distilled and demineralized water (Millipore, ρ=18 Ω.cm). Sodium acetate (ref. 6268, pro analysi, Merck), 2,3-DHP (ref. 122505, 95 % purity, Aldrich), 2,4-DHP (ref. 176964, 97 % purity, Aldrich), 2,5-DHP (ref. T23885, 95% purity, Manchester Organics) and 2,6-DHP (ref. D120006, 97% purity, Aldrich) were purchased and used without purification. Fresh DHP solutions were prepared in 50 mM sodium acetate buffer (pH adjusted to 5.00 $\pm$ 0.05) before each experiment. The DHP concentration was constant and equal to 1 mg/mL, i.e. 9.0 x 10^{-3} mol/L. Potassium hexacyanoferrate (P9387, Sigma Aldrich) was dissolved at 10^{-3} mol/L in the sodium acetate buffer to test the cleanliness of the electrodes and the permeability of the DHP-based electrodeposited coatings.

The antioxidant activity of the films was tested with 2,2-diphenyl-1-picrylhydrazyl (DPPH) bought from Sigma-Aldrich (ref. 257621).

3.2.2. Methods

3.2.2.1. Electrochemical deposition

All electrochemical experiments were performed with a CHI 604B potentiostat (CH Instruments, Austin, Texas) in a three electrode configuration. The working electrode was either an amorphous carbon disk (1 mm in diameter, ref. CHI 104 from CHI Instruments) or gold coated (1000 Å thick) microscope slides (Sigma-Aldrich, ref. 643246). These slides were cut in 10 pieces of 1.0 cm x 1.25 cm. The pieces were cleaned with an argon plasma for 10 minutes at 6 mbar, stored in a closed vessel, and rinsed with absolute ethanol before use.

The amorphous carbon electrodes were polished on a SiC cloth, rinsed with ethanol (70% v/v) and then polished on two alumina slurries (1.0 and 0.1 µm, Escil, Villeurbanne, France). Finally, the amorphous carbon electrode was sonicated twice for 2 min in a distilled water bath. The electrochemical experiments began with a CV in the presence of a 1mM hexacyanoferrate solution between -1.0 and 1.0 V vs Ag/AgCl at a potential sweep rate of 100 mV/s. The experiment was continued only if the oxidation and reduction peak potentials of hexacyanoferrate were separated by less than 80 mV (the theoretical value for a reversible one electron process being 2.3*RT/F*=59 mV at 25 °C).

The depositions of DHP based films was performed at ambient temperature (23 ± 2) °C on amorphous carbon electrodes in the presence of sodium acetate buffer at pH = 5 by performing 5 CV cycles at potential sweep rates of 10 or 100 mV/s. Some complementary experiments were performed at 10 mV/s but in the presence of 50 mM NaCl and with a pH adjusted to 10.0 in order to investigate the influence of deprotonated -OH groups on the different DHPs. Note that either at pH 5 or 10, the pyridine N atom should be deprotonated, due to its pK_a being equal to 0.1 in the case of 2,3-DHP.[30] Chronoamperometry (CA) experiments were also performed on amorphous carbon electrodes at pH=5 at a constant potential corresponding to the oxidation peak potential recorded during the first performed CV cycle.

On the gold working electrodes only CV deposition at pH = 5.0 and at a potential sweep rate of 10mV/s were undertaken. The gold electrode was chosen to perform film characterization experiments other than transmission electron microscopy (TEM), namely contact angle measurements, atomic force microscopy (AFM) and X-ray photoelectron spectroscopy (XPS).

Electrochemical impedance spectroscopy (EIS) measurements were performed on the pristine amorphous carbon electrode and on the CV-deposited DHP-based film. The frequency of the sinusoidal potential was varied between 0.01 and 10^5 Hz (with an amplitude of 5 mV superimposed to a DC signal corresponding to the oxidation peak potential of the hexacyanoferrate anions on the pristine electrode) in the potassium hexacyanoferrate(II) solution (1 mM).

The permeability of the thin films towards the same redox probe was also tested. The following steps were carried out in order to perform these assays: i) 1 CV cycle at 100 mV/s in the redox probe solution ii) 5 CV cycles at the chosen scan rate in the DHP containing solution to deposit the thin film iii) 1 CV cycle at 100 mV/s in the buffer solution (after rinse with the same buffer) to measure the capacitive and faradic current due to the film only and iv) 1 CV cycle at 100 mV/s in the redox probe solution again. The comparison of the CV curves obtained in i), iii) and iv) gives an insight of permeability of the thin films against hexacyanoferrate anions.

The films deposited on amorphous carbon by CV were scratched away for TEM characterization using a JEOL 2100 microscope under an acceleration voltage of 200 kV. The material removed from the electrode was deposited on a holey carbon coated Cu grid. A control experiment was performed by scratching the unmodified carbon electrode: no material was removed from it under these conditions.

3.2.2.2. Characterization of the deposited films

Wettability of film surfaces and of the gold electrode surface was evaluated by the averaging the left and right contact angle of 60 images of water sessile drops (4 µL) deposited by an Attention Theta Flow goniometer from Biolin Scientific (Sweden).

The morphology of the CV deposited films on gold working electrodes was characterized by AFM using a Catalyst microscope (Bruker Inc, Santa Barbara, CA, USA). The images were acquired at a frequency of 0.5 Hz in the scan assist mode and in the dry state within regions of interest (5 µm x 5 µm) and with a resolution of 512 x 512 pixels. The used cantilevers had a spring constant of 0.7 N/m as given by the manufacturer (Bruker Inc, Santa Barbara, CA, USA).

XPS measurements were carried out on a Kratos Axis Ultra *DLD* imaging photoelectron spectrometer. Measurements were carried out using the instrument's hybrid mode with a monochromatic Al Kα source (10 mA emission current and 15 kV voltage bias) in an ultra-high vacuum chamber ($1x10^{-10}$ mbar). The source line width is approximately 1.0 eV FWHM, as calibrated with the Ag 3d5/2 line. The analysis area was 700 µm x 300 µm. The data was collected using a hemispherical analyzer at an angle of 0 ° to the surface normal. Survey spectra were measured at a pass energy of 80 eV and high-resolution spectra at 20 eV pass energy.

Ellipsometric analyses were performed with a Woolam UV-NIR M2000 VASE device, equipped with an environmental chamber in which the atmosphere is controlled by two mass flow controllers mixing known amount of dry and water-saturated air. Data were collected from 200 nm to 1700 nm at 70 ° incidence.

3.2.2.3. DPPH discoloration assays

2,2-diphenyl-1-picrylhydrazyl (DPPH) is a well-known radical species used for antioxidant assays by its discoloration in the presence of antioxidants.[58] The DPPH solution was prepared with a concentration of 0.1 mM by dissolving 2,2-diphenyl-1-picrylhydrazyl in absolute ethanol. This solution was stored in a fridge and protected from light by wrapping the container with an aluminum foil. After the electrochemical synthesis, the thin films were

shortly rinsed in absolute ethanol. Then the gold coated slides covered by the films were placed horizontally at the bottom of a falcon tube containing 2.0 mL of 10^{-4} M DPPH solution (As much DPPH solution as needed to cover the whole film but not more).

3.3. Results and discussion

3.3.1. Electrodeposition on amorphous carbon electrodes

Five successive CVs of the 4 investigated DHPs (at a constant concentration of 9.0 x 10^{-3} mol/L) at a potential sweep rate of 10 mV/s in the presence of 50 mM sodium acetate buffer at pH = 5 and on amorphous carbon working electrodes are displayed in Figure 2. In these experimental conditions, the CVs of 2,4-DHP (Figure 2B) were markedly different than the CVs of the other investigated molecules in the sense that no reduction current was measured between +0.8 and -0.4 V vs Ag/AgCl. The reduction wave below -0.5 V vs Ag/AgCl in all CV curves was due to dissolved oxygen (no caution was taken to degas the solutions). This observation of irreversible CV of 2,4-DHP could imply the passivation of the electrode as observed previously in the case of resorcinol.[37] This is however not the case because CVs performed in the absence of an added redox probe (after 5 CV cycles and buffer rinse) revealed a purely capacitive current almost undistinguishable from the capacitive current measured on the polished electrode (blue curve in Figure 3B). In accordance with the assumption of no film deposition, the CV measured in the presence of 1 mM hexacyanoferrate (red curve in Figure 3B) was almost the same as the CV measured (at 100 mV/s) on the polished electrode indicating no hindrance (due to deposited impermeable material) for the redox probe to be oxidized-reduced at the electrode surface. The irreversible nature of the CVs of 2,4-DHP hence suggests the formation of an irreversibly formed quinone not undergoing a further reaction at the electrode and subsequently dissolving in the solution. Another explanation would be the

occurrence of oxidation only at higher potentials, outside the stability domain of water. This behavior differs strongly from that of resorcinol, the analogue of 2,4-DHP, which undergoes irreversible oxidation but reacts at the interface to form a film passivating the amorphous carbon electrode after only few CV cycles at 10 mV/s.[46] Clearly, 2,4-DHP does not allow to deposit coatings under several CV cycles and this molecule will be discarded in the rest of the present investigation.

On the other hand, 2,3-DHP and 2,5-DHP display a similar behaviour during their CV scans on amorphous carbon working electrodes at pH 5.0: a first set of oxidation-reduction peaks are detected between +0.2 and +0.5 V vs Ag/AgCl with some partially reversible character whereas a broad oxidation wave is detected above +0.5 V vs Ag/AgCl. This oxidation process is irreversible (no corresponding reduction wave). However, a difference appears at this level: the oxidation wave of 2,3-DHP decreases from cycle to cycle whereas the oxidation current of 2,5-DHP is strongly reduced from the first to the second CV cycle, with a concomitant anodic shift of the oxidation peak by about 0.25 V but remains almost constant from the 2nd to the 5th CV cycle (Figure 2C). Note also that the first oxidation-reduction peaks (between +0.2 and +0.5 V vs Ag/AgCl) of 2,3, 2-5, and 2,6-DHP only appear from the 2nd cycle on and evolve during the subsequent CV cycles. These almost fully reversible peaks could be due to the formation of new redox probes resulting from the nucleophilic attack of water on the 3 oxidized DHPs in a manner similar to what happens to phenol after its electrochemical oxidation.[53]

Concerning 2,6-DHP, the following observations are noticed: (i): as for 2,3-DHP the oxidation-reduction between 0.0 and +0.4 V vs Ag/AgCl only appears from the 2nd CV cycle on. (ii): a marked and sharp oxidation peak at about +0.5 V vs Ag/AgCl is measured only during the first CV cycle in addition to a broad peak centred at +0.7 V. (iii) only this 2nd peak remains on the subsequent CV cycles at an almost constant potential but with a decreasing peak current and almost disappearing at the 5th CV cycle (Figure 2D).

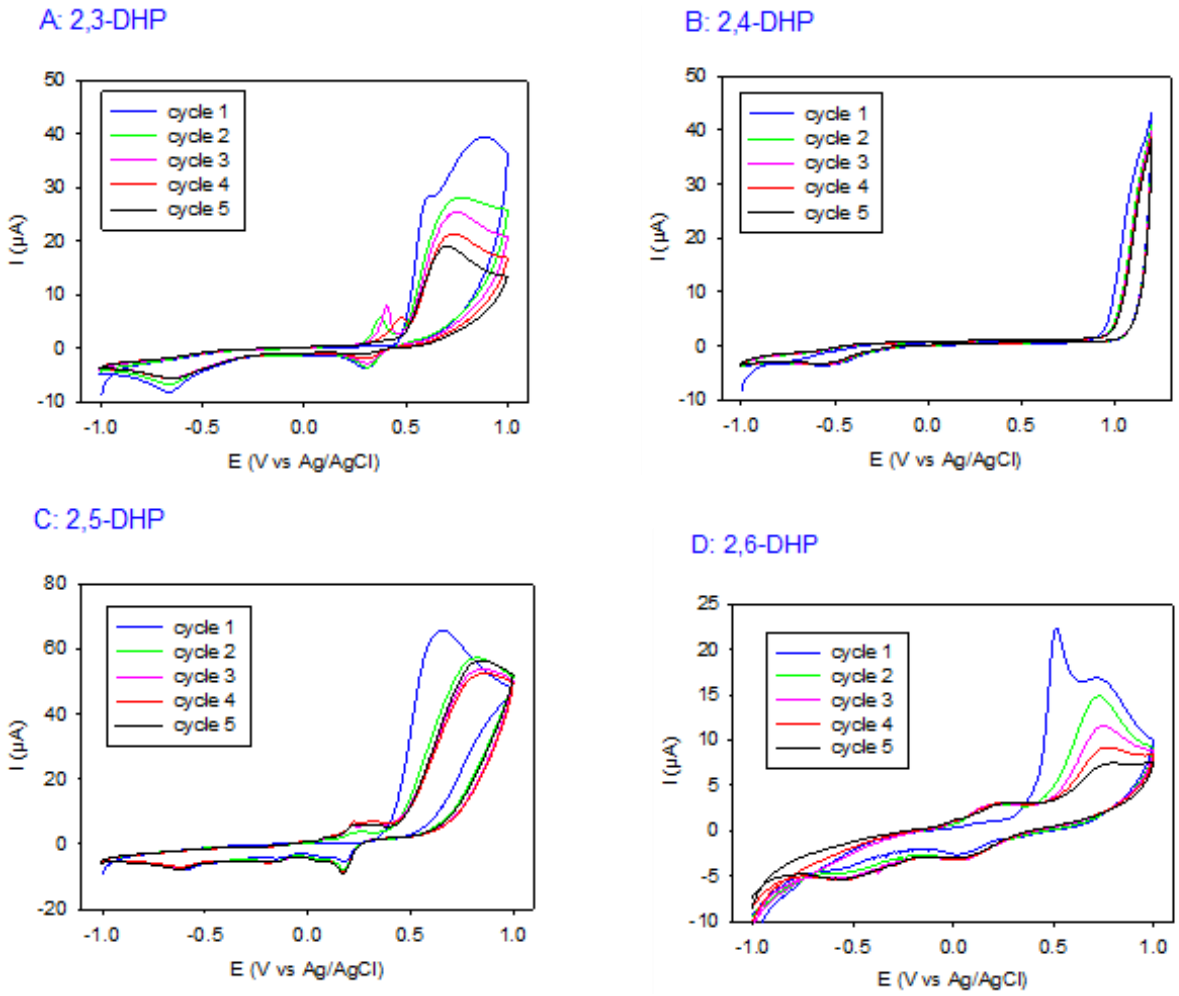

Figure 2. 5 successive CV scans at a potential sweep rate of 10 mV/s (see the inset for the correspondence between color and the cycle number) of 2,3-DHP (panel A), 2,4-DHP (panel B), 2,5-DHP (panel C) and 2,6-DHP (panel D) dissolved at 1 mg/mL in 50 mM sodium acetate buffer (pH = 5.0) on amorphous carbon working electrodes.

Hence and in marked contrast with 2,4-DHP, after 5 CV cycles (at 10 mV/s), the three other investigated dihydroxypyridines form a coating on the amorphous carbon electrode as shown by the presence of faradic currents in CVs performed at 100 mV/s in the presence of sodium acetate buffer but in the absence of an external redox probe in the solution (blue curves in Figure 3).

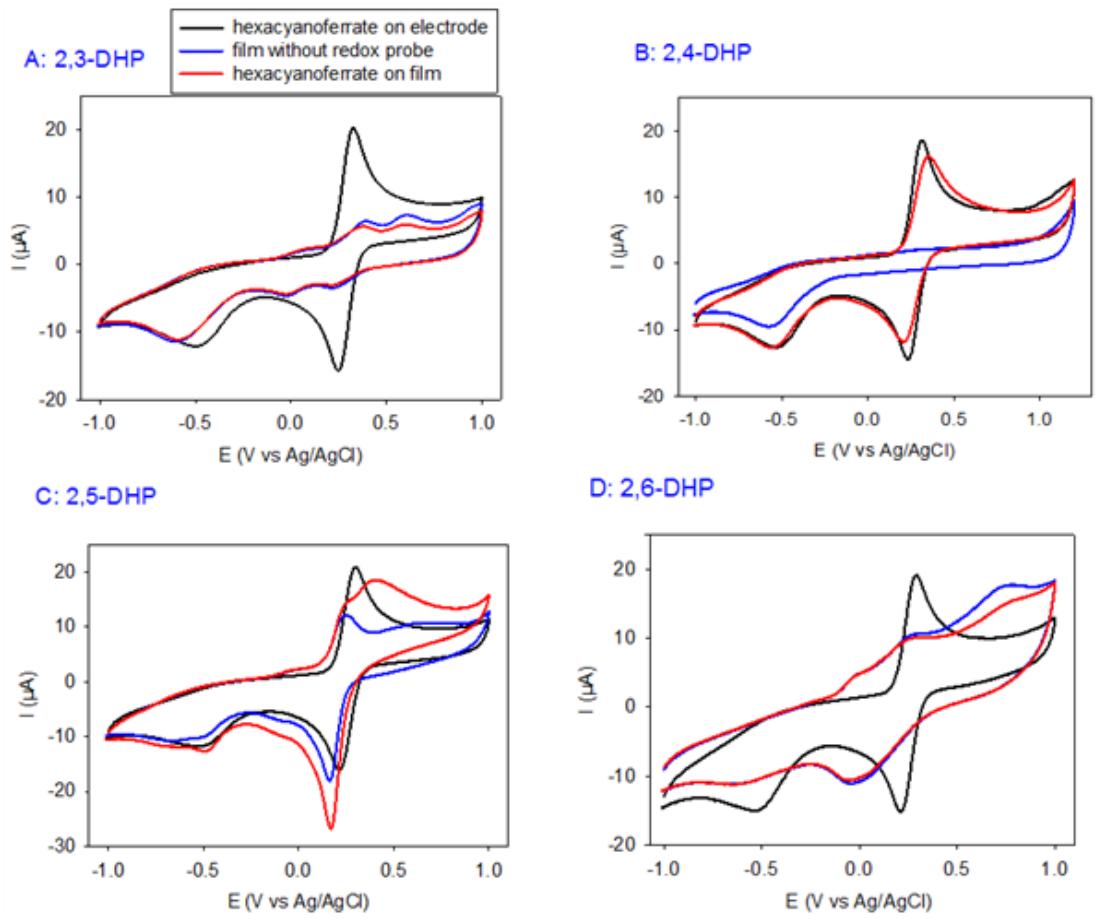

Figure 3. CVs performed at 100 mV/s in the presence of 1 mM potassium hexacyanoferrate on the pristine carbon electrodes (black full line) and on the same electrode after 5 CV deposition cycles (10 mV/s) in the presence of different DHP isomers (red full lines). The full blue lines correspond to a CV (100 mV/s) obtained after the 5 CV deposition cycles but without a redox probe in solution. All experiments were performed in the presence of 50 mM sodium acetate buffer at pH=5.0.

Next, we analyzed if the deposition process was dependent on the scan rate of the CV, by performing 5 CV cycles of all four DHP isomers at a 10-fold increased rate of 100 mV/s. The same trends are observed as for the experiments performed at 10 mV/s, however, for 2,6-DHP a faster decrease in the oxidation current from cycle to cycle (Figure 4) is found. In addition, as expected for an irreversible electron transfer process, the oxidation peak potential of the first CV shifts anodically when the potential sweep rate increases.[16] In the particular case of 2,6-DHP the first oxidation peak potential shifts from about 0.5 V to about 0.65 V (vs Ag/AgCl) when the potential sweep rate increases from 10 to 100 mV/s. All the deposits obtained at this higher potential sweep rate are electroactive, displaying a faradic current in the absence of an external redox probe (Figure 5). 2,6-DHP-based films display a second oxidation wave at around +0.75 V vs Ag/AgCl that is much more pronounced when the deposition is performed at 100 mV/s rather than at 10 mV/s (compare panel D in Figure 3 and panel C in Figure 5). In pretty marked contrast with the films obtained at 10 mV/s, the 2,3 and 2,5-DHP-based films deposited at 100 mV/s are markedly permeable to hexacyanoferrate anions (Figures 3A, 3B and 5A, 5B). The permeability of the 2,6-DHP films to hexacyanoferrate anions seems not markedly affected by the potential scan rate used during the deposition at pH = 5.0 (Figure 3D and Figure 5C).

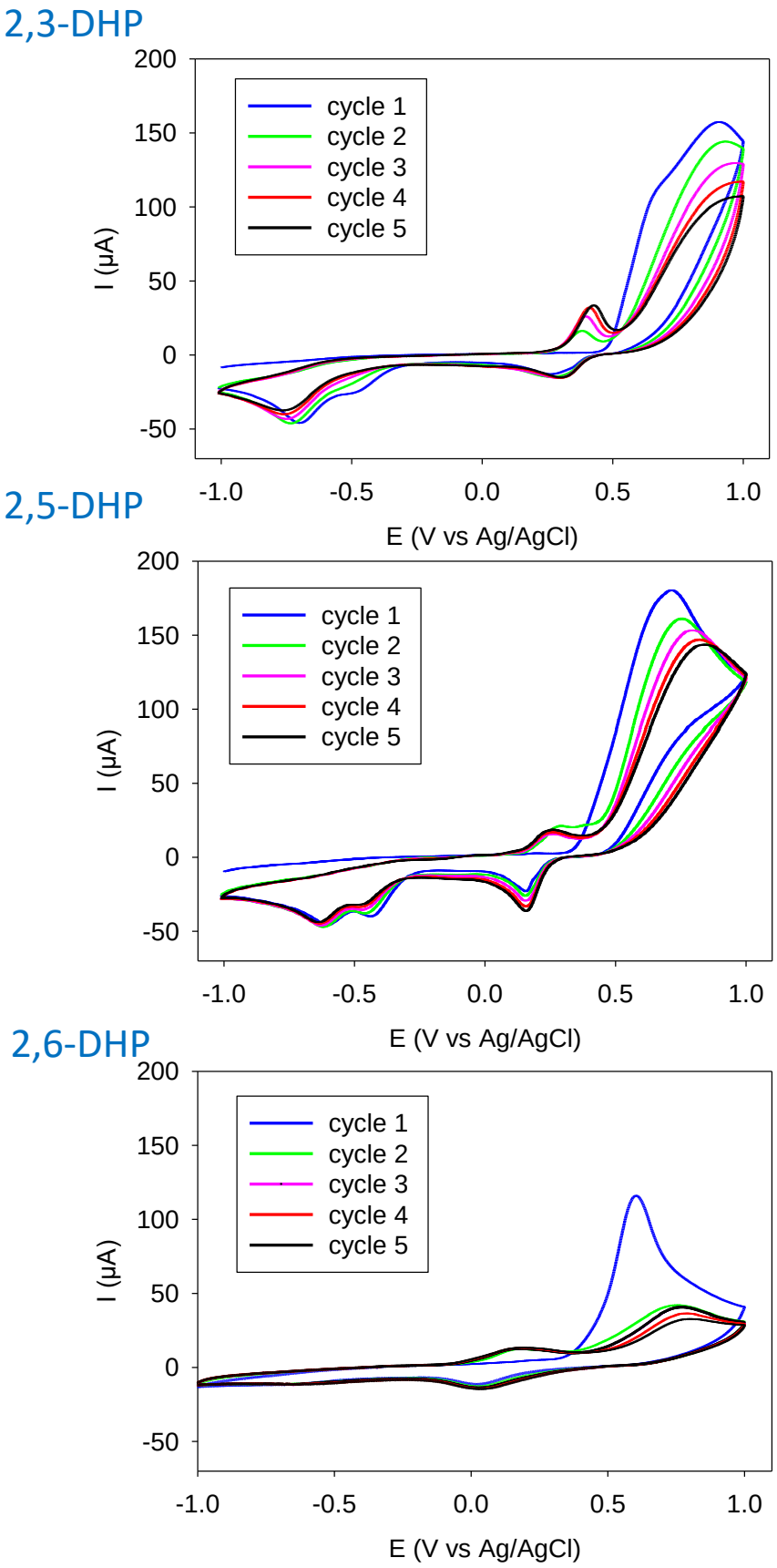

Figure 4. 5 successive CV scans at a potential sweep rate of 100 mV/s of 2,3-DHP, 2,5-DHP and 2,6-DHP dissolved at 1 mg/mL in 50 mM sodium acetate (pH = 5) on amorphous carbon working electrodes.

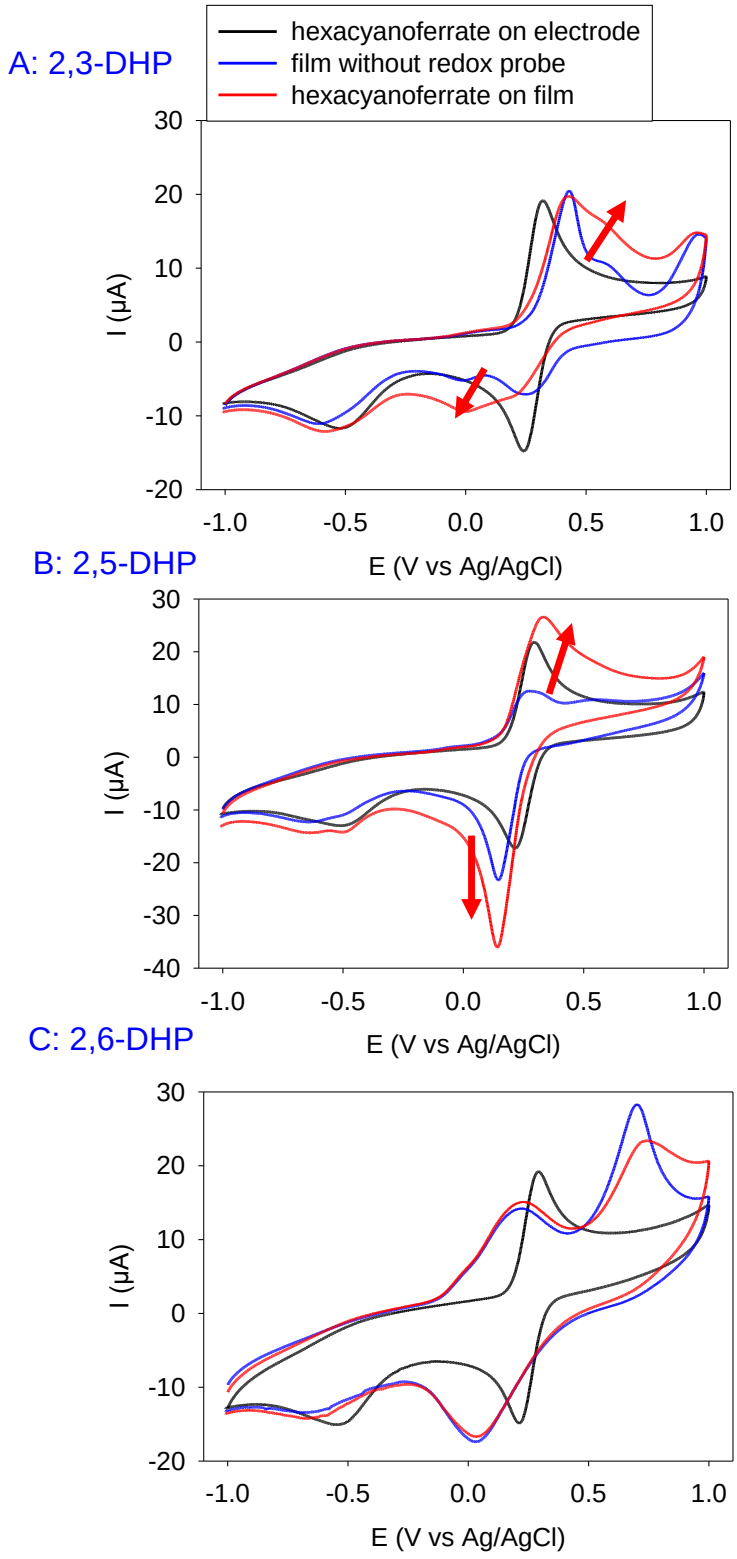

Figure 5. CV performed at 100 mV/s in the presence of 1 mM potassium hexacyanoferrate on the pristine carbon electrodes (black full line) and on the same electrode after 5 CV deposition cycles (100 mV/s) in the presence of the different DHPs (red full lines). The full blue lines correspond to a CV (100 mV/s) obtained after the 5 CV deposition cycles but in

the absence of a redox probe in solution. All experiments were performed in the presence of 50 mM sodium acetate buffer (pH = 5).

The CV of redox species in which the oxidation implies a change in the protonation state have to be pH dependent, as is the case for polyphenols.[43,51,53] Here also the electrochemical behavior changes markedly when the CVs of DHPs are performed at pH=10 (Figure 6) where the nitrogen atom of the dihydroxypyridines are uncharged and where one of the two hydroxyl group is probably deprotonated. Unfortunately, the acidity constants are determined only for 2,3-DHP:[30] pK_{a1} (deprotonation of the nitrogen atom) = 0.1, pK_{a2} (deprotonation of the OH group in position 3 of 2,3-DHP) = 8.7 and with an unknown pK_{a3} (deprotonation of the OH group in position 2). These data from the literature strongly suggest (with less confidence concerning 2,5- and 2,6-DHP) that the investigated molecules are negatively charged at pH = 10. In these conditions, the oxidation currents of 2,3- and 2,6-DHP strongly decrease between the first and the second CV cycle (Figure 6), indicating a very fast passivation of the electrode surface. In marked contrast, with 2,5-DHP the oxidation current remains pretty constant from cycle to cycle, as was already the case at pH = 5.0 (Figure 2C and Figure 2B). Interestingly, the strong reduction peak detected during the first cycle at about 0.0 V disappears during the second and the next performed CV cycles (Figure 6B). Taken together, these qualitative electrochemical experiments suggest a peculiar behavior of 2,5-DHP when compared to 2,3 and 2,6-DHP. Further analysis of the chemical structures that are obtained during electropolymerization is needed.

The oxidation peak potentials of the first cycles (E_{pa}) recorded at 10 mV/s at pH 5.0 and 10.0 are listed in Table 1.

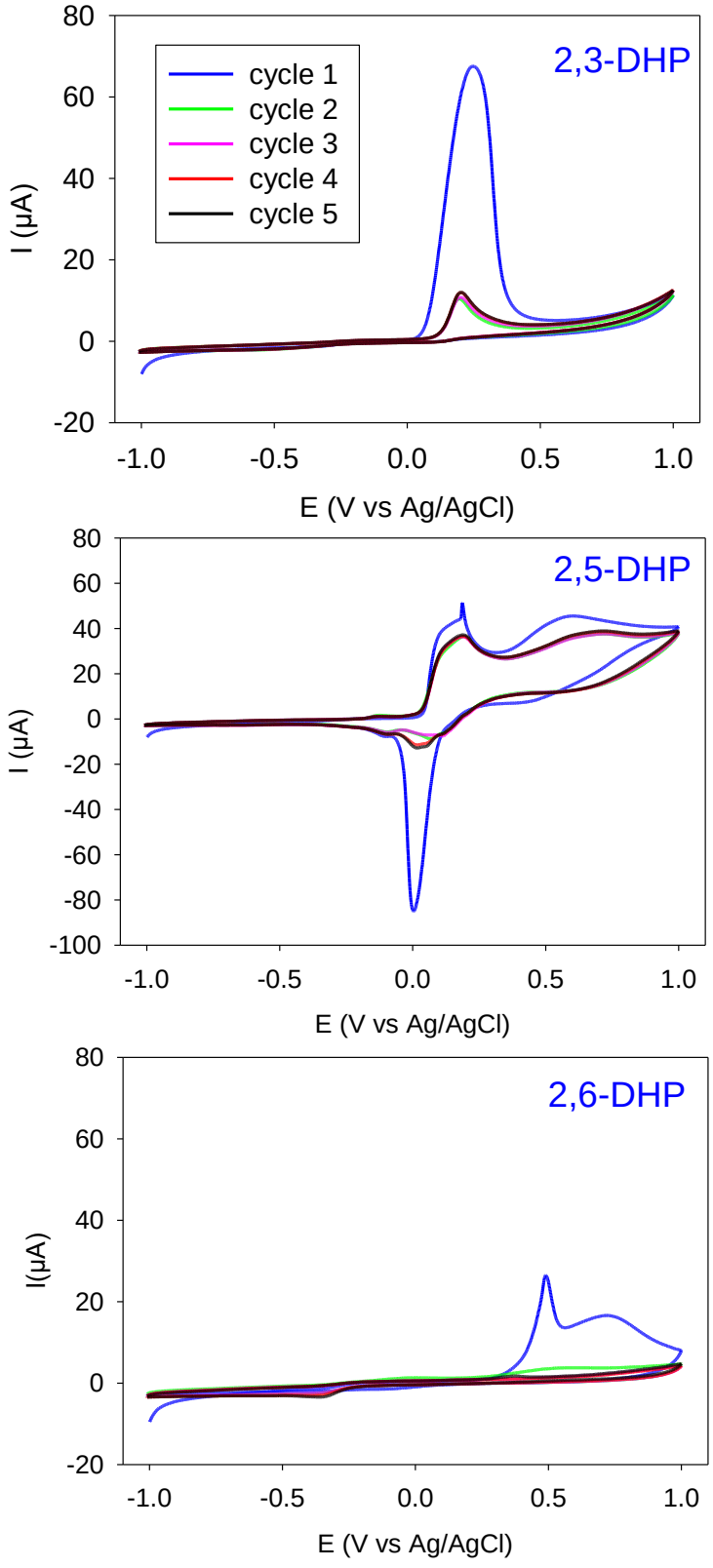

Figure 6. 5 successive CV scans at a potential sweep rate of 10 mV/s (see the inset for the correspondence between color and the cycle number) of 2,3-DHP, 2,5-DHP and 2,6-DHP dissolved at 1 mg/mL at pH = 10 on amorphous carbon working electrodes.

Table 1. oxidation peak potential measured during the first CV scan (10 mV/s) of the different DHPs at pH = 5.0 and 10.0 as well as the relative change in the peak potential position per pH unit (last row).

	2,3-DHP	2,4-DHP	2,5-DHP	2,6-DHP
E_{pa} at pH=5.0	0.608 V	>1.0 V	0.648 V	0.512 V
E_{pa} at pH=10.0	0.248 V	Not measured	0.187 V	0.490 V
$\Delta E_{pa}/\Delta pH$	-72 mV/pH unit	/	-92 mV/pH unit	-4 mV/pH unit

From Table 1 it appears that 2,6-DHP differs markedly from 2,3- and 2,5-DHP as the oxidation peak potential of 2,6-DHP is nearly pH-independent, while 2,3- and 2,5-DHP seem to show a strong pH-dependency (of course this is only a qualitative trend and more experiments will have to be performed at other pH values). The shifts in the oxidation peak potentials of 2,3- and 2,5-DHP are consistent with an oxidation in which the number of electrons and the number of protons lost during oxidation are equal. In such a case, the $\Delta E_{pa}/\Delta pH$ value should be equal to 59 mV per pH unit.[16] Since the oxidation of an -OH group on an aromatic structure requires the simultaneous loss of electrons and protons,[43,53] we assume from the results given in Table 1 that the oxidation of 2,6-DHP concerns the nitrogen atom on the pyridine ring which is deprotonated in the full pH-range between 5 and 10.

There is also interest to deposit films from redox-active molecules undergoing a post oxidation chemical change (a so-called EC process) by means of chronoamperometry (CA) which could allow to speed up the deposition process but also the production of films with different properties.

The peculiar behavior of 2,5-DHP when compared to 2,3- and 2,6-DHP appears again when CA is performed (pH=5.0) at a constant potential corresponding to the oxidation peak potential obtained during the first CV cycle (Figure 7). Indeed, the oxidation current of 2,5-DHP decreases less rapidly than for 2,3 and 2,6-DHP which behave rather similarly.

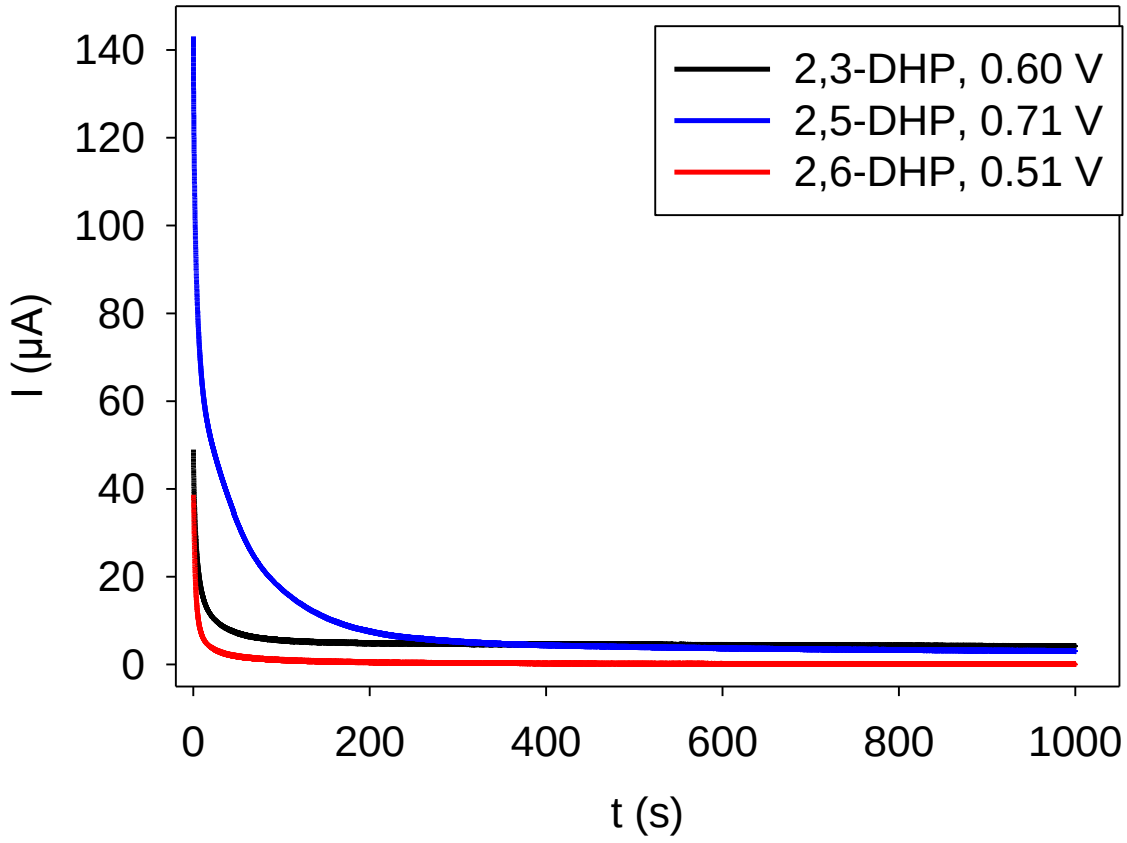

Figure 7. Chronoamperometry of DHP solutions (as indicated in the inset) at 1 mg/mL in 50 mM sodium acetate buffer at pH = 5. The deposition potentials (as indicated in the inset) were chosen equal to the oxidation peak potential measured during the first CV scan displayed in Figure 2.

Whatever the used isomer, after 1000 s of CA, the electrode is covered with an electroactive film that is highly permeable to the hexacyanoferrate probe (Figure 8). The faradic currents measured on the deposits obtained by CA are very close to those obtained when CV is performed at a high potential sweep rate, namely at 100 mV/s

(Figure 5), suggesting a similar electrochemical behavior. This is not so surprising because CA is identical to CV when the potential sweep rate becomes extremely high.

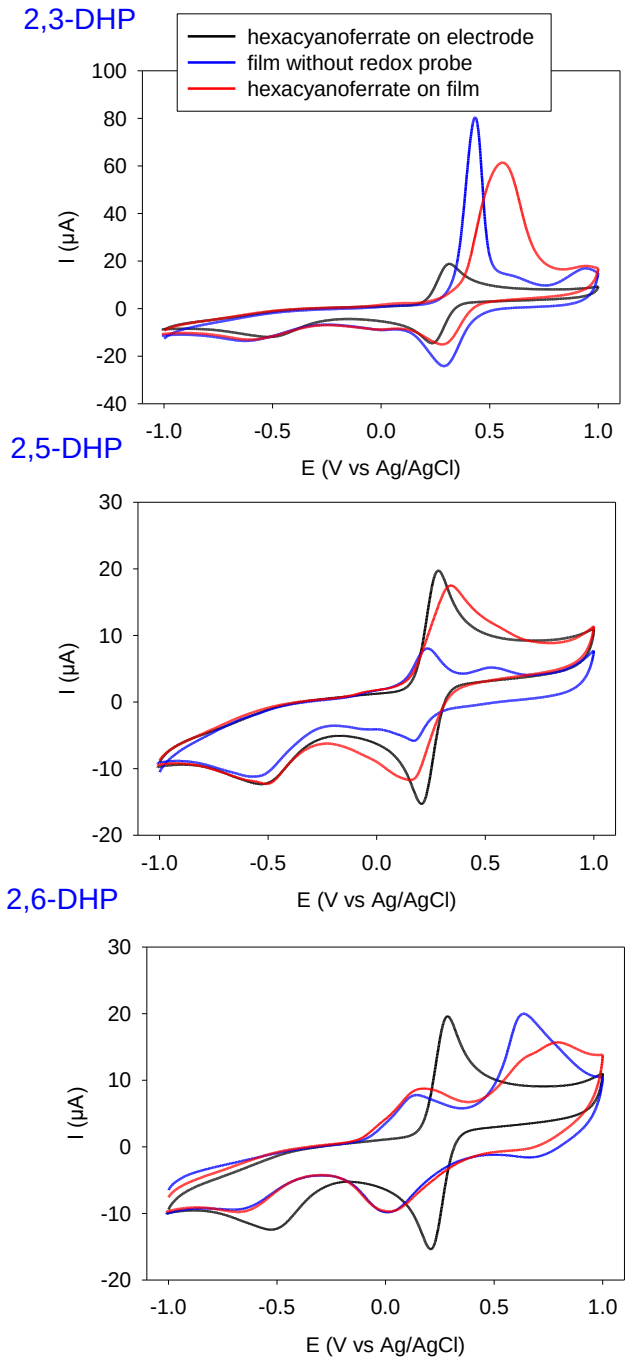

Figure 8. CV performed at 100 mV/s in the presence of 1 mM potassium hexacyanoferrate on the pristine carbon electrodes (black full lines) and on the same electrode after 1000 s of chronoamperometry (at the potentials in the inset displayed in Figure 7) in the presence of the different DHPs (red full lines). The full blue lines correspond to a CV (100 mV/s)

obtained after 1000 s of chronoamperometry but in the absence of a redox probe in solution.

In addition, the electrochemical impedance spectra of the films obtained from 2,5-DHP display a different behavior than those obtained from the two other DHPs of interest (Figure 9). The semi-circle in the Nyquist plot (-Z" versus Z', where Z" and Z' are the imaginary and real parts of the impedance) display a much lower radius in the high frequency domain for the 2,5-DHP deposit than for the 2,6- and 2,3-DHP-based ones. This suggests a much lower resistance[59] to the electron transfer across the film in the case of 2,5-DHP deposition. In turn, such a lower resistance may be due either to a more conductive or to a thinner film. This point will be addressed in the next section aimed to characterize the obtained coatings from a morphological, compositional and applied point of view. It has to be noticed that the lower electron transfer resistance of 2,5-DHP based films, and hence a higher electronic conductivity, may explain the pretty high oxidation current of hexacyanoferrate anions in the presence of the deposited film (Figure 3B). Indeed, in the case of conductive films, the redox probe has not to diffuse through pores or channels in the film but can be oxidized/reduced directly at the film/solution interface.

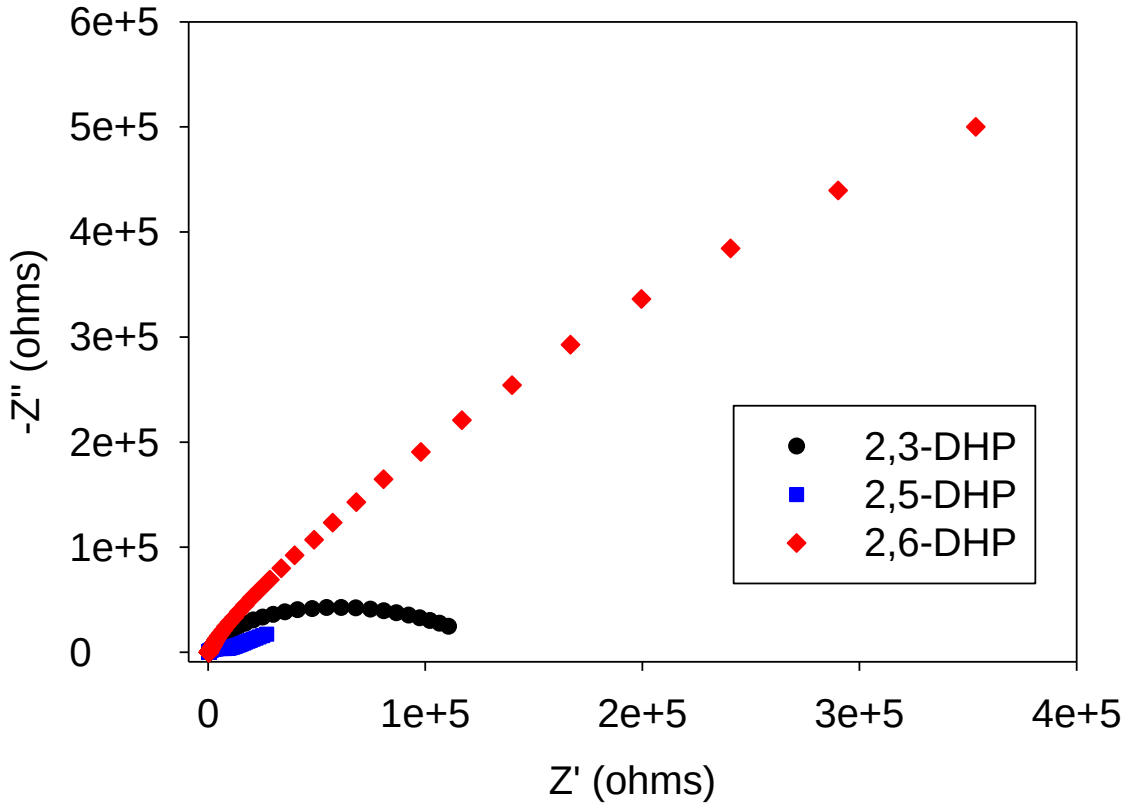

Figure 9. Electrochemical impedance spectra of the DHP-based films obtained on an amorphous carbon working electrode after 1000 s of chronoamperometry at the potential indicated in the inset of Figure 7.

DHP based films were also deposited on gold electrodes to facilitate their characterization by AFM and XPS (Figure 10). The experiments were performed at pH = 5.0 and under a potential sweep rate of 10 mV/s, hence in conditions identical to those used in Figure 2. Overall, with exception to an anodic shift of all the CVs, due to an electron transfer which is less good on gold than on carbon, the trend of the deposition is similar than on amorphous carbon. Noteworthy, with 2,5-DHP only a slight reduction in the oxidation-reduction current is observed when the number of CV cycles is increased. For all the investigated isomers, a deposit is obtained after 5 CV cycles as observed by a color change of the dried gold electrode (see later).

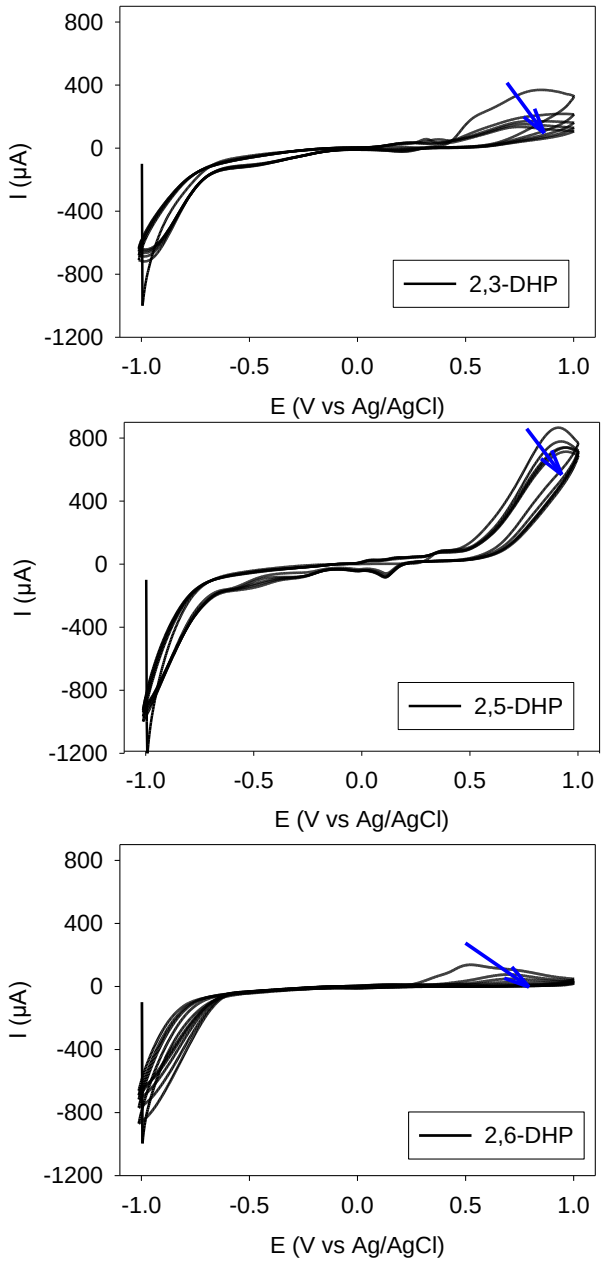

Figure 10. 5 successive CV cycles of 2,3-, 2,5- and 2,6-DHP (as indicated in the insets) recorded at pH = 5 and at 10 mV/s on gold working electrodes. The arrows indicate the current evolution upon an increase in the number of performed CV cycles.

3.3.2. Characterization of the DHP-based films

The films deposited on amorphous carbon working electrodes after 5 CV cycles performed at 10 or 100 mV/s and at pH = 5 were scratched away from the electrode and characterized by TEM (Figure 11). The material obtained from 2,3- and 2,5-DHP displayed

some crystalline domains (Figures 11A and 11C) when the deposition was performed at 10 mV/s in strong contrast with the 2,6-DHP-based material which was totally amorphous under these deposition conditions (Figure 11D). The lattice spacings were determined to be equal to 0.35 ± 0.11 nm and 0.36 ± 0.12 nm for the 2,3-DHP and 2,5-DHP-based materials produced by CV. Those values are close to expected for graphitic-based materials.

When the CVs were performed at the higher potential sweep rate of 100 mV/s the material obtained from 2,3- (Figure 11B) and 2,5-DHP (not shown) also turned to be amorphous.

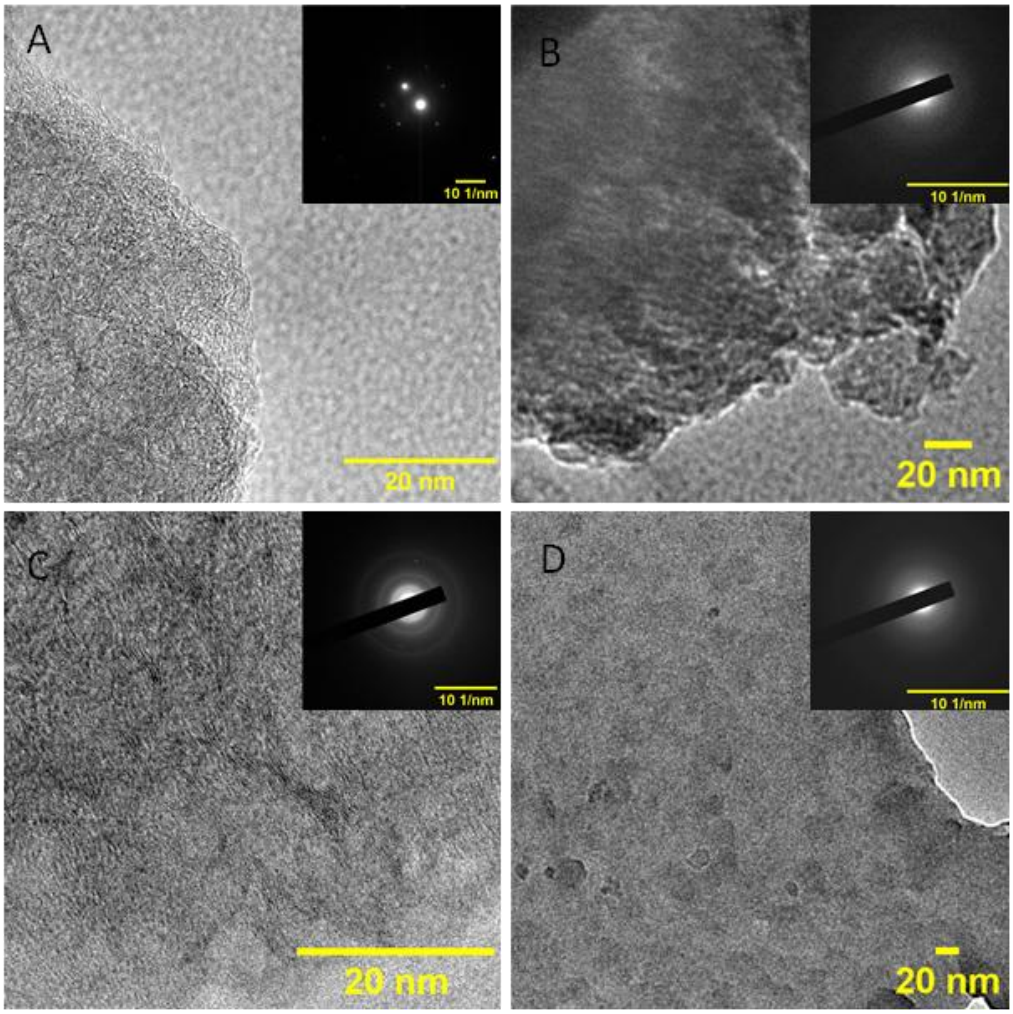

Figure 11. Transmission electron microscopy images and electron diffraction patterns (in the insets) of films obtained after 5 CV cycles on a glassy carbon electrode from A: 2,3-DHP at 10 mV/s; B: 2,3-DHP at 100 mV/s; C: 2,5-DHP at 10 mV/s and D: 2,6-DHP at 10 mV/s.

Owing to the small size of the carbon working electrode (3.14 mm² of geometric area) and its composition (carbon and oxygen being common elements with DHP), all the other film characterizations were performed on films deposited by CV (at 10 mV/s) on gold working electrodes. The presence of coatings was qualitatively confirmed after rinsing with water and drying under a stream of dried air by a color change of the electrodes (Figure 12A). The same coated electrodes were used for morphological characterization by AFM (Figure 12B), for their water wettability (Figure 12C) and for their thickness as determined by spectroscopic ellipsometry. For all the three investigated DHPs, the part of the electrode immersed in the solution during the 5 successive CV scans was covered with a brownish film (Figure 12A). The coatings obtained from 2,3-DHP, 2,5-DHP 2,6-DHP displayed a grainy morphology (Figure 12B). The root mean squared roughness (determined over 5 x 5 µm² images) was equal to 14.5, 4.7 and 17.4 nm respectively for the 2,3-DHP, 2,5-DHP and 2,6-DHP films respectively. The smoothest 2,5-DHP-based films were the less hydrophilic whereas the 2,6-DHP based films were superhydrophilic with a static water contact angle close to 5° (Figure 12C). This high wettability may be due a change in composition and/or to the increased roughness of the 2,6-DHP based coatings. Anyway, the roughness of the films made from 2,6-DHP was too high to allow for the film characterization by spectroscopic ellipsometry owing to low reflectivity and high amount of light scattering. This was not the case for the coatings made after 5 CV cycles (10 mV/s) from 2,3 and 2,5-DHP with a comparable optical thickness of 24.6 and 24.2 nm respectively (Table 2). The absence of thickness change between those two kinds of films allows to attribute the lower resistance to electron transfer of the 2,5-DHP based coatings (Figure 9) to a lower resistivity to the electron transfer between the electrode and the electrolyte solution (the resistance of thin conformal film is the product of the resistivity times the thickness divided by the surface area).

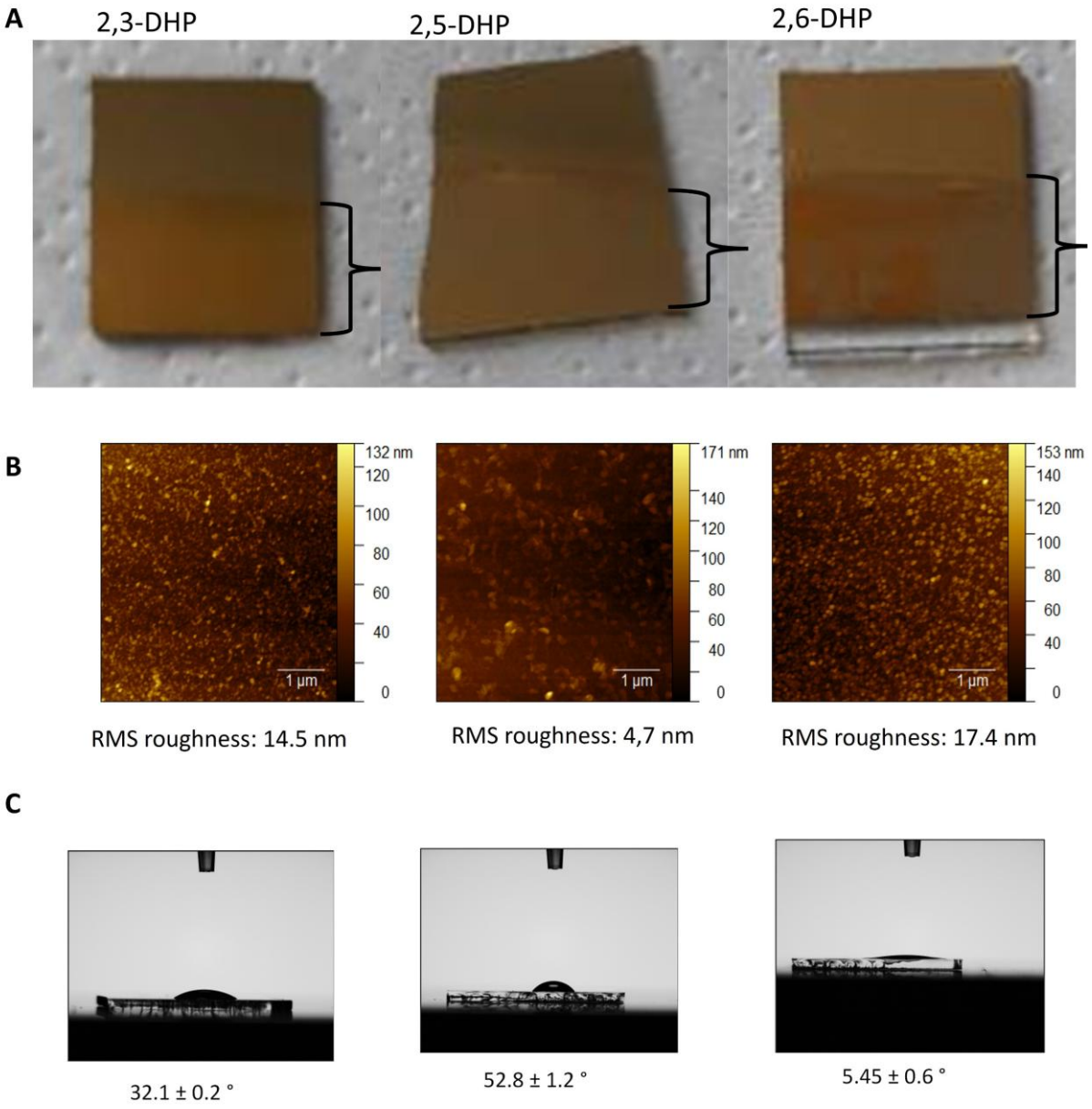

Figure 12. Characterization of the DHP based films deposited on gold working electrodes after 5 CV cycles performed at 10 mV/s (50 mM sodium acetate buffer, pH = 5.0) First, second and third column correspond to the 2,3-DHP, 2,5-DHP and 2,6-DHP based films, respectively. Rows A, B and C: optical pictures (the coated parts of the electrodes appear brownish and are marked by a brace), AFM topographies and static water contact angles respectively.

The composition of the films was characterized by means of XPS: the C1s high resolution spectrum shows that the 2,6-DHP based films are enriched in -C=O moieties when compared to the 2,3- and 2,5-DHP based coatings (Figure 13 and Table 2). The coatings obtained from 2,5-DHP also distinguish from the other ones by the presence of a lower N content (Table 2). Such a lower N content may be due to a process implying a loss of nitrogen moieties. This is totally different than in the reaction mechanism proposed by Nematollahi et al.[29] who showed that the oxidation of 2,3-DHP in acidic solution but on carbon electrodes yields to a tricyclic structure but without loss of N.

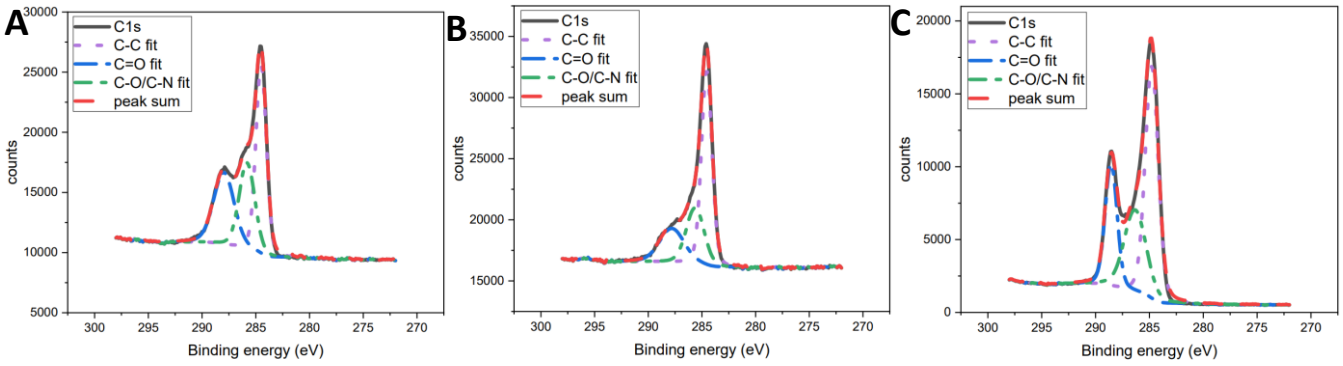

Figure 13. High resolution C1s XPS spectra of films deposited on gold electrodes after 5 CV cycles performed at 10 mV/s and at pH = 5.0 from A: 2,3-DHP, B: 2,5-DHP and C: 2,6-DHP solutions at 1 mg/mL.

However, the high resolution N1s spectra of the three kinds of films are almost similar with a peak centered at a binding energy of 400 eV (Figure 14). The N1s spectra of the electropolymerized DHP films are similar to those of self-assembled monolayers made from pyridine thiolates.[56]

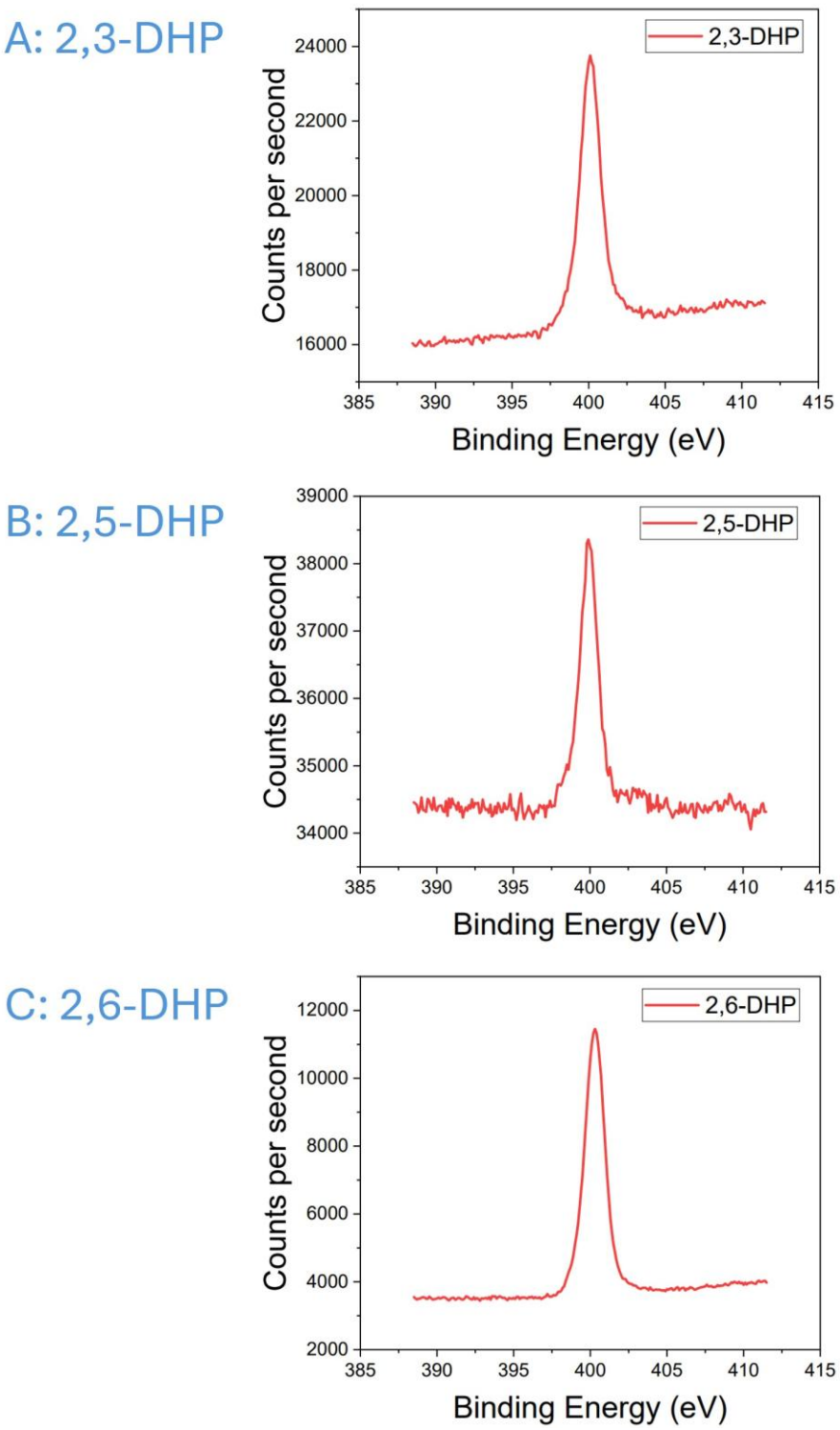

Figure 14. High resolution N1s XPS spectra of the DHP films deposited on gold electrodes from DHP solutions at 1 mg/mL (pH = 5) and after 5 CV deposition cycles performed at 10 mV/s.

Table 2. Morphological and compositional characterization of the films obtained on gold working electrodes after 5 CV cycles performed at 10mV/s at pH = 5.0.

	2,3-DHP	2,5-DHP	2,6-DHP
Thickness (nm)	24.6 ± 1.0	24.2 ± 1	Not determined
Water contact angle	32.1 ± 0.2 °	52.8 ± 1.2 °	5.45 ± 0.6 °
C (%) from XPS	66.9 ± 0.4	75.5 ± 0.9	67.8 ± 0.5
O (%) from XPS	23.9 ± 0.6	19.1 ± 0.9	22.6 ± 0.3
N (%) from XPS	9.2 ± 0.5	5.4 ± 0.3	9.6 ± 0.3

Finally, all the DHP based films deposited on gold electrodes (from a solution at pH = 5.0 and under a potential sweep rate of 10 mV/s) displayed some antioxidant activities as measured by the discoloration of 2,2-diphenyl-1-picrylhydrazyl (Figure 15), however without significant differences between the different kinds of films. This antioxidant activity corresponds to about 9 % of DPPH quenching as estimated from the relative difference between the absorption peaks of the DPPH solution (10^{-4} M) in contact with the films and the initially prepared DPPH solution (reference spectrum in Figure 15). This antioxidant behaviour may well be related to the high content in -OH groups of all the films, despite a somewhat higher oxidation degree of the 2,6-DHP based films (Figure 13C). Since those

later films display a higher roughness than the other ones (Table 2) a lower percentage of -OH groups able to have an antioxidant effect could be compensated by a higher effective concentration of those groups. Note that a quenching efficiency of 9% seems weak at first glance but this value has been obtained on a film area close to 2cm² immersed in 2 mL of DPPH solution hence in conditions of weak surface area to volume ratio.

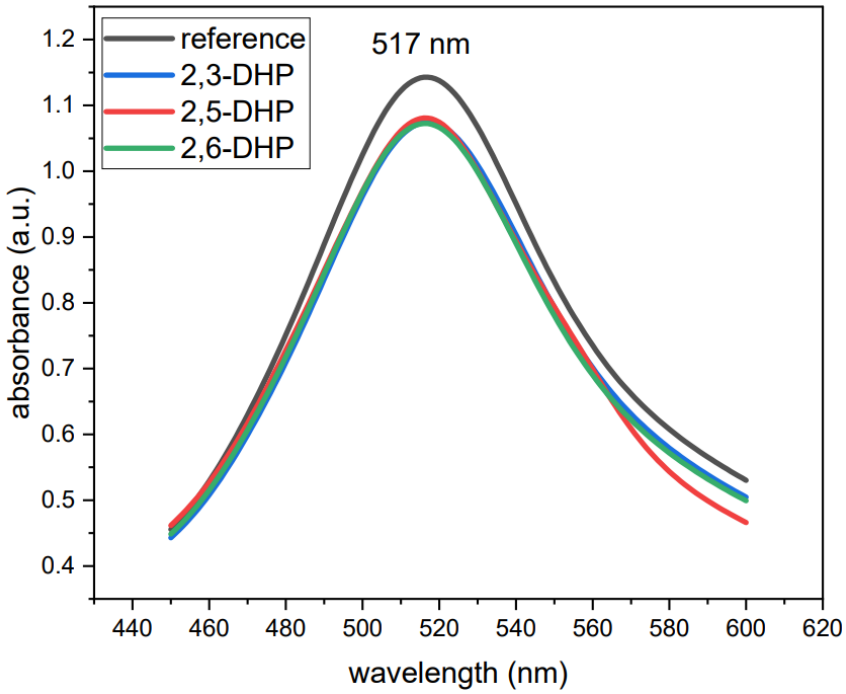

Figure 15. Antioxidant activity of the DHP films (as indicated in the insets) deposited on gold electrodes. All the deposition experiments consisted of 5 CV scans at a potential sweep rate of 10 mV/s.

3.4. Conclusions

Films made from 2,3-DHP, 2,5DHP and 2,6 DHP can be deposited on amorphous carbon and gold working electrodes using cyclic voltammetry at pH = 5.0. The films made from 2,3-DHP and 2,6-DHP are impermeable towards hexacyanoferrate anions provided they are deposited at low potential sweep rate (10 mV/s). However, those made from 2,5-DHP seem slightly permeable when deposited in these conditions. This finding may however be related to a better electrical conductivity inferred from electrochemical impedance

spectroscopy. When the deposition is performed at a higher potential sweep rate, 100 mV/s, but at the same pH, permeable films are obtained on carbon for the same isomers. At pH =10, the irreversible character of the obtained CV curves is more pronounced than at pH = 5.0 suggesting an efficient passivation of the electrodes. But more characterizations need to be performed in these conditions. Surprisingly, no film deposition is obtained from 2,4-DHP using CV at pH = 5.0. CA can also be used to deposit films from 2,3-DHP, 2,5-DHP and 2,6-DHP containing solutions at pH =5.0.

The crystallinity of 2,3-DHP, 2,5-DHP and 2,6-DHP based films was investigated using selected area electron diffraction (after deposition on a carbon electrode). Their wettability, their topography using AFM, their optical thickness using spectroscopic ellipsometry, and their antioxidant properties using DPPH scavenging were also investigated. Films made from 2,5-DHP seem the most promising for applications in electrocatalysis owing to the well-known role played by nitrogen atoms and the requirement for high electronic conductivity.

In upcoming studies, we will investigate the mechanism by which 2,5-DHP yields to partially crystalline films when the deposition by CV is performed at low potential sweep rates. In particular TEM investigations using an *in-situ* electrochemical cell will be used to investigate the structural change of the film as a function of the number of performed CV cycles. Raman spectroscopy will also be used to investigate analogy between the obtained films with N doped graphene.

3.5. Unpublished data and complementary results

The impedance of the films of DHP was discussed with the films prepared by CA on amorphous carbon electrodes. However, the data of the impedance spectroscopy of the DHP-based films prepared by CV are not presented in the article manuscript. The

corresponding Nyquist plot is represented in Figure 16. As well as observed in Figure 9, the curve obtained for the 2,5-DHP-based film suggests a much lower resistance to the electron transfer across the film deposited with 5 CV cycles at 10 mV/s compared to the films from 2,3- and 2,6-DHP.

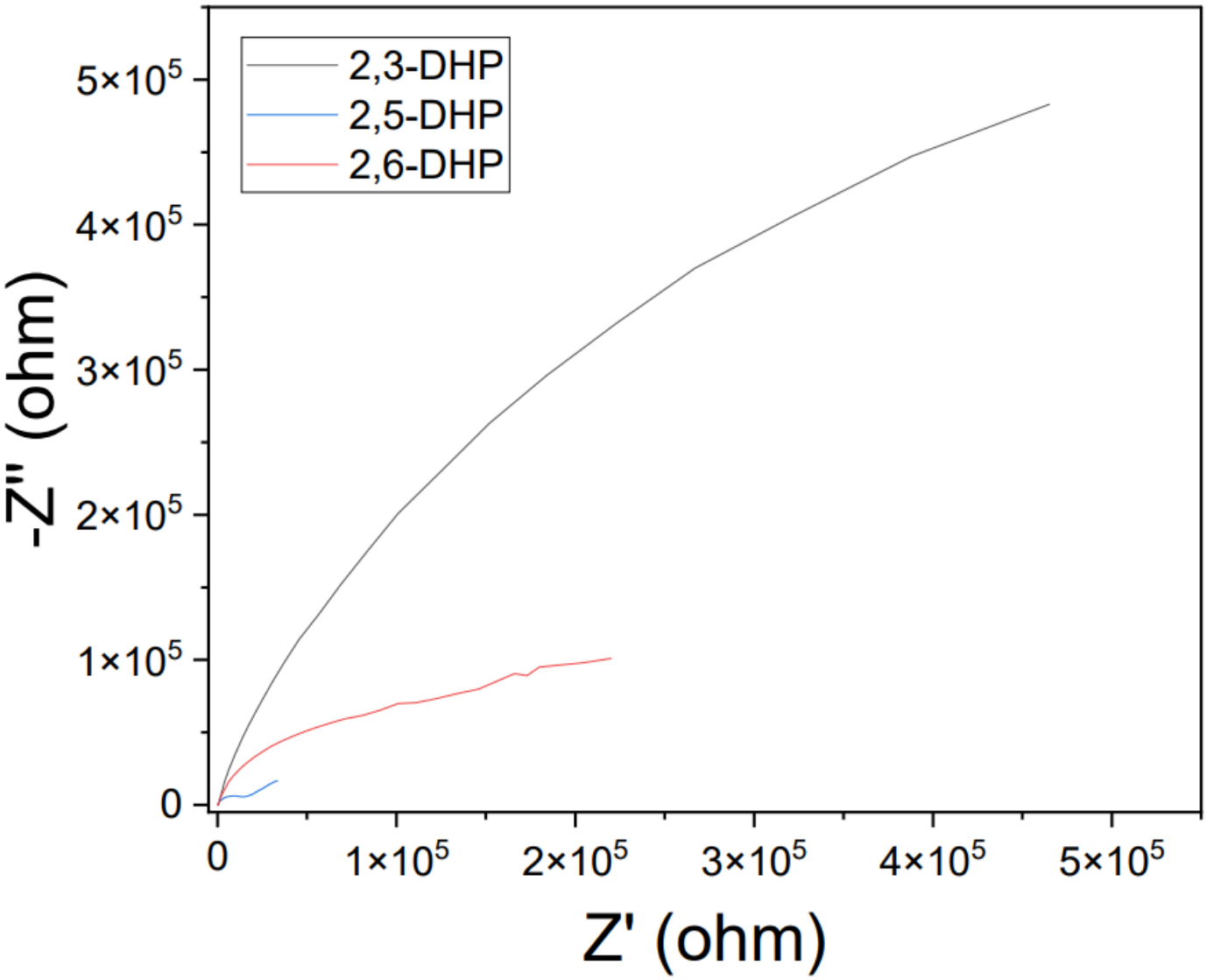

Figure 16. Electrochemical impedance spectra of the DHP-based films obtained on an amorphous carbon working electrode after 5 CV cycles at 10 mV/s.

The reason can be a thinner or conductive film for instance. The hypothesis of a conductive film was favored according to the following data obtained in ellipsometry with the films deposited on gold working electrodes.

It is also important to note that we were not able to fit these curves with typical electrical circuit models[1,59] including resistances and a capacitor, even with a Warburg component. The same difficulty was observed for the dihydroxynaphthalene films.

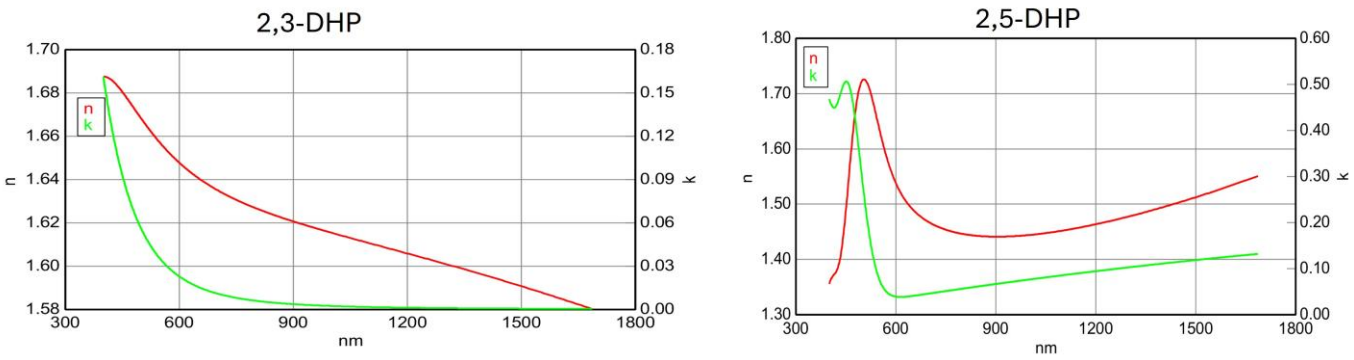

Figure 17. Optical dispersion curves obtained by ellipsometry: on left for 2,3-DHP-based films and on right for 2,5-DHP-based films. The red line is the evolution of the refractive index (n) with the wavelength and in green line the evolution of the absorption coefficient (k) with the wavelength.

Indeed, from the ellipsometric data in Figure 17, the evolution of the optical dispersion curves are different between the 2,3-DHP and 2,5-DHP-based films. In the case of the 2,5-DHP films, the evolution is similar to semi-conductors. That is why when combined with the impedance results, the 2,5-DHP-based films were expected to be conductive.

To confirm this statement, some 4-point probe measurements were performed. However, to avoid the contact between the probes (in case of the probes going through the very thin film) and the gold substrate, it was first necessary to use another substrate. To achieve this, the mechanical film transfer method (detailed in Chapter 2) used for the DHN-based films was used for the DHP films without any further modification. The DHP-based films from 2,3-, 2,5- and 2,6-DHP were transferred onto PDMS slices. However, after the polyvinyl alcohol (PVA) removal it was difficult to distinguish if films were still present in the case of the 2,3- and the 2,5-DHP because both films and substrates were transparent.

Even if a small edge of the film was observed, it was not clear if the whole film was present or if residual PVA stayed attached. In the case of 2,6-DHP, the film was brownish and its transfer was confirmed successfully (Figure 18).

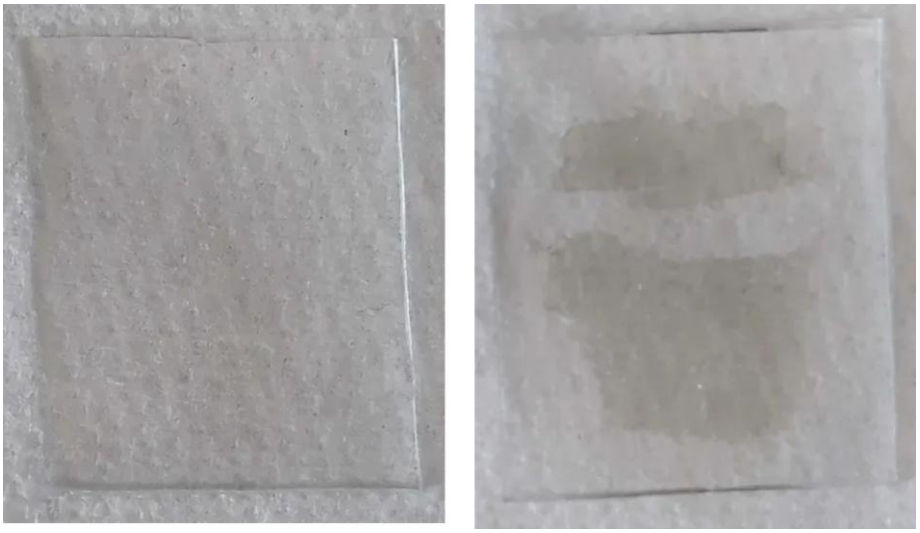

Figure 18. Pictures of the PDMS substrate with the transferred film from 2,3-DHP (left) and 2,6-DHP (right).

The 4-point probe measurements displayed no conductivity values for all the 3 films. That confirms the insulating behavior of the 2,6-DHP-based films. However, in the case of 2,3- and 2,5-DHP-based films it is impossible to make a sure statement. It can be due either to an absence of conductivity, an issue with the transfer process (if no film remains after the PVA dissolution in water and the film was gone too) or a low conductivity. In the latter case, according to the provider information on the machine and the surface size combined with the thickness of the films, the conductivity should be lower than 10 S/m.

To improve the information on the chemical composition of the DHP films, infrared spectroscopy was performed in ATR mode (Attenuated Total Reflectance). Unfortunately, only the background from the air atmosphere was measured. Indeed, the film is supported by a solid substrate that cannot mold perfectly the crystal surface. Thus, there was most likely a gap of air between the films and the crystal. If the pressing cap was tightened too

much, the substrate simply broke. An alternative would be to use the transfer method to detach the film from the substrate, but the PVA will hinder the signal of the DHP-based films.

To investigate the behavior of a co-deposition of 2 DHP precursors for future applications and perspectives, mixtures of 2,3-DHP and 2,6-DHP but also from 2,5-DHP and 2,6-DHP were prepared, and the concentration of the isomers was changed to study the evolution of the CV curves when one or the other isomer is predominant. A concentration of 100% means a concentration of 1mg/mL like previously in this chapter and 50%/50% means a concentration of both isomers at 1 mg/mL.

Figure 19 shows the curves obtained for different proportions of the mixture of 2,3-DHP and the 2,6-DHP. In a 1:1 ratio (50% of each isomer), the CV curves are similar than the curves obtained from the 2,6-DHP alone. Actually, that corresponds to the isomer that has the lower potential of oxidation (meaning also the lower energy required to get oxidized). Therefore, the 2,6-DHP is oxidized before the 2,3-DHP and dominates the reaction occurring when the potential is increased. A much higher content of 2,3-DHP is required in the initial ratio to see an evolution; here above 70% for instance. In the other cases with different mixtures of isomers, the same observation was visible.

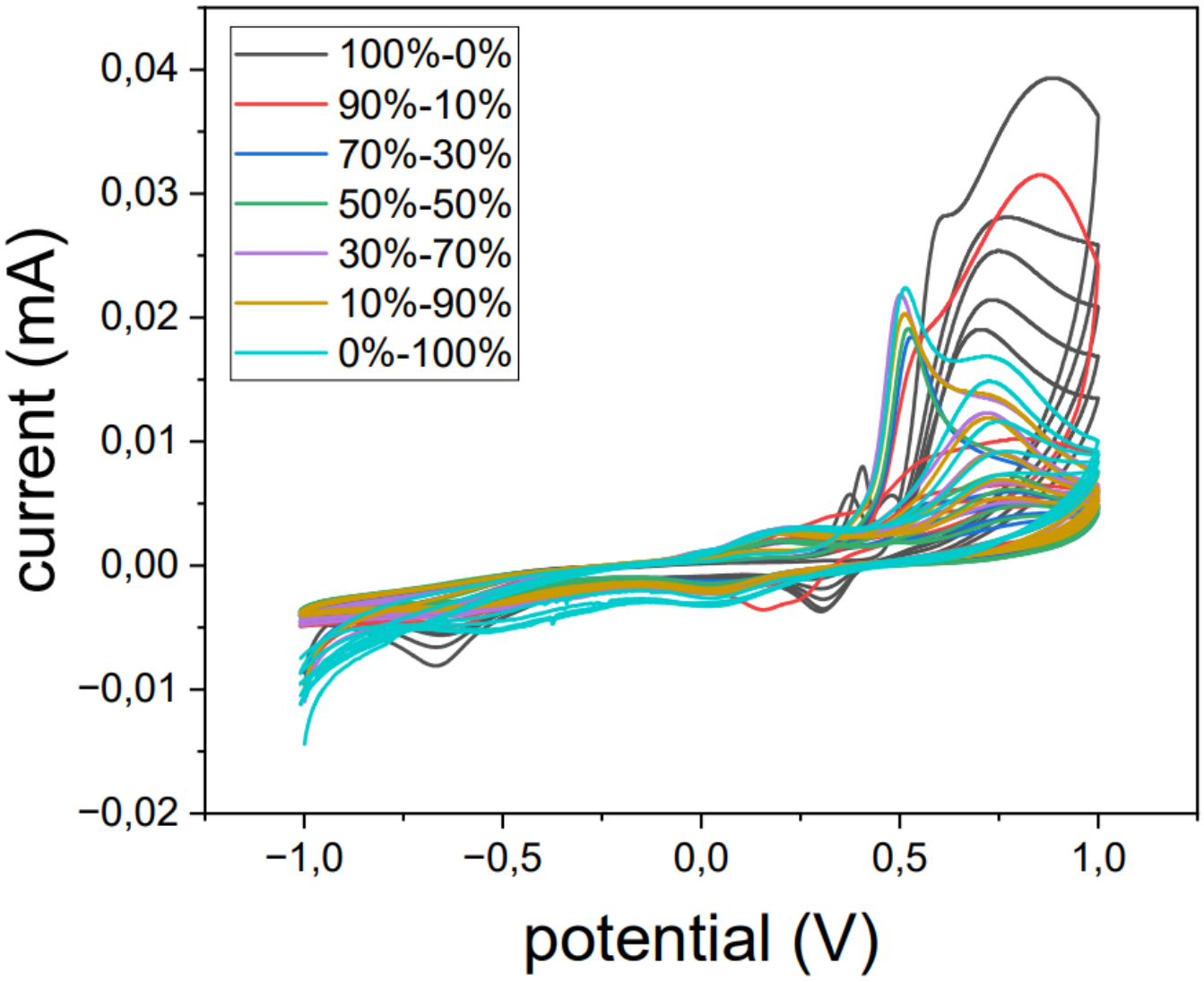

Figure 19. 5 successive CV cycles at 10 mV/s of mixtures of 2,3-DHP and 2,6-DHP. The ratio of the precursors are indicated in the inset: the percentage on left corresponds to the 2,3-DHP and on right to the 2,6-DHP. In teal lines it corresponds to 2,6-DHP alone in solution at 1 mg/mL and in black lines to 2,3-DHP alone in solution (100%) at 1 mg/mL. At 50%/50%, both isomers are at the concentration of 1 mg/mL.

Chapter 2: Electrodeposition of 1,8-dihydroxynaphthalene on gold

After the observation that ordered materials (graphene oxide-like materials) were obtained from molecules containing a single aromatic ring, a question arose: can we obtain even more ordered materials starting from precursors presenting already a higher order in the chemical structure? Then, molecules with two aromatic rings are of great interest. After few assays, the 1,8-dihydroxynaphthalene (a compound found in the nature, such as in fungi[32]) appeared as a promising candidate. Indeed, its structure includes 2 aromatic rings but also the CV curves obtained on glassy carbon (Chapter 3) were very surprising. The work on the 1,8-dihydroxynaphthalene started on glassy carbon working electrodes like with the dihydroxypyridines. Therefore, the same limitations due to the electrodes happened and the gold substrates were chosen as an alternative.

This chapter corresponds to the article manuscript submitted in *ACS Appl. Mater. Interfaces*. All the data presented in this chapter are related to electrochemical deposition on gold working electrodes only. Additional data obtained in this work but not chosen for publication are presented in section 4.5.

4.1. Introduction

Following the recommendations of the UN's 12th objective[26] that encourages more sustainable approaches, the reduction of environmental impact of material's production is paramount.

Therefore, the synthesis of functional materials from naturally occurring monomers based on low-carbon footprint processes such as electrochemical deposition from aqueous solution is emerging.

According to these approaches, biologically-based carbon materials are promising candidates for nanoscience and nanotechnology. Aromatic hydroxylated molecules are widely used for the preparation of nanomaterials and thin films opening a large range of potential applications in biomedicine,[24,53,61-68] energy storage,[63,66,69-71] environmental treatments,[24,71] catalysis,[24,66,69,70,72] sensing,[46,63-66,69,71,73] and optoelectronics[64-67,69,71,74].

Melanins are natural pigments that are well-known for their biocompatibility.[75] This group of insoluble phenolic polymers is found in many living organisms and displays strong optoelectronics, antioxidant, semiconductor-like, and metal chelating properties, among others.[34,64] Thus, these versatile materials have seen increased use in applications related to material science, biomedicine, or sensing, to name a few.[34,64] Although these compounds have received increased attention from the research community,[18] which mainly holds true for polydopamine materials, melanins still have a rich chemistry to explore.

In addition to the various strategies for the formation of polydopamine coatings,[61,63,76] literature provides strategies to deposit other melanin-like and hydroxylated materials to design functional films. Ball et al.[43,47] recently introduced pyrocatechol thin films on glassy carbon and investigated the electrochemical deposition of catechol, resorcinol, and hydroquinone, as well as the influence of the relative position of the two hydroxyl groups in the film formation.[46] Ngamchuea et al. investigated the deposition of resorcinol films[48] while Enache et al. studied phenol and different *para*-substituted phenols oxidations.[53]

Melanins can be classified into five different classes:[32,77] eumelanin, pheomelanin, neuromelanin, allomelanin, and pyomelanin. Among these classes, allomelanins represent the nitrogen-free class of melanins.[77] Among them, 1,8-dihydroxynaphthalene (1,8-DHN) found naturally in fungi[32,78] is a possible precursor of this class of melanins. Moreover, 1,8-

DHN is slightly soluble in water and therefore, its oxidative polymerization can be performed under green chemistry conditions.[79] The oxidation of 1,8-DHN and subsequent polymerizations was mainly studied in solution,[33,64,77,78,80] usually leading to investigations on precipitates or nanoparticles. For example, Manini et al. obtained 1,8-DHN thin films via oxidation in solution[34] and an ammonia-induced solid-state polymerization.[81] To the best of our knowledge, the development of functional 1,8-DHN coatings via an electrochemical reaction has not yet been described in the literature.

In this work, we present the electro-assisted synthesis and characterization of thick carbon-based functional films from 1,8-DHN that exhibit both radical scavenging and antimicrobial properties.

4.2. Experimental section

4.2.1. Chemicals and materials

1,8-dihydroxynaphthalene (96%), Potassium hexacyanoferrate(II) trihydrate (98.5%), 2,2-diphenyl-1-picrylhydrazyl, Hexaammineruthenium(III) chloride (98%), Copper(II) chloride, and Poly(vinyl alcohol) (80% hydrolyzed, 9500-10500 Da) were bought from Sigma Aldrich and used without further purification. Anhydrous sodium acetate (ACS, Reag. grade) was obtained from Merck Chemicals. Hydrochloric acid (37%) and Ethanol absolute anhydrous (ACS, Reag. grade) were bought from Carlo Erba Reagents. All these chemicals were used without further purification. Gold coated (1000 Å-thick) microscope slides were purchased from Sigma Aldrich. These slides were cut into 10 pieces of 1 cm x 1.25 cm prior to use. They were cleaned either with an argon plasma for 10 minutes at 6 mbar (model PDC-002 from Harrick Plasma) or an air plasma for 5 minutes (PDC-32G-2 from Harrick Plasma). The cut and plasma-cleaned gold-coated slides were used as substrates for electrodeposition. A dental piece of a Co-Cr alloy (a cut piece from a metal frame

denture, Vitallium alloy with composition $Co_{0.64}Cr_{0.28}Mo_{0.06}$ and traces of Si, Mn, and C, from Flecher, France) was also used as a substrate for electrodeposition.

4.2.2. Preparation of the solutions

The sodium acetate buffer solution was prepared with a concentration of 50 mM by dissolving anhydrous sodium acetate in water (Millipore, 18 Ω.cm) and adjusting the pH with hydrochloric acid (37%) until pH 5.0 was reached. Solutions of 1,8-DHN were prepared with a concentration of 1 g/L in a 50%/50% mixture of a sodium acetate buffer solution (50 mM, pH 5.0) and ethanol (70% vol.). Ethanol is added here to increase the solubility of the 1,8-DHN precursor, the resulting pH of the 1:1 mixture was 5.75. The 1,8-DHN solutions were sonicated for 10 minutes (Ultrasonic cleaner USC from VWR) at room temperature to break up agglomerates and improve the dissolution of the 1,8-DHN precursor.

4.2.3. Electrochemical synthesis

Syntheses were carried out using either a CH Instruments Electrochemical Analyzer potentiostat from CH Instruments or an Autolab PGSTAT 204 potentiostat from Metrohm. The electrochemical cell used for electropolymerization was a typical three-electrodes system. An Ag/AgCl electrode (CHI111 from CH Instruments) was served as the reference electrode; therefore, all reported potentials are given versus this Ag/AgCl reference electrode. A Pt electrode (CHI115 from CH Instruments) was used as the counter electrode. Plasma-cleaned gold-coated slides were employed as working electrodes. A solution of 1,8-DHN (1 g/L) was used in all synthesis conditions. The film depositions were carried out either by cyclic voltammetry (CV) or chronoamperometry (CA) in air atmosphere and room temperature without degassing of the solutions. In the case of a CV deposition, a cyclic sweeping process with 25 cycles from -1 V to +1 V at scan rates of 20

mV/s, 200 mV/s and 1000 mV/s was used. Additional samples were prepared in CV mode with 100 cycles to investigate the influence of higher cycle numbers on the film thickness. In the case of deposition by CA, the thin films were obtained using a constant applied potential of 0.33 V during 1000 s (equivalent to the duration of 25 CV cycles at 100 mV/s) and 5000 s (equivalent to the duration of 25 CV cycles at 20 mV/s). The applied potential was chosen just below the potential where the maximum oxidation peak is observed at 20 mV/s (0.35 V). A CV deposition has also been carried out on the Co-Cr alloy substrate with 25 CV cycles from -1 V to +1 V at 200 mV/s.

Complementarily, some films were produced by CV (25 cycles at a potential sweep rate of 20 mV/s) from 1,8-DHN solutions containing $CuCl_2$. In those experiments, aimed to show the possible incorporation of Cu in the DHN films, the Cu^{2+}/1,8-DHN ratio was maintained equal to 0.25.

4.2.4. Electrochemical characterizations of the 1,8-DHN-based films

The same potentiostat instruments and three-electrode configurations described above were used for electrochemical characterizations of the obtained coatings, namely the redox probe permeability and impedance measurements. The permeability of the thin films towards two redox probes was tested, namely potassium hexacyanoferrate(II) and hexaammineruthenium(III) chloride, prepared at a concentration of 1 mM by dissolving respectively potassium hexacyanoferrate(II) trihydrate and hexaammineruthenium(III) chloride in the sodium acetate buffer (50 mM, pH 5.0). The following electrochemical analysis steps were carried out to perform these assays: i) 1 CV cycle at 100 mV/s between -0.4 V and +0.7 V in the redox probe solution, rinsed with water, and followed by ii) 25 CV cycles at the chosen scan rate in the 1,8-DHN solution to deposit the thin films between -1 V and +1 V, rinsed with water, and followed by iii) 5 CV cycles at 100 mV/s

between -0.4 V and +0.7 V in the buffer solution to measure the current in the absence of a redox probe, and finally iv) 1 CV cycle at 100 mV/s between -0.4 V and +0.7 V in the redox probe solution again. Step iii) includes 5 CV cycles to stabilize the peak current since it decreases during the first few cycles. The comparison of the CV curves obtained in steps i), iii) and iv) gives an estimation of the degree of permeability of the thin films against the redox probe used. In the case of hexaaminеruthenium(III) the steps i), iii) and iv) were performed by starting the CV cycles with the reduction pathway between +0.7 V and -0.4 V.

Electrochemical impedance spectroscopy measurements were performed between 10^{-1} and 10^{5} Hz in the potassium hexacyanoferrate(III) solution (1mM) with an AC amplitude of 10 mV and a DC potential chosen to correspond to the oxidation peak potential of the hexacyanoferrate(II) in step i).

4.2.5. Film characterizations

4.2.5.1. Transmission electron microscopy (TEM)

The TEM pictures were obtained with a JEOL 2100 microscope operating at 200 kV with a LaB_6 filament as the electron source. The thin films were gently rubbed against the TEM grids to transfer fragments of the films. These grids are TEM copper grids covered with a lacey carbon membrane.

4.2.5.2. Contact angle measurements

The wettability of film surfaces and of the gold electrode surface was evaluated from the average of left and right contact angles of 60 images of water sessile drops (4 µL) deposited by an Attention Theta Flow goniometer from BIOLIN Scientific (Sweden).

4.2.5.3. Atomic force microscopy (AFM)

Atomic force microscopy measurements were performed using a Nikon Eclipse Ti-S microscope coupled with a Bioscope Catalyst instrument (Bruker, Mannheim, Germany) in the ScanAsyst mode. A ScanAsyst-fluid cantilever (Bruker, 150 kHz, 0.7 N/m) was used in the liquid mode and a ScanAsyst-air cantilever (Bruker, 70 kHz, 0.4 N/m) was used in the air mode. In liquid mode, the films freshly deposited on the gold electrodes were rinsed with water and directly measured in a small water bath. In the air mode, the films deposited on the gold electrodes were washed with water and dried before the measurements in the ambient atmosphere. To determine the thickness, scratches were made on the film surface with a diamond pen. AFM images were taken with scans of 5 µm x 5 µm. The roughness (RMS) was estimated using the freeware software Gwyddion 2.64 (GNU, Boston, MA, USA) dedicated to scanning probe microscopy analysis.

4.2.5.4. Ellipsometric measurements

Ellipsometric analyses were performed with a Woolam UV-NIR M2000 VASE ellipsometer, equipped with an environmental chamber in which the atmosphere is controlled by two mass flow controllers mixing known amounts of dry and water-saturated air. Data were collected from 200 nm to 1700 nm at 70 ° incidence. Refractive index characterizations were obtained by modeling Psi and Delta parameters with the Complete Ease 5.0 software. The substrate was made of 100 nm gold supported onto float glass slides. A single carbon-based layer was modeled using a Genosc model with one Cody-Lorentz and three Lorentz oscillators. The influence of relative humidity on film thickness and refractive index was obtained by modeling in the spectral range with the least light absorption (700 nm to 1700 nm).

4.2.5.5. Scanning electron microscopy (SEM)

SEM measurements were performed using a JEOL 6700F microscope operated at 10 kV and 10^{-6} mbar. After the film deposition, samples were dried under an air flow. The coated gold electrodes were simply scratched with a diamond pen (to determine the thickness), attached to the SEM support with a double-side adhesive tape, and no further metallization of the surface was required. A lower secondary electron (LEI) detector was used. The cross-section to determine the thickness was observed at an angle of 10 °.

4.2.5.6. *X-ray photoelectron spectrometry (XPS)*

XPS measurements were carried out on a Kratos Axis Ultra *DLD* imaging photoelectron spectrometer. Measurements were carried out using the instrument's hybrid mode with a monochromatic Al-Kα source operating at 10 mA emission current and 15 kV voltage bias in an ultra-high vacuum chamber with a base pressure of approximately $1x10^{-10}$ mbar. The source line width is approximately 1.0 eV FWHM, as calibrated with the Ag 3d5/2 line. The analysis area was 700 µm x 300 µm (i.e., X-ray spot size). The data was collected using a hemispherical analyzer at an angle of 0 ° to the surface normal. The takeoff angle was kept fixed along the surface normal in all experiments. Survey spectra were measured at a pass energy of 80 eV and elemental spectra at 20 eV pass energy.

4.2.5.7. Raman spectroscopy

Raman spectroscopy was performed with a Witec Confocal Raman spectroscopy System Alpha 300 R (WITec, Germany) instrument. The excitation wavelength of the Nd:YAG laser was 532 nm and the power used to characterize the films was 2.5 mW, while integration time was 20 s. The Zeiss (Carl Zeiss, Germany) objective lens of the microscope had a x100 magnification.

4.2.5.8. *UV-visible spectroscopy and antioxidant assays*

UV-visible spectroscopy measurements were performed with polystyrene cuvettes (ref. 67.742 from Sarstedt) and an UVmc² instrument from SAFAS (Monaco). UV-visible spectroscopy was used to detect the antioxidant activity of the thin films deposited on gold electrodes. 2,2-diphenyl-1-picrylhydrazyl (DPPH) is a well-known radical species used for such assays by its discoloration.[82] The DPPH solution was prepared with a concentration of 0.1 mM by dissolving 2,2-diphenyl-1-picrylhydrazyl in absolute ethanol. This solution was stored in a fridge and protected from light by wrapping the container with an aluminum foil. After the electrochemical synthesis, the thin films were shortly rinsed in absolute ethanol. Then the gold coated slides covered by the films were placed horizontally at the bottom of a falcon tube containing 2.0 mL of 10^{-4} M DPPH solution (As much DPPH solution as needed to cover the whole film but not more). Otherwise, the number of radicals reacting may be too low compared to the total amount of them in the given volume and no measurable change in the UV-visible spectrum would be detected.). The films were immersed for 20 minutes in the DPPH solution before measuring the solution spectrum with respect to an absolute ethanol reference solution. As a control measurement, another 2.0 mL DPPH solution was prepared and measured after a pristine gold electrode was immersed for 20 minutes.

4.2.5.9. Antibacterial assays

Inhibition of biomass formation: Pseudomonas aeruginosa PAO1[79] and *P. aeruginosa* PA14[80] were cultivated in 5 mL of lysogeny broth medium (Carl Roth GmbH + Co. KG, Karlsruhe, Germany) for 16 h at 37 °C while shaking at 150 rpm, respectively. Gold electrodes (1 cm²) with 1,8-DHN films prepared with 25 CV cycles at 200 mV/s (6 mm diameter) and without 1,8-DHN films (negative/untreated control) were disinfected using

70 % (*v/v*) ethanol before antimicrobial testing and placed in 24-well plates (Sarstedt AG & Co. KG, Nümbrecht, Germany). The films were subsequently inoculated with 1 mL of *P. aeruginosa* PAO1 or PA14 (OD_{600} = 0.0001) and incubated for 24 h at 37 °C without agitation to follow adherence on the surfaces. Afterwards, the planktonic phase was removed, and the wells were washed twice with 1 mL of demineralized water and the remaining biomass was stained with 200 µL of 0.1 % (*w/v*) crystal violet solution for 15 minutes.[85] After crystal violet removal, the slides were washed again twice with 1 mL demineralized water, and the stained biomass was dried for 24 h at 25 °C. Then the slides were transferred to a fresh well plate to only dissolve biomass formed on the surface and the dried biomass was dissolved with 200 µL of 30 % acetic acid and transferred to a new 96-well plate after 15 minutes. The absorbance at 560 nm was measured using a Tecan Infinite F200 microplate reader (Tecan Groupe Ltd, Männedorf, Switzerland). The resulting absorbance values were normalized, evaluated against the negative controls (gold-only electrodes), and data were plotted as the biomass per surface area (OD_{560} per 1 mm^2).

Viability reduction assay: To further analyze the antibacterial potential of the films, a life-dead staining assay was performed. Cells and films were prepared as described above and after incubation for 24h at 37°C the planktonic phase was removed, and the films were washed with 1 mL of demineralized water. 200 µL of fresh LB broth with 20 µL of 0.15 mg/mL resazurin solution was added and incubated for 2 h at 37°C. The viable cells reduce resazurin to the fluorescent resorufin by the production of NADPH and cell viability was then quantified by measuring the amount of produced resorufin by fluorescence measurements at an excitation wavelength of 535 nm and an emission of 595 nm using a Tecan Infinite F200 microplate reader (Tecan Group Ltd., Männedorf, Switzerland).

Lipid peroxidation assay: The potential of the 1,8-DHN-based films to oxidize bacterial cell membrane fatty acids was investigated using a lipid peroxidation assay as described previously.[86,87] In brief, bacterial cells and films were treated accordingly; however, 24 h incubation was performed under agitation at 100 rpm to allow all planktonic cells to have contact to the films. After incubation, 100 µL of the planktonic phases of P. aeruginosa PAO1 and PA14 were treated with trichloroacetic acid (200 µL; 10% w/v) for 2 h at room temperature followed by centrifugation at 11000 rpm for 35 min to collect the supernatant. Then the solution was centrifuged again for 20 min at 11000 rpm for complete removal of precipitated proteins and the supernatant was mixed with a thiobarbituric acid solution, incubated at 100 °C for 10 min, cooled to RT and the absorbance of the malondialdehyde-TBA adduct was recorded at 532 nm using a Spark® multimode microplate reader (Tecan Group Ltd., Männedorf, Switzerland).

Statistical significance analyses were performed using unpaired Student's *t*-test where *p* values < 0.05 were considered significant, ** denotes $p < 0.01$ and *** $p < 0.001$. Standard deviations were presented as error bars by experiments conducted in triplicate.

4.2.5.10. Film transfer method

The process is derived from the polydopamine film transfer method reported by Marchesi D'Alvise et al.[88] Briefly, the film was washed with water after the deposition on gold, then a layer of a 10% (w/v) solution of polyvinyl alcohol (PVA, 0.2 mL) was distributed over the film, the substrate was placed in an oven at 40 °C for 30 minutes, the PVA-DHN layer was stripped off and placed on a new substrate, the new substrate was placed in a water bath at 40 °C for 30 minutes to dissolve the PVA and the last step was to dry the film in an air atmosphere or with a nitrogen or air flow. The films prepared from 1,8-DHN were not able

to stay attached to non-treated glass slides. However, the transfer was successful on a polydimethylsiloxane slice (PDMS).

4.2.5.11. Strain Induced Elastomer Buckling Instability for Mechanical Measurements (SIEBIMM)

The film prepared with 25 CV cycles at 200 mV/s was transferred to a polydimethylsiloxane (PDMS) substrate. The PDMS substrate was synthesized by mixing the base and the curing agent (Sylgard) with a weight ratio of 10:1. The mixed solution was then placed in a vacuum chamber for degassing until no bubbles were formed anymore. Afterwards, the solution was poured into a Petri dish and was placed in the oven for 3 h at 70 °C for curing. PDMS samples of 6 cm x 2 cm x 0.1 cm were cut out from the Petri dish using a scalpel, pre-stretched (30 % stretch), and fixed on a custom-designed apparatus. The film was transferred, using the described method above, with the PVA layer on top and attached to the pre-stretched PDMS substrate and placed in a water bath (40 °C) for 1 h to remove the PVA. After drying the transferred film and cooling down to room temperature, the stress was slowly released. The formed wrinkles were measured by AFM (Dimension Icon FastScan, Bruker) using tapping mode and the Young modulus was calculated from those data and from the measured film thickness.[89] The Poisson's ratio was estimated similar to polydopamine films at 0.33.

4.3. Results and discussion

4.3.1. Film Deposition

The synthesis of 1,8-DHN films was conducted via electropolymerization using cyclic voltammetry with gold-coated glass slides as substrates.

First, we studied the electrodeposition behavior of 1,8-DHN under different sweeping rates as shown in Figure 20. Figure 20a is a global scheme of the study on the 1,8-DHN films. The CV curves of 1,8-DHN on gold electrodes at 1 mg/mL in a mixture of the sodium acetate buffer and ethanol (1:1 v/v pH = 5.75) using scan rates of 20 mV/s, 200 mV/s, and 1000 mV/s for 25 cycles are displayed in Figures 20b, 20c, and 20d, respectively. In all cases, an oxidation peak and a reduction peak were observed, but the oxidation current progressively decreased upon successive potential sweep cycles. This is a sign of electrode fouling and hence of film formation.[46,47,73,90] The access of dissolved unoxidized 1,8-DHN to the electrode surface was blocked thus progressively inhibiting the oxidation of more precursor molecules. This observation was previously reported for aromatic organic compounds such as phenols, catechols, and their derivatives. As expected, and consistent with findings by others, the oxidation peak was shifted to more anodic potentials when the scan rate is increased (Figure 20e) as the usual behavior of irreversible electrochemical processes.[91] The maxima of the first peak are obtained for +0.33 V, +0.52 V, and +0.92 V, respectively for 20 mV/s, 200 mV/s, and 1000 mV/s. At 20 mV/s and 200 mV/s, the current measured at the oxidation peak increases between the 1st the 2nd cycle and decreases between the 2nd and the 3rd cycle but stagnated thereafter up to the 25th cycle. In all three cases, the reduction peak is obtained at around -0.2 V, and the current increased for consecutive cycles. A 2nd oxidation peak is observed at 20 mV/s starting on the 2nd cycle at about +0.18 V. These differences could be explained by the time allowed for the reaction between each oxidation and reduction steps depending on the scan rate used. Indeed, at a high scan rate (1000 mV/s) the time allowed for non-electrochemical reactions at the electrode surface is very short between successive CV cycles. However, with a slow scan rate (20 mV/s) the reaction time is more pronounced, and the deposited molecules may undergo some slow non-electrochemical reactions.[92,93]

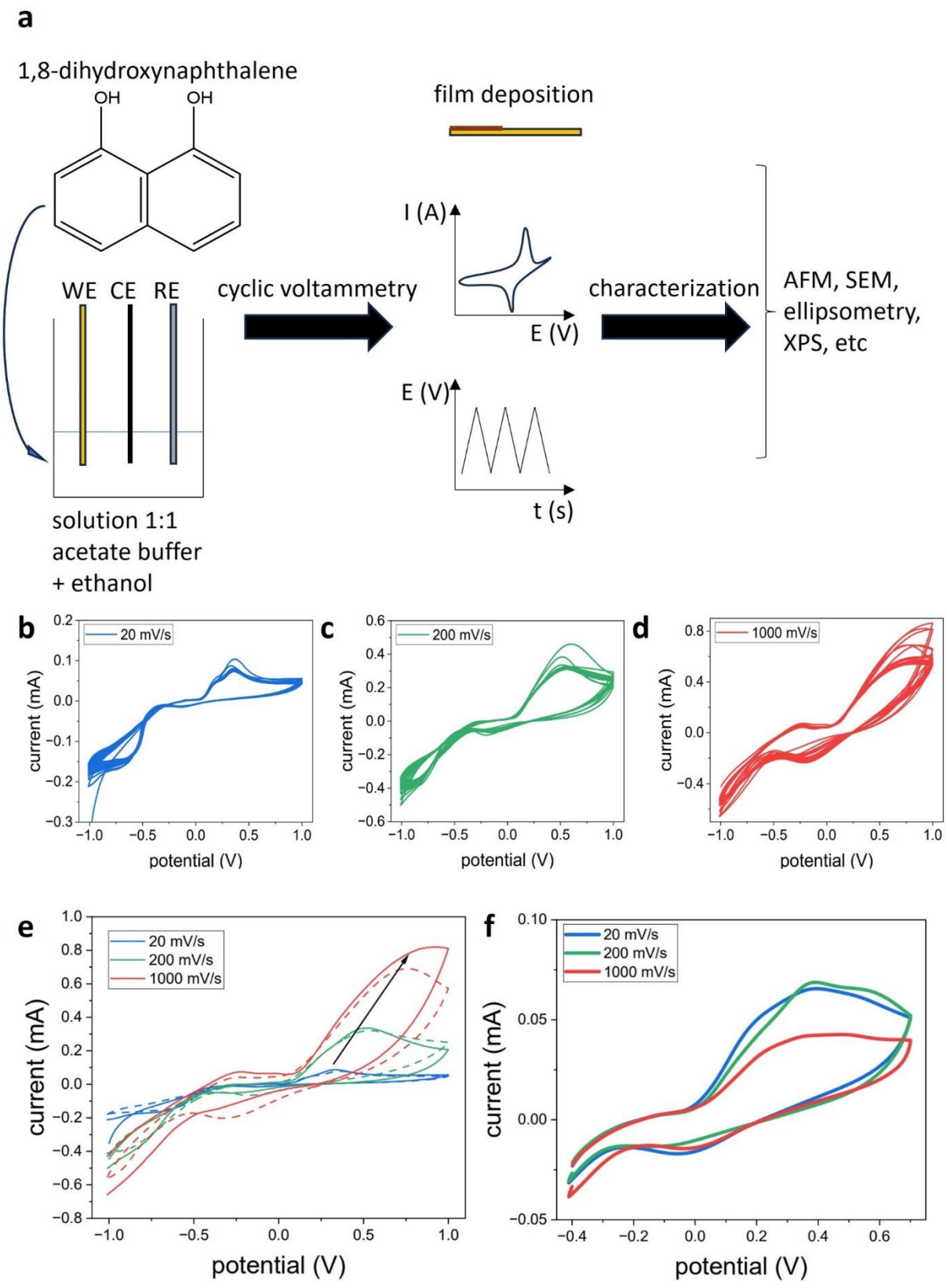

Figure 20. (a) General scheme of the electropolymerization of 1,8-DHN: from the precursor solution to film deposition and characterization. WE represents the working electrode, CE is the counter electrode and RE represents the reference electrode. 25 CV curves have been performed at a potential sweep rate of (b) 20 mV/s (c) 200 mV/s and (d)

1000 mV/s in the presence of 1,8-DHN at 1 mg/mL in sodium acetate buffer and ethanol mixture (1:1 v/v). The substrate is a gold working electrode. (e) 1st (full line) and 5th (dashed line) CV cycles in the presence of 1,8-DHN at 1 mg/mL with a scan rate of 20 mV/s (blue), 200 mV/s (green), and 1000 mV/s (red). The black arrow indicates the evolution of E_p, the potential at the oxidation peak, with the scan rate. (f) 1 CV cycle at 20 mV/s (blue), 200 mV/s (green), and 1000 mV/s (red) in the buffer-ethanol mixture without any redox species after the film deposition.

4.3.2. Film characterizations

The plot of the maximum current's logarithm at the oxidation peak of the first cycle as a function of the scan rate's logarithm is given in Figure 21a. Additional single CV scans at scan rates of 10 and 50 mV/s were used to get a more accurate value of the electron transfer process. The slope of that plot indicates if the oxidation is controlled by adsorption or diffusion: values of 1.0 indicate adsorption as the rate limiting step, while a value of 0.5 is found for diffusion of the redox probe to the electrode surface as the rate limiting step.[93] Here, a value of 0.47 was found (Figure 21a), most probably corresponding to a diffusion-controlled reaction. The plot of the potential where the maximum current is measured at the oxidation peak of the first cycle as a function of the scan rate's logarithm is given in Figure 21b. The dependence of the peak potential versus the scan rate's logarithm indicates an irreversible process because the peak potential increases with an increase of the scan rate. The slope includes the overall electron transfer coefficient according to the following equation valid for irreversible diffusion-controlled reactions:[91,92]

$$E_p = \left(\frac{RT}{2\beta n_\beta F}\right) \ln \nu + const \quad [1]$$

where E_p is the potential at the oxidation peak, R the universal gas constant, F the Faraday constant, T the absolute temperature, βn_β the overall electron transfer coefficient

and *v* the scan rate. The overall electron transfer coefficient obtained from equation 1 was 0.038 for the 1st oxidation peak. This coefficient is lower than the coefficients reported by Nady et al.[91] for phenol, resorcinol and pyrogallol (between 0.146 and 0.431), suggesting a slower electron transfer than in these three systems. However, they used different conditions such as a Pt working electrode at pH=3.0.[91]

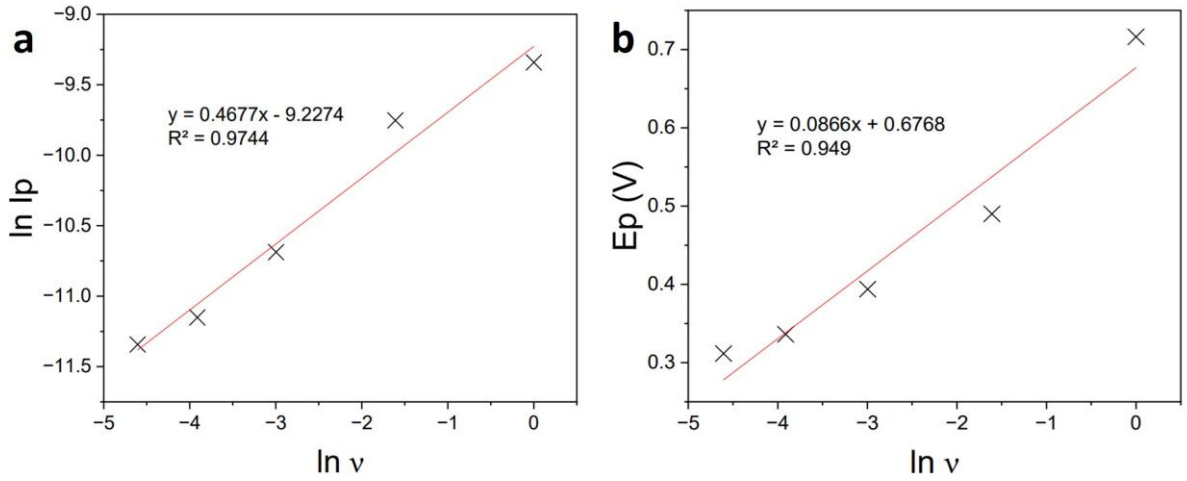

Figure 21. Dependences of (a) ln I_p versus ln v and (b) E_p versus ln v. With I_p the oxidation (anodic) peak current, E_p the oxidation peak potential and v the potential scan rate.

Figure 20f displays 1 CV cycle of the films measured at 100 mV/s in the buffer solution. This current is obtained in the absence of any redox species in solution. The appearance of a broad oxidation peak at around +0.4 V suggests the presence of an electroactive film at the electrode's surface. This means that the films formed at the electrode's surface have electrons available that can be further oxidized. Figure 22 shows the evolution of this oxidation current displayed by the deposited material with the number of CV cycles performed. For all three samples, a strong change in the current is visible between the first and second CV cycle, where decreases in the oxidation peak (ca. +0.4 V) and in the reduction peak (ca. -0.1 V) occur. The peak intensities further decrease with consecutive CV cycles, but the changes between successive CV scans become gradually less

pronounced. This behavior indicates that the further oxidation of the films is irreversible but slow.[94]

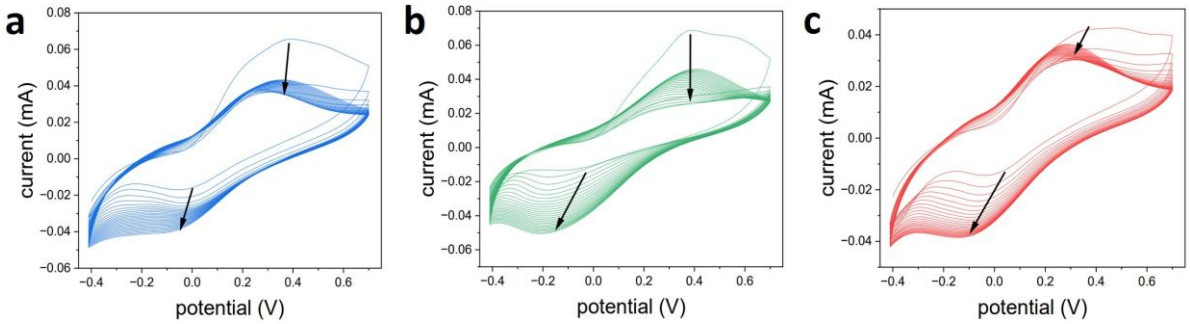

Figure 22. 25 CV cycles at 100 mV/s in presence of the buffer-ethanol mixture without any redox species in solution. The CV cycles were performed after the film deposition at (a) 20 mV/s, (b) 200 mV/s and (c) 1000 mV/s. The black arrow indicates the evolution of the current intensity upon an increase in the number of CV cycles.

Electrochemical impedance spectroscopy was also carried out on the different films as well as on a pristine gold electrode as a control (Figure 23) to determine the main electrical properties of the deposited films through the modeling of the spectra.[92] The difference between the spectrum of pure gold and the spectra of the films indicates a material deposition. The imaginary part of the impedance (Z") is changed and the shape of the curves has a minor visible difference while increasing the scan rate. The fits of the films' impedance with standard equivalent circuits like the Randles circuit were not possible. However, the measured curves suggest an insulating material behavior for the films obtained at the three potential sweep rates. Indeed, the gold impedance shows a short semi-circle and low imaginary and real parts, both typical for a conductive material, but in case of the 1,8-DNH based films, the semi-circle has a high radius. This suggests that the 1,8-DHN based films are insulating.[92]

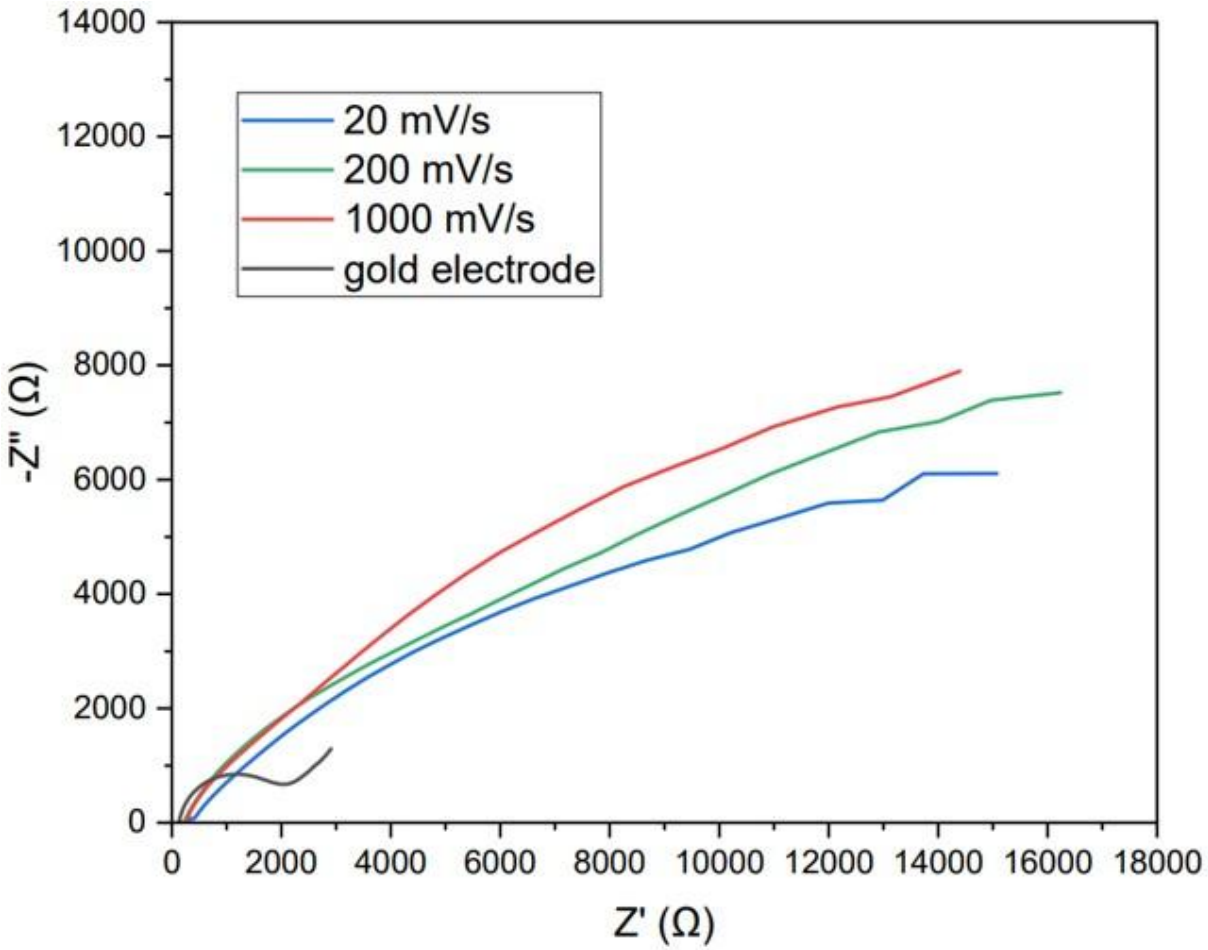

Figure 23. Electrochemical impedance spectroscopy (Nyquist plots) of the films deposited at 20 mV/s (blue), 200 mV/s (green) and 1000 mV/s (red) and a pristine gold electrode (black). *Z*'' is the imaginary part of the impedance and *Z*' the real part.

The permeability of the films towards redox probes was also investigated (Figure 24). To measure the permeance of the redox probe through the film, three CV curves are required: (i) before the film deposition and in the presence of the redox probe, (ii) after the film deposition in the absence of the redox probe, and (iii) after the film deposition in presence of the redox probe. The comparison and evolution of these CV curves allow assessing the permeability of the film for the used redox probe. To detect any charge effect of the film, both a positively charged and a negatively charged redox probe were used: hexaammineruthenium (III) chloride and potassium hexacyanoferrate (II), respectively. They also have a similar ionic radius of 5-10 Å,[95,96] thus avoiding a size effect in the comparison.

If the film is completely permeable to the redox probe, the CV curves in the presence of the redox probe before and after the film deposition would be identical. One could also consider the situation where the film accumulates the redox probe: in this case the oxidation and reduction current of the redox probe are increased in the presence of the film with respect to the pristine electrode. In contrast, if the film is completely impermeable, the CV curves after the film deposition in the absence and in the presence of the redox probe would overlap. Figure 24 shows that all the three films are semi-permeable to both redox probes. Indeed, the CV curves are very different after the film deposition, but the peak currents are higher in the presence of the redox probes.

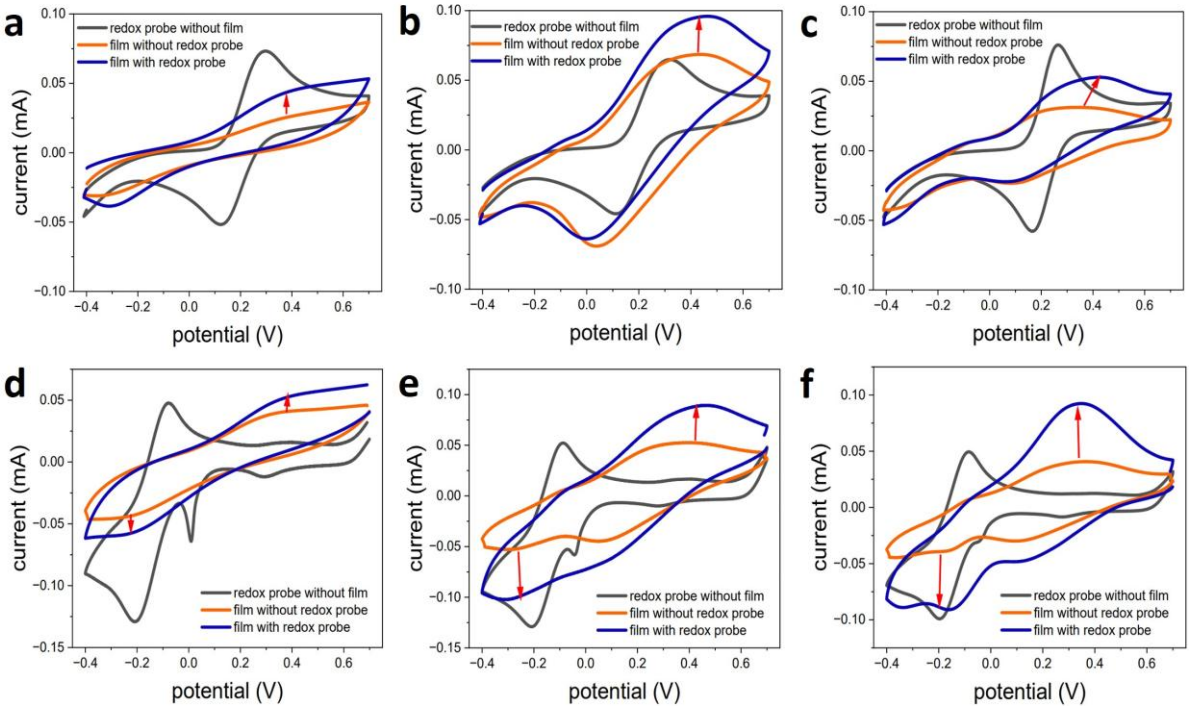

Figure 24. CV curves at 100 mV/s in presence of potassium hexacyanoferrate before the film deposition (black line), after the deposition in the buffer solution only without the redox probe (orange line) and in presence of potassium hexacyanoferrate after the deposition (blue line) with the film deposition performed at (a) 20 mV/s, (b) 200 mV/s and (c) 1000 mV/s with 25 CV cycles. CV curves obtained by replacing potassium hexacyanoferrate by hexaammineruthenium for a film deposition with 25 CV cycles at (d) 20 mV/s, (e) 200 mV/s

and (f) 1000 mV/s. Red arrows indicate the shift of the curves between the absence and the presence of the redox probe after the film deposition.

Deposition by chronoamperometry (CA) has also been performed from 1,8-DHN solutions on gold working electrodes (Figure 25) at a constant applied potential of 0.33 V for 1000 s (equivalent in time with 25 CV cycles at 100 mV/s but without dynamics induced by the potential scanning) to compare with the CV method. The oxidation current falls to a steady state value of about 10^{-5} A in about 100 s with almost no decrease even after 1000 s of potential application (Figure 25a). The Nyquist plot (Figure 25b) suggests that the obtained coating is insulating, similar to the coating obtained after CV deposition. In addition, the obtained film was almost impermeable to potassium hexacyanoferrate (II) ions (Figure 25c).

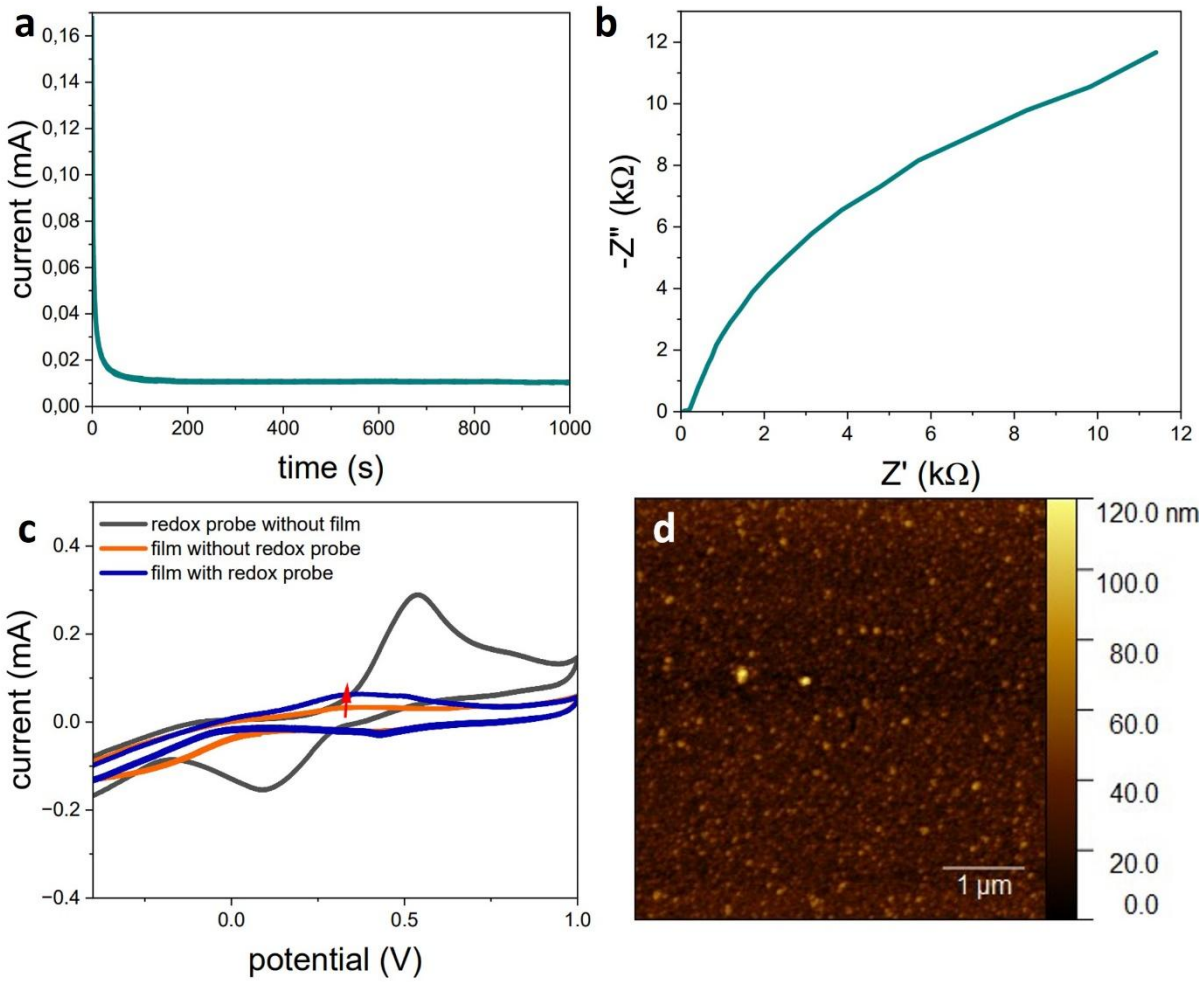

Figure 25. (a) Chronoamperometry at a constant applied potential of 0.33 V for 1000 s. (b) Electrochemical impedance spectroscopy (Nyquist plot) of the film deposited by CA. (c) CV curves at 100 mV/s between -0.4 V and +1 V in presence of potassium hexacyanoferrate before the film deposition (black), after the film deposition in the buffer only in absence of the redox probe (orange) and in presence of potassium hexacyanoferrate after the film deposition (blue), with the film deposited by CA. (d) AFM surface topography of the film deposited by CA.

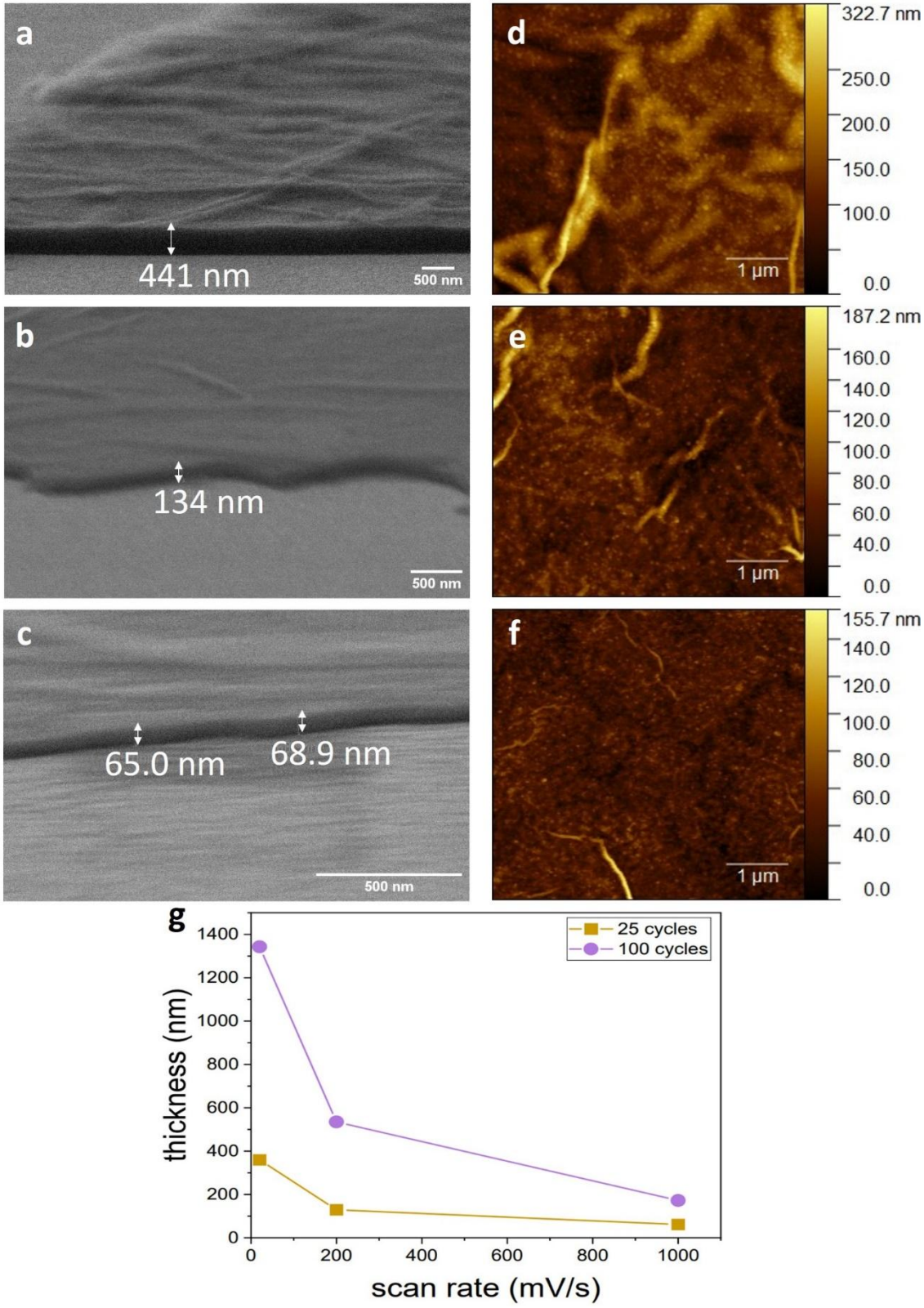

Figure 26. SEM images of the films deposited after 25 CV cycles at (a) 20 mV/s, (b) 200 mV/s and (c) 1000 mV/s. AFM surface topographies of the film obtained after 25 CV cycles at (d) 20 mV/s, (e) 200 mV/s and (f) 1000 mV/s. (g) Ellipsometric thickness of the 1,8-DHN based films as a function of the potential sweep rate after 25 CV cycles (dark yellow) and 100 CV cycles (purple). Straight lines in this figure are only aimed to guide the eye.

After studying the electrochemical deposition in detail, we next investigated the topography of the deposited films using microscopy and ellipsometry techniques (Figure 26). Figures 26a, 26b, and 26c show the SEM image for the films prepared at 20 mV/s, 200 mV/s, and 1000 mV/s, respectively, after 25 CV cycles. The AFM images of the same films are displayed in Figures 26d, 26e, and 26f. The ellipsometric thicknesses obtained for the three thin films after 25 and 100 CV cycles are plotted in Figure 26g. The thickness of the 1,8-DHN based films increases when the scan rate is decreased after either 25 or 100 deposition cycles (Figure 26g) in probable relation to increased deposition time at low potential sweep rates. The surface roughness of the film changes in the same way. From SEM measurements, the determined thicknesses were 418 ± 13 nm, 152 ± 15 nm, and 63 ± 5 nm for the films obtained at 20 mV/s, 200 mV/s, and 1000 mV/s, respectively. However, these values might be slightly overestimated due to the observation tilt angle of 10 °. According to ellipsometry analysis, the film thickness was determined as 360 nm, 130 nm, and 60 nm for a deposition performed at 20 mV/s, 200 mV/s, and 1000 mV/s, respectively, after 25 CV cycles and 1340 nm, 535 nm, and 170 nm, respectively, after 100 CV cycles. The thickness is increased by a factor of 3-4 when the number of cycles is increased by a factor of 4. The thicknesses measured by AFM were in excellent agreement with the ellipsometry results and provided values of 350 ± 30 nm, 132 ± 6 nm, and 65 ± 8 nm respectively for 20, 200, and 1000 mV/s after 25 CV cycles. All of the obtained thickness values are reported below in Table 3. As shown by the ellipsometric thicknesses, the amount of material deposited increases with the number of cycles even after 100 cycles. It seems possible to get even thicker films by increasing the number of CV cycles, but we make the assumption that the rate of film growth quantified by its thickness increase per CV cycle might decrease. Indeed, we observe that the higher the number of performed CV cycles, the lower is the increase in oxidation-reduction currents.

Anyway, such high film thicknesses are surprising when compared to the film thickness obtained during the electropolymerization of catechol or resorcinol monomers, which do not exceed a few tens of nanometers.[46] Such high thicknesses reached after CV deposition are very surprising for a material showing an insulating behavior as suggested from the EIS data (Figure 23). However, the observation of thick film formation could be explained by a swelling effect. Indeed, the films could swell, which allows the monomer to access the electrode surface, thus leading to a continuous deposition. The swelling of the films in water was determined from ellipsometric measurements performed at different relative pressures introduced in the measurement cell as shown in Figure 27. The swelling ratio increases as the relative pressure of water increases and as well as the scan rate increases. The swelling is only partially reversible for the films obtained at 20 and 200 mV/s (Figure 27). The swelling reversibility could however not be investigated for the films deposited at 1000 mV/s because of strong water condensation on those films when 100 % relative humidity is reached. If we consider the deposited films as polymer networks, the lower swelling after 25 CV cycles at 20 mV/s (Figure 27) is a sign of a higher degree of reticulation when compared to the films obtained at 200 and 1000 mV/s.

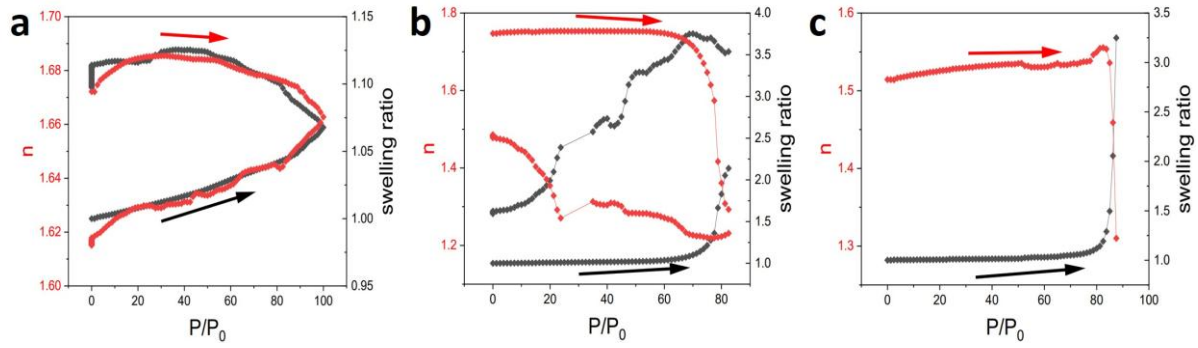

Figure 27. Evolution of the refractive index (red; measured at a wavelength of 1200 nm) and the swelling ratio (black) with H_2O sorption isotherms of the films deposited after 25 CV cycles at (a) 20 mV/s, (b) 200 mV/s and (c) 1000 mV/s. Desorption is missing for the film prepared at 1000 mV/s due to water condensation at the film surface. Arrows indicate the direction of the evolutions.

The RMS roughness was also measured with AFM and values of 45 nm, 20 nm, and 12 nm were obtained respectively for 25 CV cycles at 20, 200, and 1000 mV/s. The AFM images (Figures 26d, 26e, and 26f) also displayed some wrinkles on the film surface. They do not originate from mechanical stresses due to the solvent evaporation step because similar features appear when the imaging is performed in the liquid state (Figure S1). The most likely explanation is that such features are intrinsic to the CV deposition, reflecting the presence of nuclei from which the film grows in the average plane of the polycrystalline gold electrode as well as in thickness. The topography of the sample deposited by CA (Figure 25d) observed in AFM is grainy and, thus very different from that of the CV method. The corresponding roughness (RMS) that was obtained was 10 nm. The thicknesses of two films prepared by CA with 1000s and 5000s of synthesis time (equivalent time of 25 CV cycles at 100 mV/s and 20 mV/s, respectively) were measured. The thicknesses as-obtained were 61 nm and 187 nm, respectively. Therefore, the thickness of the films obtained by CA is lower than those prepared by CV.

Due to the permeability of the films to redox probes, we wanted to investigate the porosity of the films and their structures. Figure 28 displays some representative TEM images. The film appeared similar at 20 mV/s and 200 mV/s: a homogeneous and very probably, amorphous surface was observed. However, at a scan rate of 1000 mV/s the film showed a pattern of little structures with an average diameter of a few nanometers. These features could be agglomerates formed in the reaction because there was not enough time for the molecules to reorganize at such a high potential sweep rate. In the literature, such kinds of patterns are called “basic structural units” in carbon-based materials.[97] Interestingly, the film nevertheless remains amorphous. The greyscale analysis (Figure S2) suggests that the film prepared with 25 CV cycles at 20 mV/s is smoother than the films prepared at 200 mV/s and 1000 mV/s. In addition, the films seem to have more granular structures as the scan rate increases. In all cases, several layers were distinguishable at the edges of the films. No apparent pores were observed anywhere on the film surfaces. This observation is surprising given the permeable behavior of the films towards the hexacyanoferrate(II) and hexaammineruthenium(III) redox probes (Figure 24). However, since the ionic radii of these ions are close to 1 nm,[95,96] micropores with such a small diameter may not be visible due to the observation conditions used in the experiments and the thickness of the analyzed fragments.

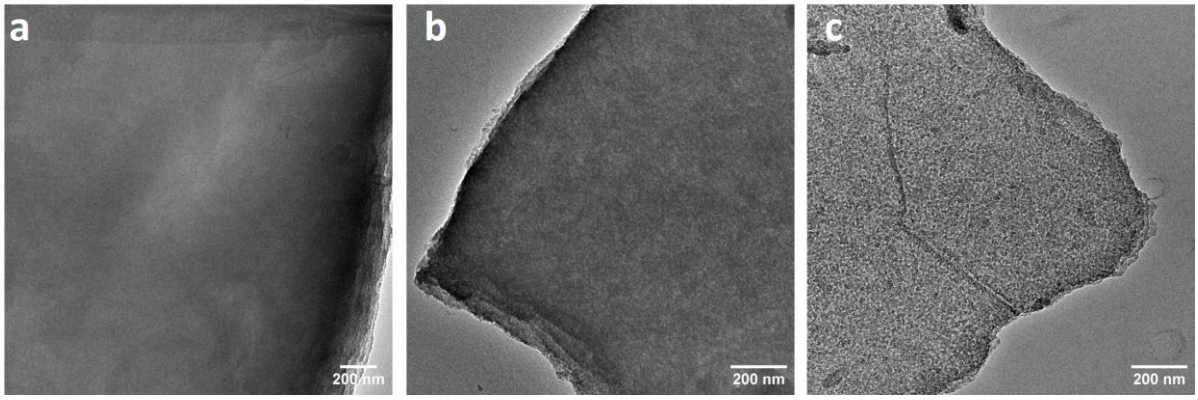

Figure 28. TEM images of the films removed from the gold electrodes after 25 CV cycles performed at (a) 20 mV/s, (b) 200 mV/s, and (c) 1000 mV/s. Scale bars represent 200 nm.

Other properties of the films were characterized in more detail, such as the refractive index and the water contact angle evolution with the potential sweep rate. The refractive indexes of the different films were calculated from the ellipsometric angles obtained at a wavelength of 800 nm (Figure 29). The average refractive index was measured to be 1.74. This value is in good agreement with values obtained for other oxygen-containing carbon-based materials. For example, Schöche et al. reported similar indexes for graphene oxide (around 1.75 at 800 nm).[98] Figure 27 showed that the swelling ratio increases as the relative humidity increases and the refractive index evolves consistently in the opposite direction, i.e. it decreases as the relative pressure of water increases. The decrease in refractive index with an increase in water pressure is more pronounced when only 25 CV cycles are performed (Figure 29) compared with 100 CV cycles suggesting that longer deposition and probably higher crosslinking induces a smaller sensitivity to water induced swelling.

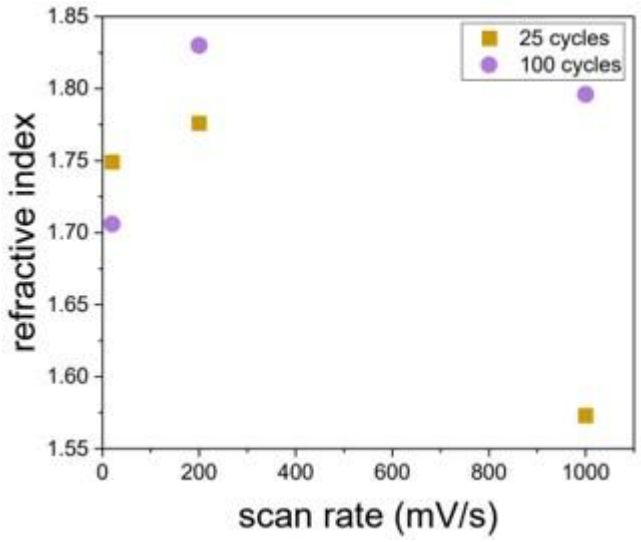

Figure 29. Ellipsometric refractive index evolution with the applied scan rate for films prepared after 25 CV cycles (dark yellow) and 100 CV cycles (purple). The wavelength used for the refractive index determination was 800 nm.

Contact angle measurements were done with a sessile water drop at 25 °C (Figure 30) on the three films (after 25 CV cycles) and a pristine gold electrode as reference material. The gold electrode had a hydrophobic surface with a contact angle of 88 ± 4 °. However, a hydrophilic behavior was observed after the deposition of the three films with angles of 24 ± 1 °, 23 ± 1 °, and 21 ± 1 ° for films deposited at scan rates of 20 mV/s, 200 mV/s, and 1000 mV/s, respectively. Even though some structural or compositional differences may exist between the films, they do not appear to significantly affect the contact angle values.

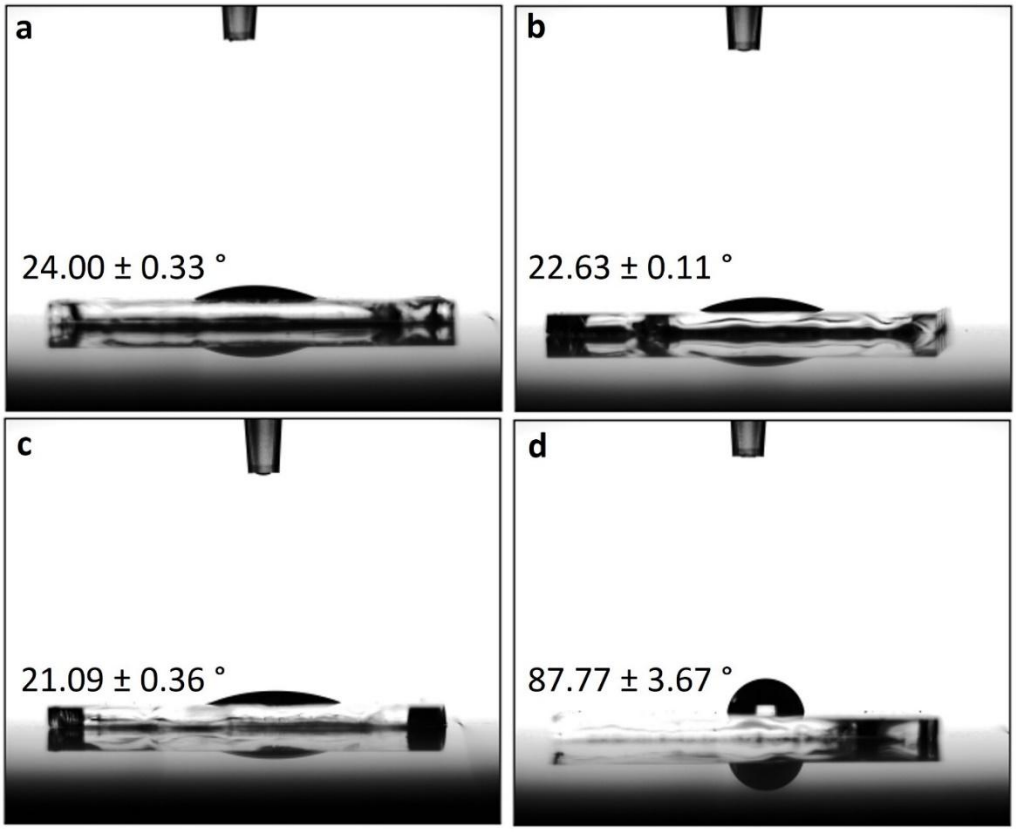

Figure 30. Pictures of water droplets (4µL) at 25 °C on the films deposited after 25 CV cycles at (a) 20 mV/s, (b) 200 mV/s and (c) 1000 mV/s and (d) on a pristine gold electrode.

Next, we analyzed the stability of the films against common solvents. A film produced at a scan rate of 200 mV/s was immersed in water, ethanol, acetone, isopropanol, dimethylsulfoxide, dichloromethane and hexane (Figure S3). No dissolution or apparent degradation of the films was found even after 7 days of immersion. This emphasizes the stability and high internal cohesion of the 1,8-DHN-based films, which is a major advantage for future applications, but it makes a detailed characterization of the inner chemical structure rather challenging.

The high stability and cohesion of the films obtained by CV on gold from 1,8-DHN solutions would in principle allow transferring them from the gold electrode to flexible substrates using a previously established mechanical stripping process.[88] Figure 31 depicts a representative film that was deposited on the gold working electrode and transferred to a PDMS substrate. The experiment was repeated three times and, in all cases, intact films were obtained.

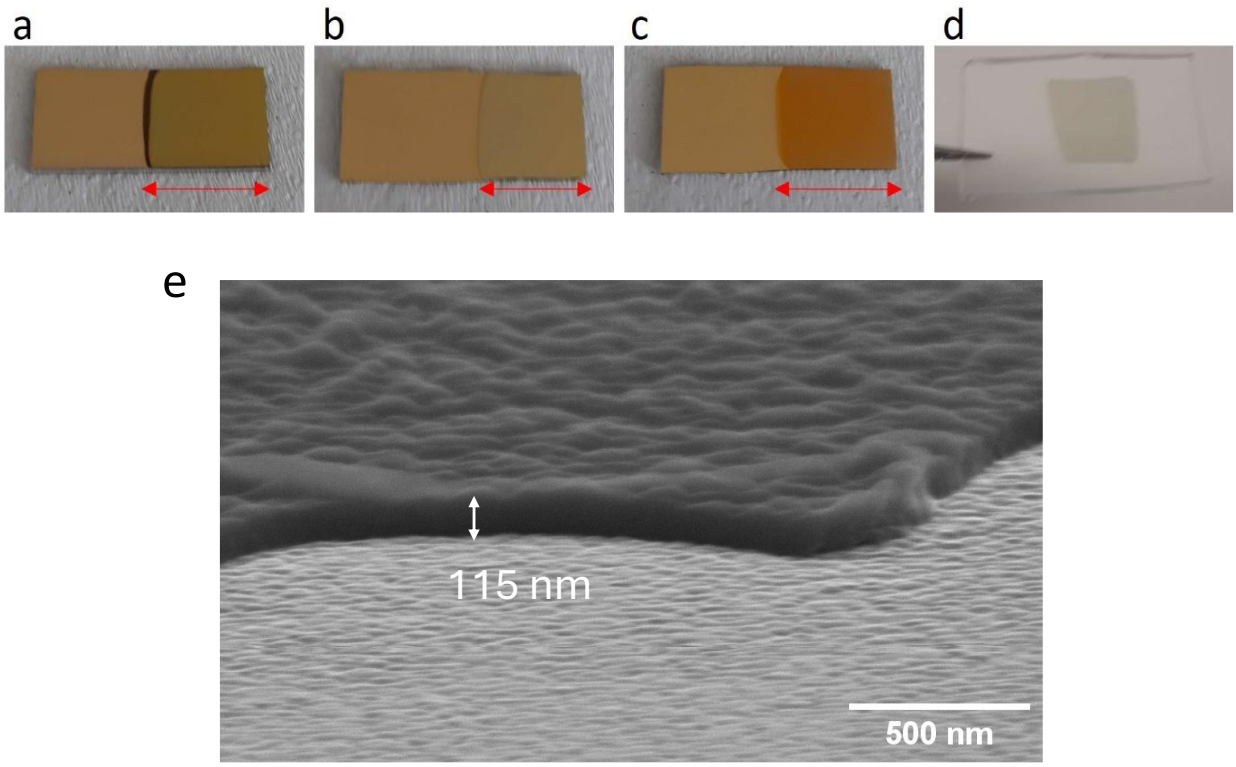

Figure 31. Pictures of the deposited films on gold working electrodes after 25 CV cycles at 20 mV/s (a), 200 mV/s (b) and 1000 mV/s (c) and the picture of a film prepared at 200 mV/s and transferred on a piece of PDMS (d). Double-head red arrows indicate the part transferred (1.2 cm x 1.0 cm). (e) SEM micrograph of the transferred film.

The free-standing membranes detached after 25 CV cycles (200 mV/s) on gold and redeposited on a substrate had a thickness of 128 ± 9 nm as determined by SEM (Figure 31e). This thickness value is undistinguishable from the 132 ± 6 nm measured directly on the supporting gold working electrode. The static water contact angle on the transferred membrane was equal to 37 ± 1° (Figure S4a) a value significantly larger than on the

untransferred pristine film, 23 ± 1 °, but lower to a pure PVA layer (64 ± 1 °). This finding suggests that the film undergoes some slight changes upon transfer with the PVA method. It will be discussed further in a following discussion.

The transfer of the 1,8-DHN based films onto PDMS also unlocked the possibility to measure the elastic modulus with the SIEBIMM method.[89] Here, the film prepared with 25 CV cycles at 200 mV/s was used. An elastic modulus of 656 ± 252 MPa was obtained. This high value suggests a strong crosslinking of the monomers and a dense polymeric network. Interestingly, the Young modulus of these 1,8-DHN based films is significantly lower compared to polydopamine films,[88,99] which could explain their higher swellability.

Raman spectroscopy (Figure 32), and an IR spectrum calculated from the spectroscopic ellipsometry data (Figure 33) and XPS (Figure 34) were used to characterize the structure of the 1,8-DHN films obtained by CV. Raman spectra of all three films shown in Figure 32 have observable bands at 1292 cm^{-1}, 1372 cm^{-1}, 1400 cm^{-1}, 1593 cm^{-1}, and 1620 cm^{-1}. The first band corresponds to aromatic C-H bending vibrations, the three following ones are attributed to aromatic C-C stretching and the last band is attributed to C=O stretching vibrations, respectively.[74,75] The increasing drift of the Raman signal, particularly with the sample prepared at 20 mV/s, above 2000 cm^{-1} might be induced by a heating effect of the laser on the gold substrate. The fact that this effect is more pronounced for the thickest film (Figure 32) may be explained that it is able to store more thermal energy. Therefore, it is difficult to attribute the area around 2880 cm^{-1}.

The IR spectrum in Figure 33 is obtained from the absorption coefficient k measured in ellipsometry from the film deposited with 25 CV cycles at 200 mV/s. 5 bands are observed above 1000 cm^{-1}. The first one at 1263 cm^{-1} can be attributed to C-H vibrations. The following band at 1344 cm^{-1} can be due to C-O-H stretching. The band at 1425 cm^{-1} may correspond to C-C stretching. The band at 1614 cm^{-1} can be attributed to C=O vibrations and the large peak at 3448 cm^{-1} to -OH stretching vibrations.[75,81] This spectrum is in very good agreement with the Raman spectroscopy data.

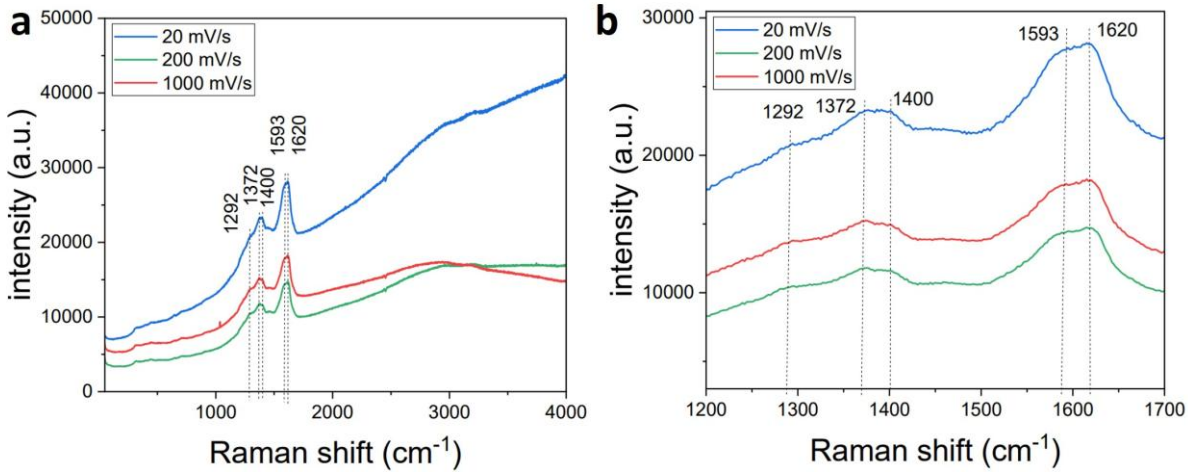

Figure 32. (a) Raman spectra of the films prepared after 25 CV cycles at 20 mV/s (blue), 200 mV/s (green) and 1000 mV/s (red). (b) Zoom in the wavenumber range between 1200 and 1700 cm^{-1}.

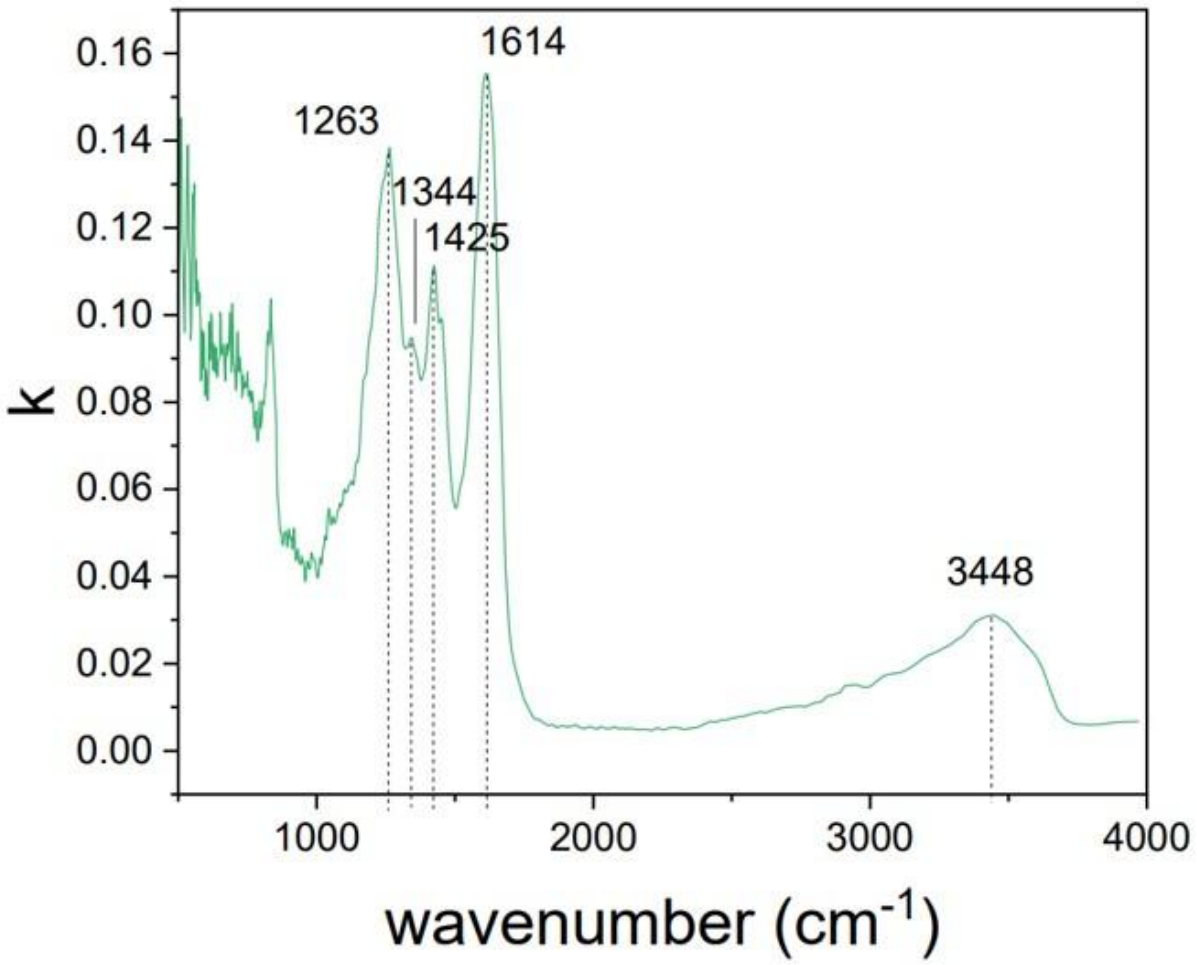

Figure 33. IR spectra obtained from the absorption coefficient measured by ellipsometry for the film deposited after 25 CV cycles at 20 mV/s.

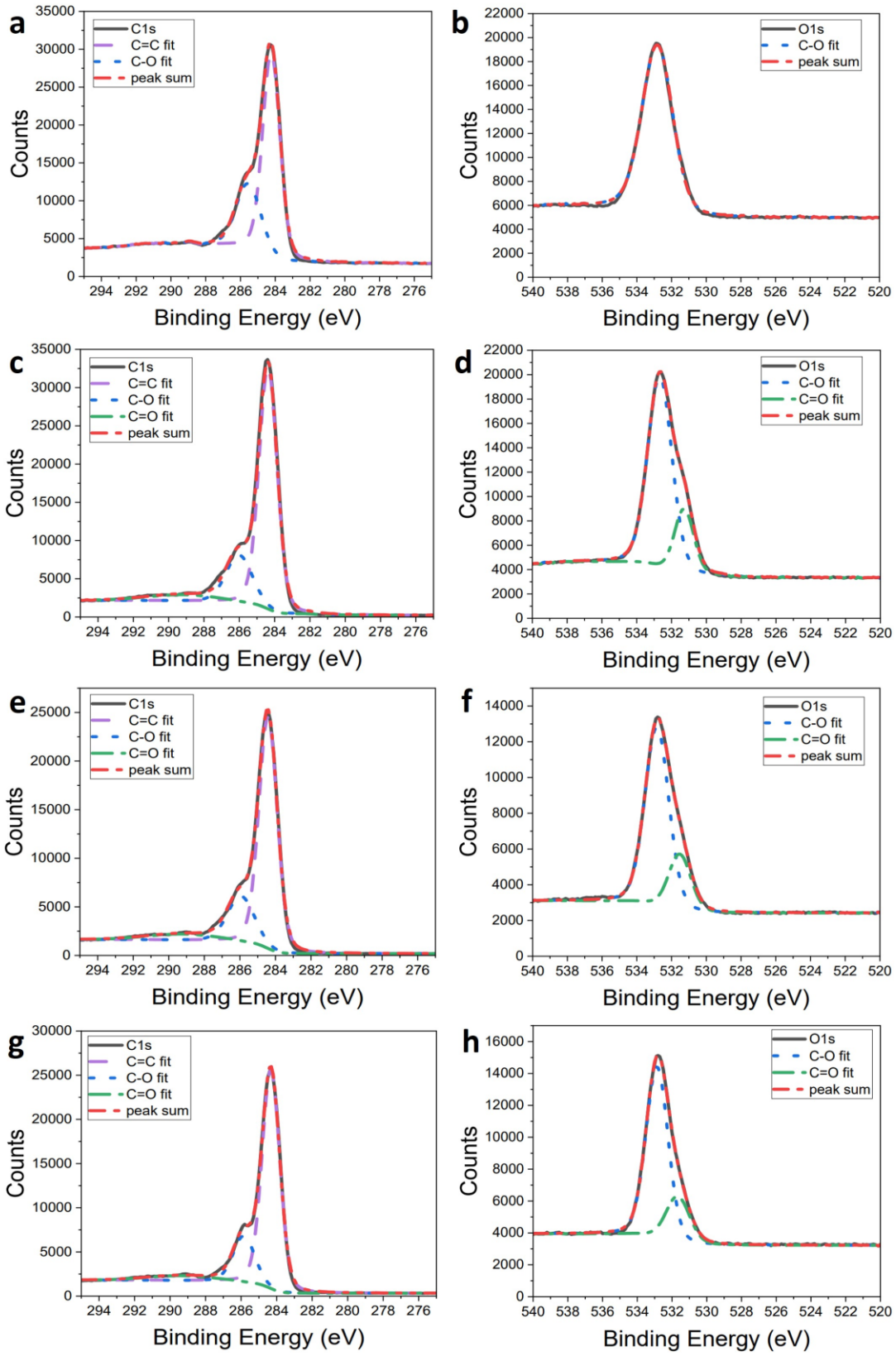

Figure 34. High resolution XPS C 1s and O 1s spectra of the films deposited after 25 CV cycles and a drop casted solution of the precursor. (a) C1s for the precursor, (b) O1s for the precursor, (c) C 1s for the film at 20 mV/s, (d) O 1s for the film at 20 mV/s, (e) C 1s for the film at 200 mV/s, (f) O 1s for the film at 200 mV/s, (g) C 1s for the film at 1000 mV/s and (h) O 1s for the film at 1000 mV/s.

The theoretical C/O ratio of the 1,8-DHN precursor is equal to 5. XPS measurements (Figure 34) determined similar ratios of 4.9, 5.2 and 5.2 for the films deposited at 20 mV/s, 200 mV/s, and 1000 mV/s, respectively. C 1s and O 1s spectra of the three films show the presence of both C=O groups (289.3 eV in C 1s and 531.5 eV in O 1s) and C-OH groups (285.9 eV in C 1s and 532.8 eV in O 1s).[71,73,82,100] The C-OH/C=O ratio is around 3 independent of the potential sweep rate used for the film deposition. As expected, the C 1s spectra also indicates the presence of C-C bonds (284.4 eV). Raman, FTIR and XPS spectroscopies combined allow us to determine the presence of C=O and C-OH bonds and also aromatic rings. No carboxylic acid, ester or ether groups were found. This suggests that the aromatic rings are only connected via C-C bonds. No oxygen elimination is observed either. Thus, C-OH from alcohol groups correspond to the same unoxidized groups present in the precursor and C=O groups are the ketones obtained from these groups under their oxidized form.

In the case of the transferred film, its surface composition as inferred from XPS spectroscopy is enriched in OH groups (Figure S4b): the percentage of O atoms implied in C-O bonds as in alcohols is now of 35 $\pm$ 1% with a C-OH/C=O ratio increased to 4.9 whereas it was only equal to 3.0 in the as deposited film (Table 3). This finding strongly suggests that during the last step of the free-standing film formation, the immersion in hot water to dissolve PVA required for the film detachment, some PVA remains on the film.

Table 3. Summary of the films' characterization data obtained for the 1,8-DHN based films obtained after 25 CV cycles.

Scan rate	20 mV/s	200 mV/s	1000 mV/s
E_p (at the first CV cycle)	0.33 V	0.52 V	0.92 V
SEM thickness	418 ± 13 nm	152 ± 15 nm	63 ± 5 nm
Ellipsometric thickness	360 nm	130 nm	60 nm
AFM thickness	350 ± 30	132 ± 6 nm	65 ± 8 nm
AFM roughness (RMS)	45 nm	20 nm	12 nm
Refractive index (800 nm)	1.75	1.78	1.58
Contact angle	24 ± 1 °	23 ± 1 °	21 ± 1 °
Elastic modulus	Not measured	656 ± 252 MPa (SIEBIMM)	Not measured
C/O XPS ratio	4.9	5.2	5.2
C-OH/C=O XPS ratio from C 1s	2.9	3.0	3.1
C-OH/C=O XPS ratio from O 1s	3.3	3.2	3.2

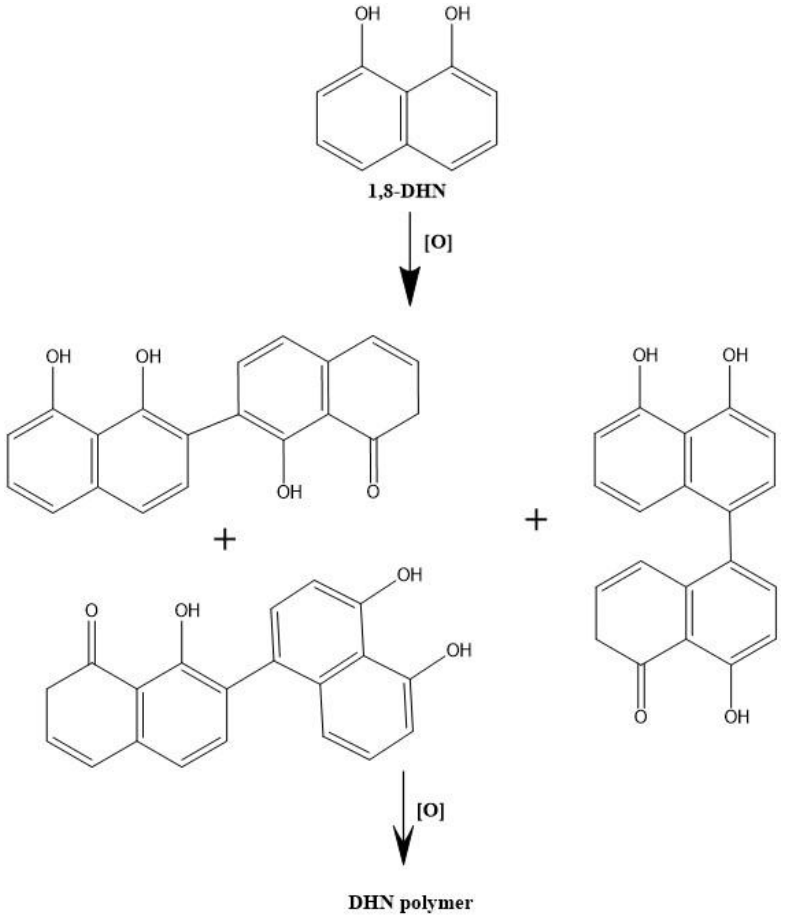

Scheme 4. Proposed 1,8-DHN dimerizations to afford the electropolymerized 1,8-DHN based films.

Scheme 4 summarizes our assumptions on the structure of 1,8-DHN-based films obtained via the oxidative electropolymerization according to the chemical characterization data obtained from Raman spectroscopy, IR, and XPS: monomers are linked via C-C coupling, there is no oxygen loss, and the ratio of alcohol/ketone groups is close to 3 (Table 3). d'Ischia et al. and Manini et al. reported similar structures for materials formed via chemical oxidation of 1,8-DHN in solution.[34,80,81] Unfortunately, the degree of polymerization of the 1,8-DHN-based films is not yet known. Their structure is likely a combination of covalent and non-covalent bonds such as hydrogen bonds made by non-oxidized -OH groups on the 1,8-DHN monomers as well as π-π interactions that may contribute to the overall cohesion. The situation may hence be similar to that of polydopamine films.[61]

4.3.3. Subsequent use in applications

The fact that the 1,8-DHN-based films display some oxidation peak current (not a single capacitive current, Figure 20f) indicates that the deposited material has some reductive properties. This behavior is comparable to that of polydopamine films[82,101] and incited us to investigate potential antioxidant properties of the films. Furthermore, it is known that 1,8-DHN by itself, as the precursor dissolved in solution or as artificial allomelanin nanoparticles,[33,77,78,102] displays strong antioxidant activity, that may be due to H-atom-donating ability from the presence of alcohol (-OH) functional groups and the films display -OH groups, too (Table 3). We conducted DPPH assays,[82,100] where the antioxidant properties of the films are expressed as a decrease of the absorbance at 517 nm compared to the pristine electrode control, due to the DPPH radicals reacting with the films. The spectra displayed in Figure 35a show the absorbance of 10^{-4} M DPPH solutions after samples were immersed for 20 minutes. The absorbance of the DPPH solution at λ = 517 nm decreased in the presence of the three films, indicative of their strong antioxidant behavior. Thus, the 1,8-DHN electropolymerized films may be useful in biomedical applications such as wound healing where radical scavenging behavior is known to reduce inflammatory reactions or to protect against oxidative stress causing damage to tissues.[62,103,104] Moreover, Liu et al[105] reported that reactive oxygen species can also provide new wound healing opportunities by protecting against infections. This decrease of the absorbance of DPPH in the presence of the films is more pronounced when the scan rate used in the synthesis is slower, suggesting that the activity is improved when the thickness is increased. This likely means that the radicals of DPPH are not only able to be neutralized at the films' surface, but also deeper in the films. Here, the absorbance was decreased by 15 % per cm² of film, 20 % per cm² of film, and 38 % per cm² of film for the films prepared at 1000 mV/s, 200 mV/s, and 20 mV/s, respectively. The reduction of DPPH

discoloration from 20 % per cm² for the deposited film with 25 CV cycles at 200 mV/s to 9 % per cm² for the detached film (Figure S4c) is probably due to the remaining PVA. However, the film detachment does not change the overall film thickness and morphology and offers many new possible applications. Since the 1,8-DHN precursor is known to have a radical scavenging activity, a calibration curve (Figure S5) was established from solutions of the 1,8-DHN precursor to determine an equivalent concentration of 1,8-DHN solution for the radical scavenging activity of the films. The film prepared with 25 CV cycles at 20 mV/s has the same antioxidant activity than a $3.49x10^{-6}$ M 1,8-DHN solution in ethanol, the film prepared at 200 mV/s has an activity equal to a $4.20x10^{-7}$ M 1,8-DHN solution and the film synthesized at 1000 mV/s is comparable to a $1.96x10^{-7}$ M 1,8-DHN solution. With this equivalent concentration, an estimation of the volumetric mass and the calculated volume of the films (calculated from the measured thicknesses), an estimation of the number of molecules that reacted with DPPH in the films was done. Around $4.3x10^{-5}$ % of the molecules reacted in the film prepared with 25 CV cycles at 20 mV/s, $5.2x10^{-6}$ % in the film prepared at 200 mV/s and $2.4x10^{-6}$ % in the film prepared at 1000 mV/s. These relatively small percentages of moieties able to give electrons to DPPH reflect that fact that most of the available -OH groups are not accessible to the bulky probe, only those at the surface of sufficiently large and accessible pores are available. Nevertheless, the finding that redox moieties present in the bulk of the film are accessible to DPPH is consistent with the growth regime of the films (Figure 26) and its high swellability (Figure 27). To our knowledge this constitutes an unprecedented result for polyphenol-based films.

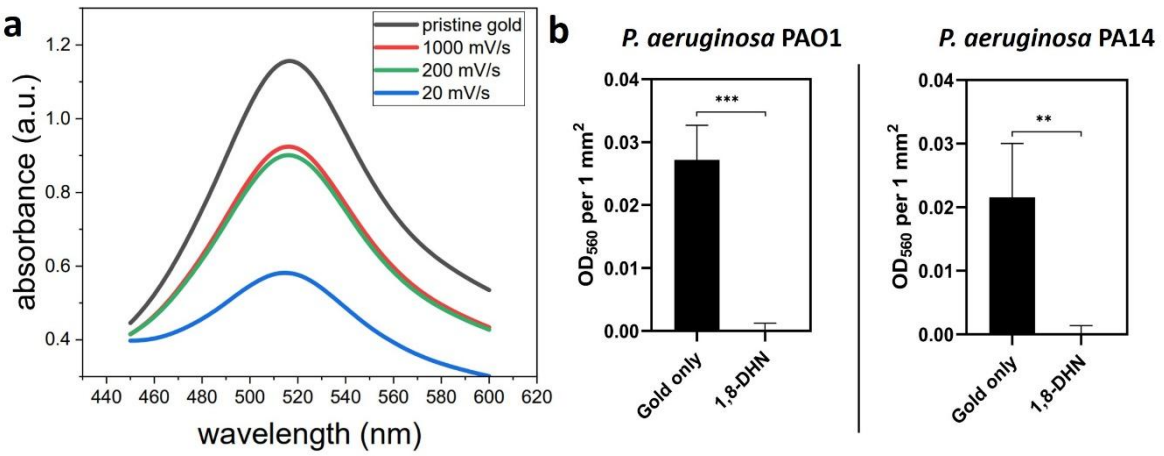

Figure 35. (a) UV-visible spectra between 450 and 600 nm for a DPPH 10^{-4} M solution in contact during 20 minutes with the thin films prepared at 20 mV/s (blue), 200 mV/s (green), 1000 mV/s (red), and a pristine gold electrode as a control measurement (black). (b) Optical density of the bacterial biomass (560 nm) on a clean gold electrode and on 1,8-DHN films (obtained from 1,8-DHN at 1mg/mL after 25 CV cycles at 200 mV/s). Antibacterial properties were quantified by crystal violet biomass staining after 24 h of incubation with *P. aeruginosa* PAO1 (left panel) and *P. aeruginosa* PA14 (right panel). Errors bars represent experiments conducted as triplicates and values were considered as statistically significant for $p < 0.05$. ** denotes $p < 0.01$ and *** $p < 0.001$.

The pathogenic Gram-negative bacterium *P. aeruginosa*, with strains including *P. aeruginosa* PAO1 and *P. aeruginosa* PA14,[83,84] are classified to be among the most threatening pathogens with the highest demand for novel antibiotics by the World Health Organization[106] due to resistances even against last-resort therapeutics. Infections with such multi-resistant pathogens, especially with nosocomial infections being one of the most challenging tasks, are a general global threat and represent the leading cause for mortality worldwide.[107] There is an urgent need for the development of new treatment technologies against *P. aeruginosa*. In this study, *P. aeruginosa* PAO1 and *P. aeruginosa* PA14 were used as the model pathogens to demonstrate antibacterial properties of the

1,8-DHN films prepared with 25 CV cycles at 200 mV/s. Growth of both strains was perfectly prevented in contact with the films when compared to the biomass formed on the gold electrodes as a control (Figure 35b). Since Liu et al[100] reported evidence suggesting that reactive oxygen species (such as polydopamine) are potential antimicrobial agents, the antioxidant activity of the 1,8-DHN films may play a role in the antibacterial properties observed here. Accordingly, in a life-dead assay using resazurin the bacterial killing capability of the films was verified (Figure 36a) as non-viable cells could be determined on the 1,8-DHN material. To further demonstrate the antibacterial potential a lipid peroxidation assay[86,87] was performed to show the oxidative damage of bacterial membrane lipids as the membrane fatty acids gets oxidized by the films. Malondialdehyde (MDA) serves as a widely accepted biomarker for oxidative stress,[108] where MDA levels in biological fluids can be detected through interaction with thiobarbituric acid (TBA) as an MDA-TBA complex. The 1,8-DHN films showed higher lipid peroxidation potential against *P. aeruginosa* PAO1 and PA14 compared to the pure gold electrodes, respectively (Figure 36b), as higher levels of the MDA-TBA complex were formed upon treatment. Therefore, the oxidative damage of the bacterial membrane is a possible mechanism to explain the observed antibacterial properties of the films. Indeed, Sarker et al.[87] reported that the permeability of the bacterial cell membrane gets compromised when the oxidation of the membrane lipids occurs. Thus, leading to bacterial cell death by cytoplasmic leakage or binding from the 1,8-DHN films with cellular macromolecules. Another possibility is the enhanced expression of apoptotic genes and oxidative proteins to cause the bacteria's apoptosis in presence of reactive oxygen species,[87] as it is the case with the 1,8-DHN films (Figure 35a).

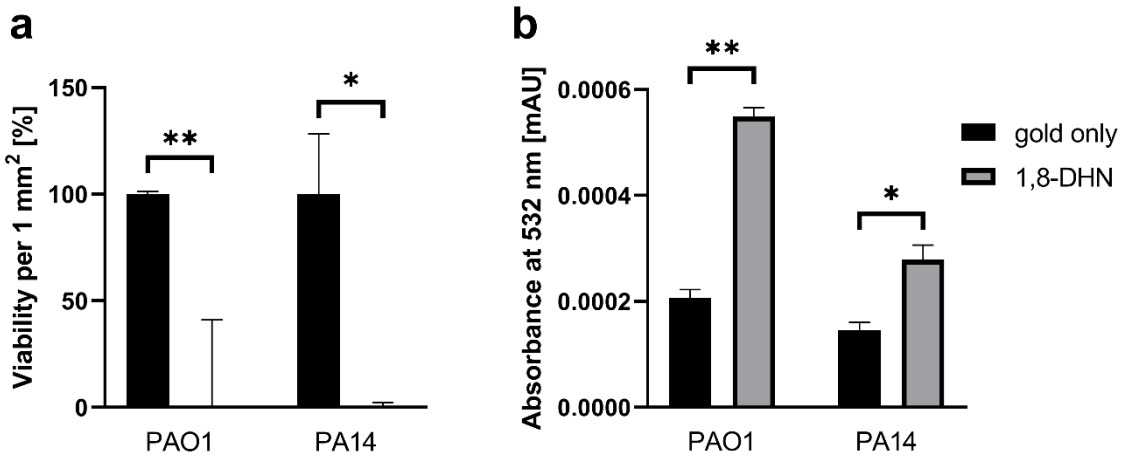

Figure 36. Antibacterial activity of 1,8-DHN films towards *P. aeruginosa* PAO1 and PA14. (a) Antibacterial properties were quantified in a resazurin-reduction assay after 24 h of incubation with *P. aeruginosa* PAO1 and *P. aeruginosa* PA14. Obtained viabilities on a clean gold electrode (black bars) and on 1,8-DHN films (grey bars) represented as relative fluorescence intensities [%] normalized to the material area [mm^2]. (b) Lipid peroxidation potential of 1,8-DHN films. The absorbance of the MDA-TBA adduct was measured at 532 nm. Errors bars represent experiments conducted as triplicates and values were considered as statistically significant for $p < 0.05$ and ** denotes $p < 0.01$.

Overall, very thick and porous films can be produced by CV and CA from 1,8-DHN containing solutions. The OH content remains high (Table 3) and affords some hydrophilic as well as antioxidant and antibacterial properties. As another conceivable application, the 1,8-DHN based films could be used as a protective layer of protheses with antioxidant activity. Figure 37 illustrates the feasibility of film deposition on metals of biomedical interest as CV curves on a Co-Cr alloy after 25 CV cycles obtained from a 1,8-DHN solution at 1 mg/mL in a mixture of a sodium acetate solution and ethanol (pH = 5.75) using a scan rate of 200 mV/s (Figure 37a). Co-Cr alloys are used in dental care. A film deposition was observed by the naked eyes on the piece used as working electrode (Figure 38) and as expected the alloy was afforded with antioxidant activity (Figure 37b).

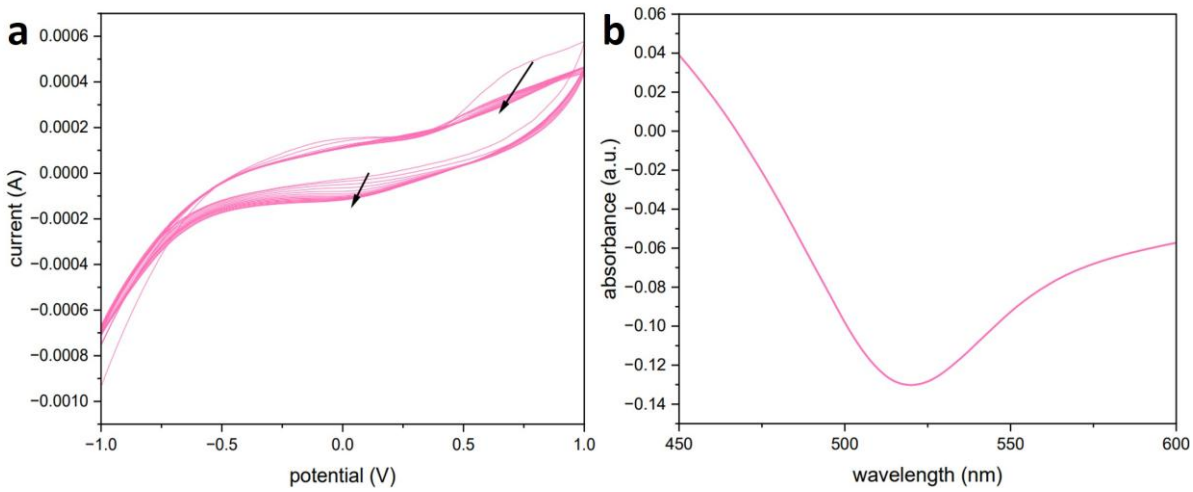

Figure 37. (a) 25 CV cycles performed at a scan rate of 200 mV/s from a 1,8-DHN solution at 1 mg/mL in sodium acetate buffer and ethanol mixture solution on a piece made of a Co-Cr alloy. Black arrows show the evolution of the oxidation and reduction peaks current. (b) UV-visible spectrum of a DPPH 10^{-4} M solution in contact with the film deposited for with 25 CV cycles at 200 mV/s on the Co-Cr piece with respect to a 10^{-4} M DPPH solution in the reference cuvette of the spectrophotometer. The reference is not absolute ethanol like with the films deposited on gold, then the plot is a difference between two spectra and the minimum indicates a reaction of DPPH in contact with the film.

Figure 38. Picture of the Co-Cr piece after 1,8-DHN film deposition (dark part).

Due to the insolubility of the films in the most common solvents and their mechanical properties, the films may also have potential applications as protective coatings. Their electroactive, antioxidant, and antibacterial properties allow them to be good candidates in applications in the fields of environmental treatment and biomedicine, among others. The transferability of the films also opens the way to other applications and the films may be used as membranes for instance.

Finally, 1,8-DHN was electrodeposited by CV (25 cycles performed at 20 mV/s) in the presence of $CuCl_2$ (at a ¼ Cu^{2+}/DHN molar ratio). The obtained CVs as well as the CVs obtained after film deposition and water rinse are displayed in Figures 39a and b respectively. The obtained films incorporate copper as shown by XPS directly on the film surface (Figures 39c, d, e, f and g), by EDX (Figures 39h, i and j) and by ICP-MS (Inductively Coupled Plasma - Mass Spectrometry) after film dissolution in the presence of 10 mL H_2O_2 at 35 % (v/v). The incorporation of copper in the DHN in a one pot process will offer the opportunity for applications in catalysis[109] and will be the subject of future investigations.

The primary copper peak appears at 931.6 eV (Figure 39f), suggesting the presence of Cu (I) as it is lower than the expected value for Cu (II). The broadness of the peak rules out Cu (0). According to the NIST data bank (National Institute of Standards and Technology), the binding energy for CuCl also tends to be lower.[110] However, due to the signal-to-noise ratio in the XPS measurement, there remains some uncertainty. An analytical CV was conducted after film deposition (Figure 39b), revealing an oxidation potential of +0.1 V and a reduction potential of -0.23 V. Taking into account the chelation of the incorporated and the formal oxidation potential of Cu (I) to Cu (II) at 0.159 V,[111] along with the XPS results, it is plausible that the film contains Cu (I).

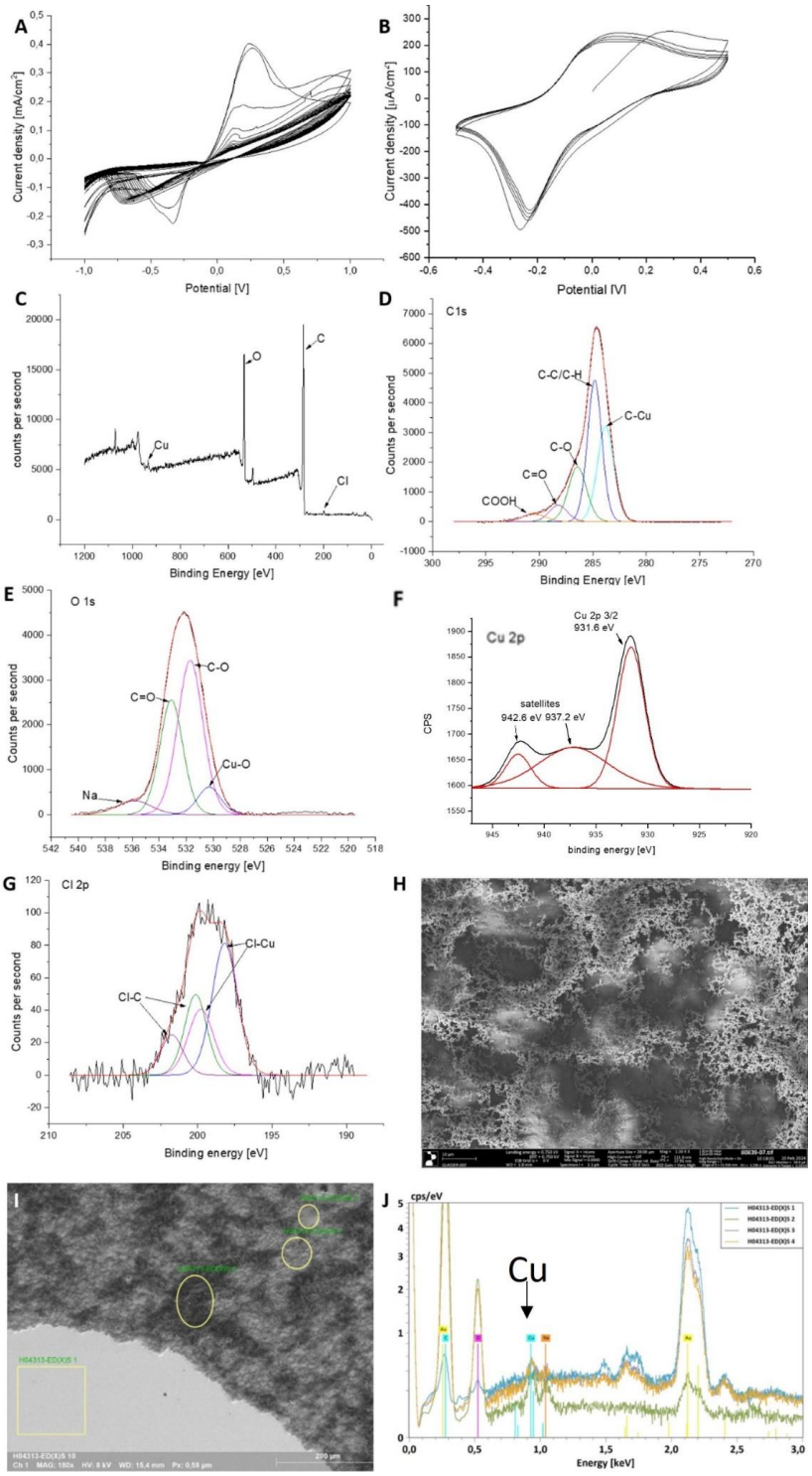

Figure 39. (A) 25 cycles CV curves performed at a potential sweep rate of 20 mV/s in the presence of 1,8-DHN at 1 mg/mL and $CuCl_2$ at 0.256 mg/mL in sodium acetate buffer. (B) 5 CV cycles at 100 mV/s in presence of the buffer-ethanol mixture without any redox species in solution. The CV cycles were performed after the film deposition. (C) XPS survey spectra of the Cu containing film and the high resolution XPS C 1s (D), O 1s (E), Cu 2p (F) and Cl 2p (G) spectra. (H) SEM image of the Cu containing film and with the measured EDX spots (I). (J) EDX results of the measured areas (I).

4.4. Conclusions and perspectives

Herein, the electrodeposition of 1,8-DHN films on gold electrodes using CV and CA synthesis methods was investigated under environmentally friendly conditions using low electrical potentials at ambient temperature in an ethanol-sodium acetate buffer solution at pH = 5.75. The potential scan rate used in the CV deposition allows to tune the film thickness up to hundreds of nm at 20 mV/s, which is unprecedented for electrodeposited films based on polyphenols. Regardless of the used scan rate, the obtained films display some electroactivity and can be further oxidized or reduced which is consistent with their strong antioxidant activity. Interestingly, these antioxidant properties increase with the film thickness, suggesting that the used probe is able to access the whole film thickness in relation to its porosity and ability to swell in the presence of a solvent such as water. The feasibility of the electrodeposition of 1,8-DHN was also extended on a dental Co-Cr alloy. Interestingly, the 1,8-DHN-based electrodeposited films are antibacterial against *Pseudomonas aeruginosa* without further chemical film modification. We assume this biological property to be related to its special redox properties and/or to their high hydrophilicity. To investigate the structure of those electrodeposited films, their transferability on flexible polymer substrates like PDMS will be exploited in a future work.

4.5. Unpublished data and complementary results

To determine a possible conductivity in the films, C-AFM (Conductive–AFM) measurements were carried out. As a reference of a non-conductive material, a film from 3-amino-L-tyrosine was also used. In the case of the reference and the 3 films of DHN (20, 200 and 1000 mV/s), a constant current of 14 pA was measured at 3 different potentials applied: +0,7 V, +5 V and +7 V. These results strongly suggests that the films are not conductive.

Scheme 4 presents our assumptions on the oxidative electropolymerization pathway. However, the mechanism is even less evident. Since a mechanism involving radicals was expected, electron paramagnetic resonance (EPR) measurements were performed to detect the presence or the absence of radicals. To place the material from the films in the quartz sample tube for EPR, the films were scratched with a spatula and the small amount of powder from ~1cm² of surface deposition was sufficient because EPR is a very sensitive technique. Figure 40 shows the spectra obtained with the deposited material prepared at 20 mV/s at different powers and those for the precursor powder.

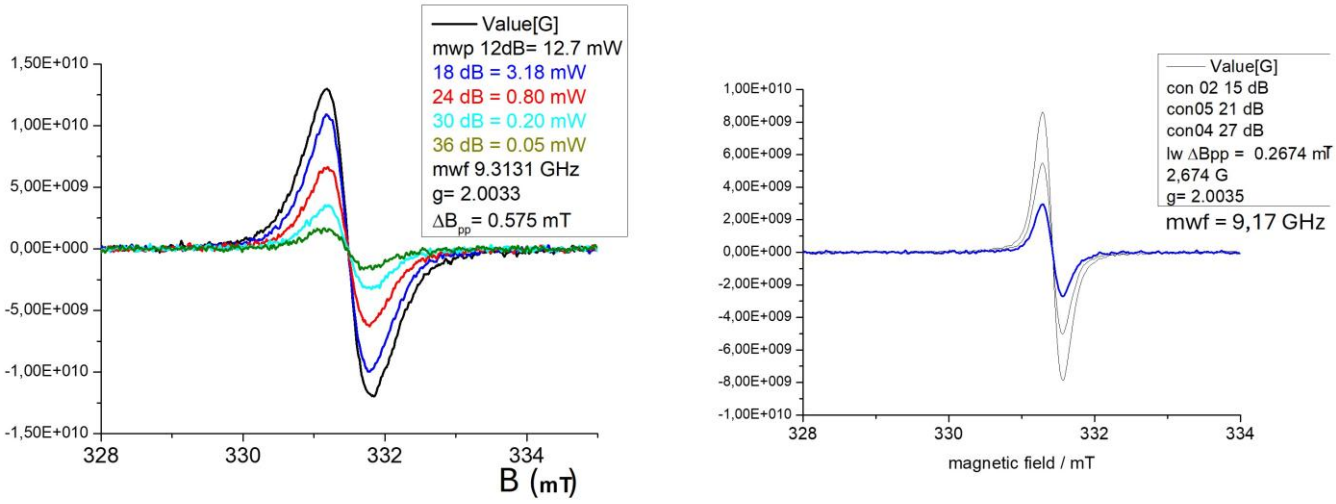

Figure 40. EPR spectra of a DHN film prepared with 25 CV cycles on gold electrode at 20 mV/s (left) and of the 1,8-DHN precursor (right). The measurements were performed at ambient temperature.

First, signals were obtained. Thus, radicals were detected in the film material. Surprisingly, signals were also obtained in the precursor powder. Therefore, the precursor already contains radicals. However, it is difficult to determine if it is a spontaneous mechanism or only after a long time of storage, even stored in a fridge at 4 °C. The g-factor for the film is equal to 2.0033 and for the precursor equal to 2.0035. The g-factors obtained are typical from carbon-centered radicals.[67,112] The signal amplitude (ΔB) was determined in both

cases and also with a film prepared at 1000 mV/s. For the film prepared at 20 mV/s, the signal amplitude was equal to 0.58 mT (= 5.8 G); a similar amplitude of 0.55 mT (5.5 G) was obtained for the film prepared at 1000 mV/s; and a very different value of 0.27 mT (2.7 G) was determined. The values observed for the films are close to values found in the literature for melanin[112] and polydopamine[67] radicals. The lower signal amplitude with the precursor suggests a greater homogeneity of the free-radical components compared to the free-radical components in the films. Unfortunately, the presence of radicals has also drawbacks. For instance, nuclear magnetic resonance (NMR) is not possible to be performed with compounds containing radicals. This technique could have been efficient to help to determine the global structure of the films.

As an alternative, mass spectrometry measurements were carried out to get clues about the structure of the films. ToF-SIMS measurements were performed, and the results are presented in Figure 41. Unfortunately, this technique creates a huge fragmentation of the samples. A lot of fragments were detected and only relatively small fragments. Thus, it is very complex to reconstruct the structures from these data. However, it is noticeable that for every polarity (positive or negative) the fragments detected are exactly identical for both films, independently of the scan rate used in the CV. This results strongly suggests similar or identical structures of both materials.

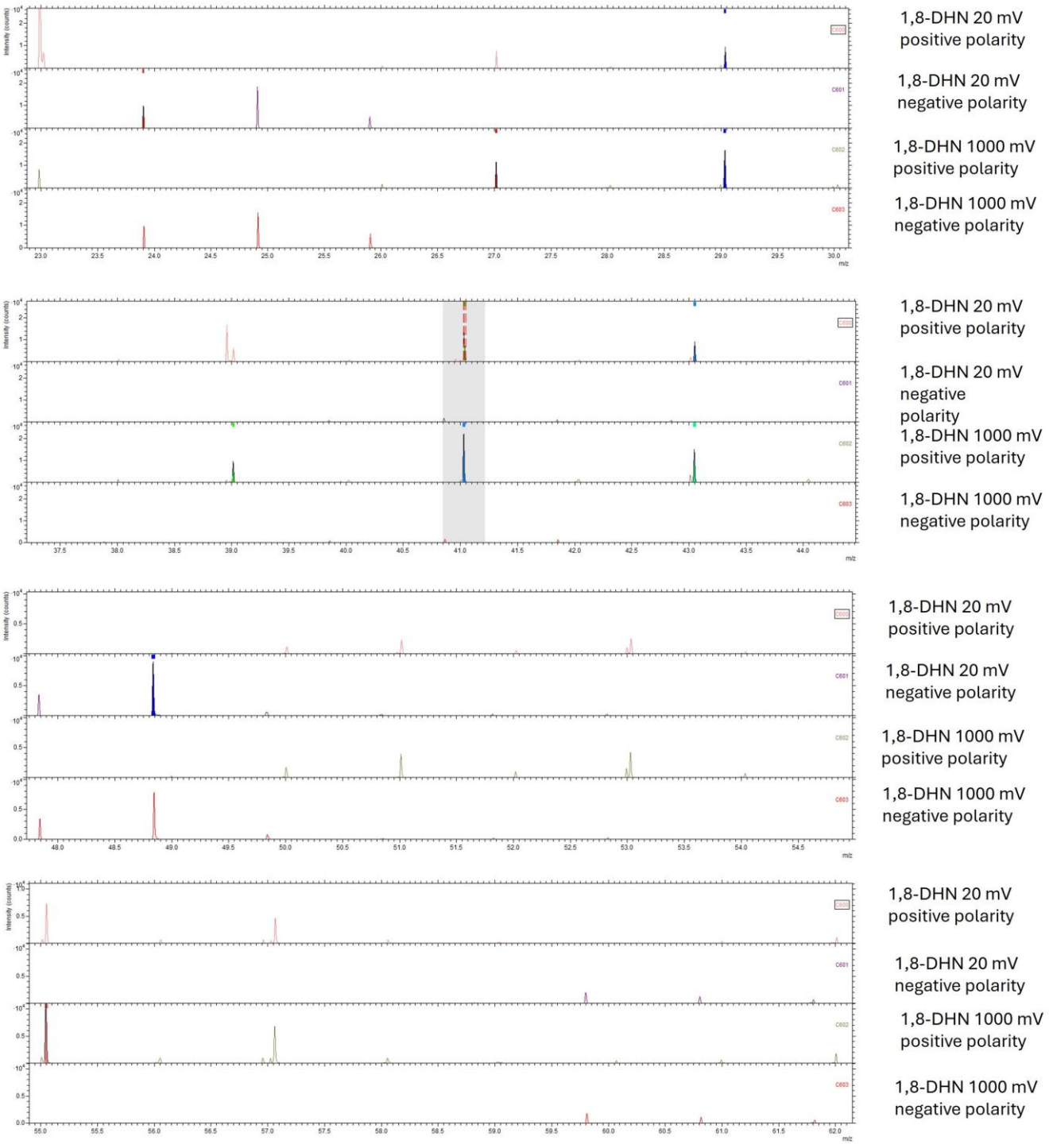

Figure 41. ToF-SIMS measurements on the films prepared at 20 mV/s and 1000 mV/s in the mass-to-charge ratio range from 23 to 62 (increasing from left to right and from the top to the bottom).

In Figure 39 were presented characterizations made on the films co-deposited with $CuCl_2$ to prove the presence of Cu in the obtained films. As perspectives of applications, such materials can be used in catalysis. An example is the CO_2 electroreduction reaction

(CO_2RR). Indeed, copper has been reported to be a good catalyst in CO_2RR.[27] Electrochemical tests were carried out to determine if the DHN-based films containing copper can be efficient CO_2 electroreduction. Film samples were prepared with 25 CV cycles at 20 and 200 mV/s. First an additional CV of 10-20 cycles was done in 0.1 M $KHCO_3$ electrolyte to stabilize the redox activity of the samples (discussed with Figure 22) to avoid misinterpretation of the following experiments. Then, a linear sweep voltammetry (LSV) experiment was done in Ar-saturated atmosphere as a reference and in CO_2-saturated atmosphere to investigate if there is a reaction with CO_2. Unfortunately, the samples prepared at 20 mV/s were not stable at all. Indeed, even after washing the samples with water after the synthesis it was possible to see degradations of the material. When starting the 20 CV cycles before the LSV, the film was completely removed from the electrode to the solution. Figure 42 shows pictures of both films after they were washed with water consecutively to the synthesis. The film prepared at 200 mV/s looks more homogenous. However, even if it was more stable in the washing step and in the electrochemical performance, the film was falling from the electrode in the product analysis process. Indeed, after the LSV and based on the potential window at which CO_2RR takes place, an electrolysis was performed at control potential in a gas-tight cell for 2-3 hours and the products produced, gas or liquid, are collected (to investigate the selectivity of the catalyst). In this electrolysis, higher negative and positive potentials can be applied and are a possible cause of the degradation of the films. However, the general stability of the films containing copper seemed affected and in particular when prepared at 20 mV/s. This observation compared to the high stability of the films without copper (Figure S3) strongly suggests that the adsorption on the gold surface is different between the presence and the absence of copper. It is expected that the copper can create a complex with the hydroxyl groups of 1,8-DHN. Therefore, it is possible that the adsorption of the 1,8-DHN on gold

was done via the hydroxyl groups but in presence of copper this adsorption was impacted by the presence of copper already complexed with the hydroxyl groups, resulting in a lower adhesion of the films containing copper to the electrode surface.

Figure 42. Pictures of films of 1,8-DHN co-deposited with $CuCl_2$ with 25 CV cycles at 20 mV/s (left) and 200 mV/s (right).

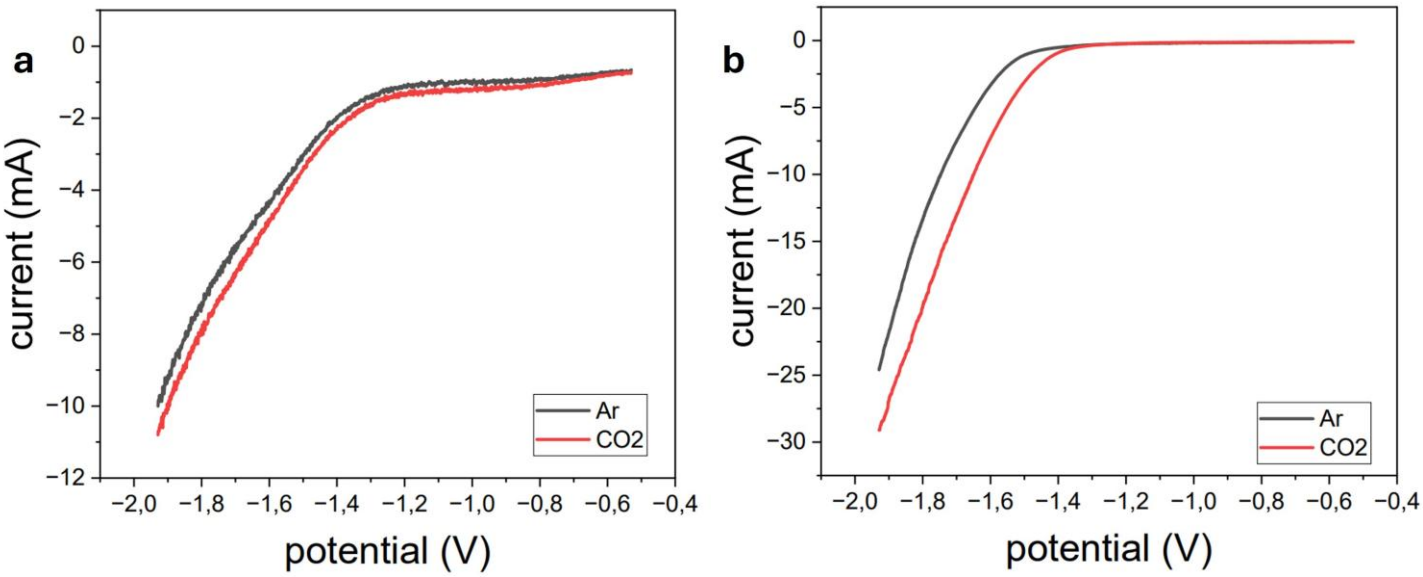

Figure 43. LSV tests on (a) the pristine gold electrode and (b) the film containing copper prepared with 25 CV cycles at 200 mV/s. The black lines correspond to a LSV in Ar-saturated atmosphere as reference and the red lines to a LSV in CO_2-saturated atmosphere. Potentials are given here vs SCE (saturated calomel electrode).

The LSV curves obtained in Figure 43a represent the currents measured in Ar- and CO_2-saturated atmospheres with the pristine gold electrode, while Figure 43b represents the currents measured with the electrode covered with the deposited Cu-containing film prepared with 25 CV cycles at 200 mV/s. In the case of the pristine gold working electrode, no difference is visible between both atmospheres. However, a shift of the onset potential and an increase of current is observed in the case of the film when Ar gas is replaced by CO_2 gas. This strongly suggests that the CO_2 is reacting with the film. Therefore, the DHN-based films containing copper are promising for CO_2RR, but the film stability must be improved.

Chapter 3: Electrodeposition of 1,8-dihydroxynaphthalene on glassy carbon

The work on the 1,8-DHN started on glassy carbon electrodes. The type of electrode used is a disc of glassy carbon assembled with a polymer tube and a Ni metal connecting wire (Figure 44a). This kind of electrode will be referred to as “disc electrode” in this manuscript. Due to the shape of the assembled electrode and the difficult access to the surface for further measurements without sacrificing a lot of electrodes (by cutting the edge containing the carbon disc), a limitation to only few techniques was inevitable. Later, mainly after the whole work on gold working electrodes, different glassy carbon electrodes with a plate shape (Figure 44b) were purchased and used for additional characterization on the films deposited on glassy carbon with the aim to compare the depositions on both substrates (gold and carbon) and study the influence of their chemical nature. This kind of electrode will be referred to as “plate electrode” in this manuscript.

Finally, few investigations were performed to produce and characterize hybrid systems combining 1,8-DHN and DHPs on glassy carbon electrodes. The chosen DHP precursor was the 2,5-DHP that seems the most promising according to the TEM, impedance and ellipsometric data (Figures 11c, 16 and 17 respectively).

All the experiments were carried out with the same conditions described in Chapter 1 (glassy carbon electrode preparation and electrochemical cell setup), and in Chapters 1 and 2 (techniques used). Any differences will be specified. The carbon plate electrodes were purchased from Sigma Aldrich (3 mm x 20 mm x 60 mm) and cut in pieces of 3 mm x 1 cm x 2 cm.

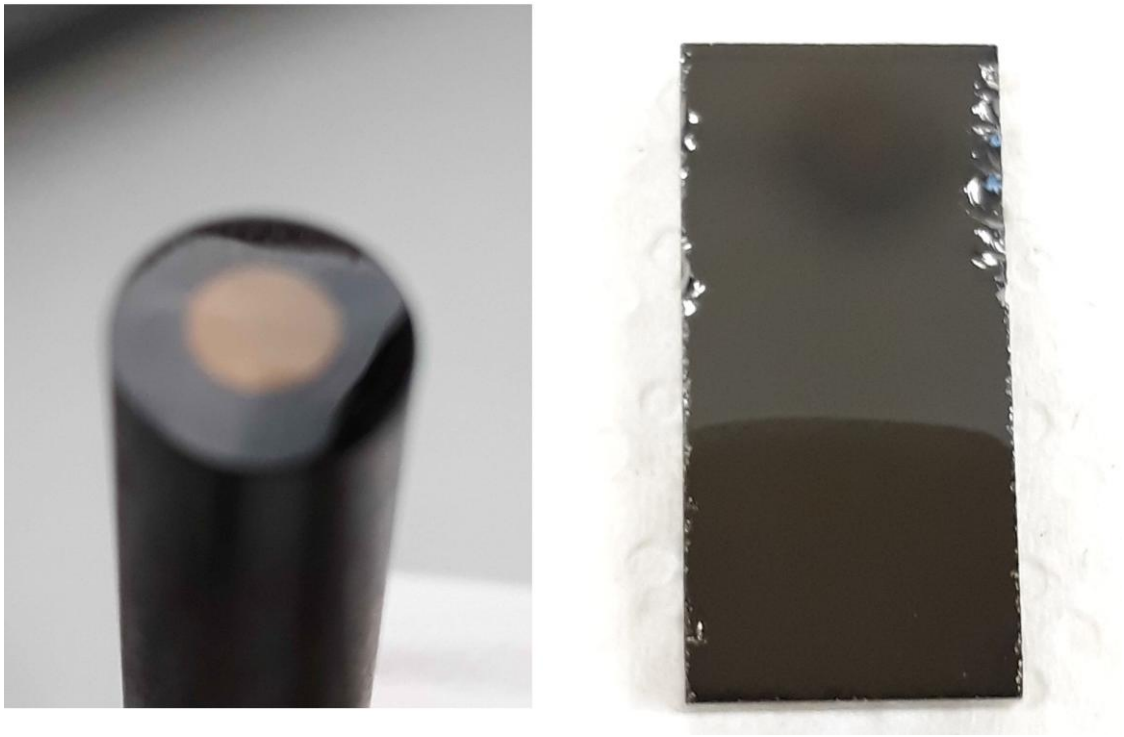

Figure 44. Pictures of the glassy carbon electrodes: (a) the disk-shaped working electrode and (b) the plate-shaped working electrode. Both are covered by a brownish 1,8-DHN-based film deposited with 25 CV cycles at 1000 mV/s.

5.1. Electrodeposition of 1,8-DHN on the carbon disc electrode

The synthesis of 1,8-DHN films was conducted using cyclic voltammetry with an arbitrary choice of 25 CV cycles. We wanted to investigate the effect of the scan rate on the obtained material, like it was done with DHPs, and then decided to work at 20, 200 and 1000 mV/s to get a large range of scan rates.

The CV curves obtained with 25 CV cycles on the glassy carbon disc electrode at 20, 200 and 1000 mV/s are reported in Figure 45. The 1,8-DHN had a concentration of 1 mg/mL in the same sodium acetate buffer and ethanol mixture described in Chapter 2 with a pH of 5.75. In all cases, oxidation and reduction peaks were observed. The maxima of the first peak are obtained for +0.284 V, +0.418 V and +0.602 V, respectively for 20 mV/s, 200 mV/s and 1000 mV/s. After 2-3 cycles, the peak currents decreased. However, after 4-5

cycles, both oxidation and reduction currents increased again. This is not in agreement with an electrode fouling. This phenomenon was observed up to 25 cycles. This surprising observation can be the sign of a conductive or a porous (and maybe swelling) material, so that electrons can still be exchanged at the surface of the electrode after that many cycles.

Investigations were conducted at 50 mV/s on different DHN isomers (1,8-DHN, 1,7-DHN and 1,6-DHN) to identify if this is a unique behavior of the 1,8-DHN or a common behavior for similar precursors. As shown in Figure 46a, the previously described behavior was observed only with the 1,8-DHN-based film formation. The impedance spectroscopy of these isomers (Figure 46b) showed that the film produced from 1,8-DHN also has a significantly different electrical behavior and tends to have a similar short semi-circle than conductive materials for instance. Based on these comparisons, the 1,8-DHN was chosen as a promising candidate for our study to investigate if a molecule with already 2 aromatic rings can lead to films with higher structural order or crystallinity compared to catechol or the DHPs for example.

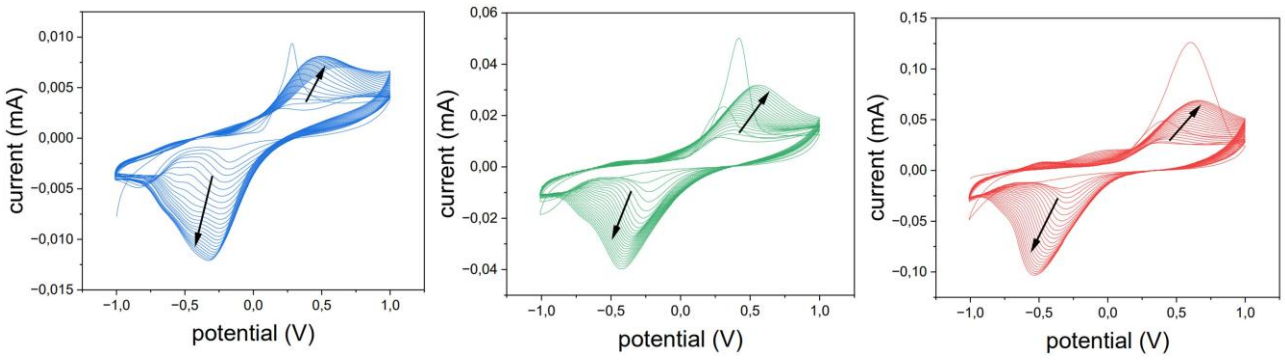

Figure 45. 25 CV cycles with 1,8-DHN (1 mg/mL in sodium acetate buffer and ethanol, pH 5.75) at 20 mV/s (blue), 200 mV/s (green) and 1000 mV/s (red) on the glassy carbon disc electrode. Black arrows indicates the evolution of the peak currents when the number of cycles increases.

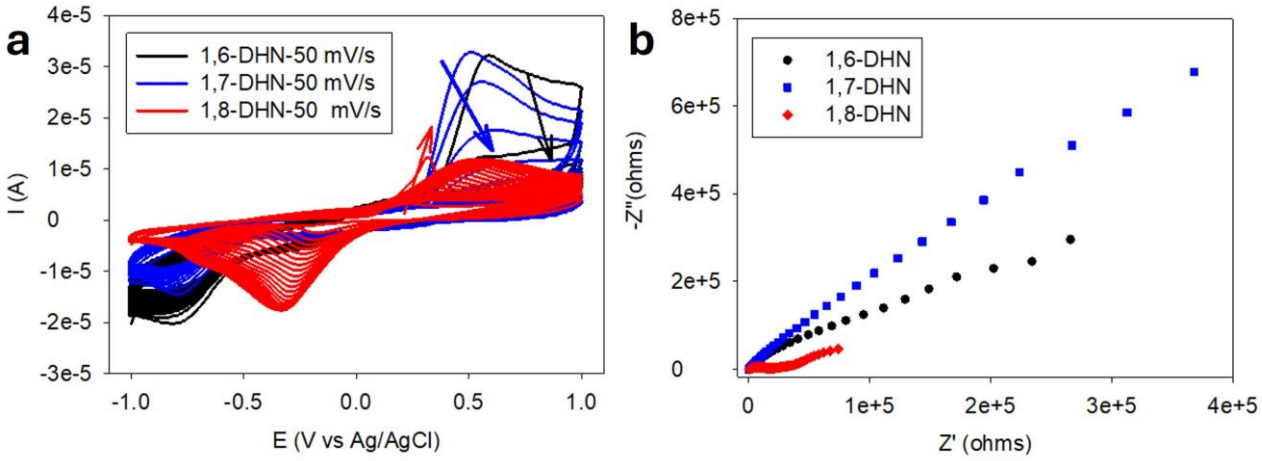

Figure 46. (a) 25 CV cycles at 50 mV/s of a few isomers of DHN at 1 mg/mL on the disc electrode: 1,8-DHN in red, 1,7-DHN in blue and 1,6-DHN in black. (b) Impedance spectroscopy after the 25 CV cycles of the same isomers.

Electrochemical investigations were also performed to determine the need of the whole potential window. Figure 47 shows a CV of 1,8-DHN with 25 CV cycles at 100 mV/s between +0 V and +1 V instead of -1 V and +1 V. The CV is not only shortened by half, but also includes only the oxidation reaction because the reduction occurs at lower potential than 0 V (Figure 45). The oxidation at the first cycle remains unchanged compared to the CVs in Figure 45. However, the successive cycles are completely different. Indeed, we observed a clear decrease in the oxidation current at the 2nd cycle and this current was stabilized until 25 cycles. The previous increase in the oxidation current does not occur in these conditions. The CV curves suggest a strong passivation of the electrode's surface after the first CV cycle. Therefore, with comparison to Figure 45, it is assumed that the reduction reaction plays an important role in the 1,8-DHN film growth and mechanism.

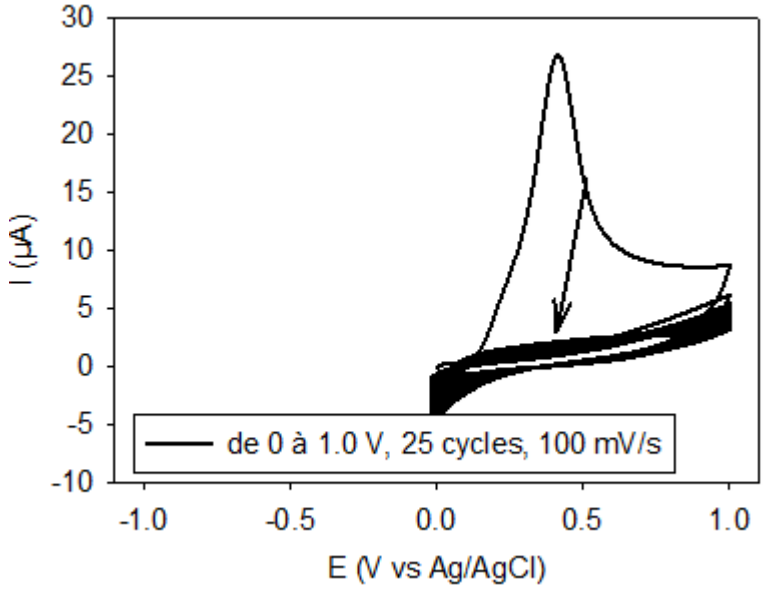

Figure 47. 25 CV cycles at 100 mV/s of 1,8-DHN at 1 mg/mL on the disc electrode between 0 V and +1 V.

Except electrochemical analysis, not a lot of techniques were possible to use to characterize the films without sacrificing plenty of electrodes. However, it was possible to get a transfer of material on a copper TEM grid (as described in Chapter 2) to perform TEM measurements. The obtained images are presented in Figure 48. The film prepared with 25 CV cycles at 20 mV/s had large amorphous areas but containing several domains with a mosaic aspect (around 200 nm in width, Figure 48a) which was highly crystalline (Figure 48b). The film at 200 mV/s presented less structural order and had less crystalline areas (Figure 48c), which was again contained in the mosaic aspect domains (Figure 48d) but the reverse is not true, some of these domains were not crystalline. The lower crystallinity apparent proportion in the sample prepared at 200 mV/s is not surprising because with a higher scan rate, the time reaction time is lower, and molecules have less time to reorganize between 2 successive redox cycles. Surprisingly, the film prepared at 1000 mV/s was not less crystalline than the one at 200 mV/s. It was even fully crystalline (Figures 48e and f). This is not very clear how exactly, but the high reaction speed rate

induces strong differences in the obtained material structure. Lattice spacings measured were 3.4 ± 0.3 Å, 3.5 ± 0.3 Å and 3.5 ± 0.3 Å, for respectively the films at 20, 200 and 1000 mV/s. Another visible observation is the amorphous layer on top of the sample at 1000 mV/s (Figure 48e, but actually it was observed at different areas on all the film fragments). This layer was simply pulled off from the electrode surface. Thus, indicating a strong adhesion between the carbon-based film and the electrode surface.

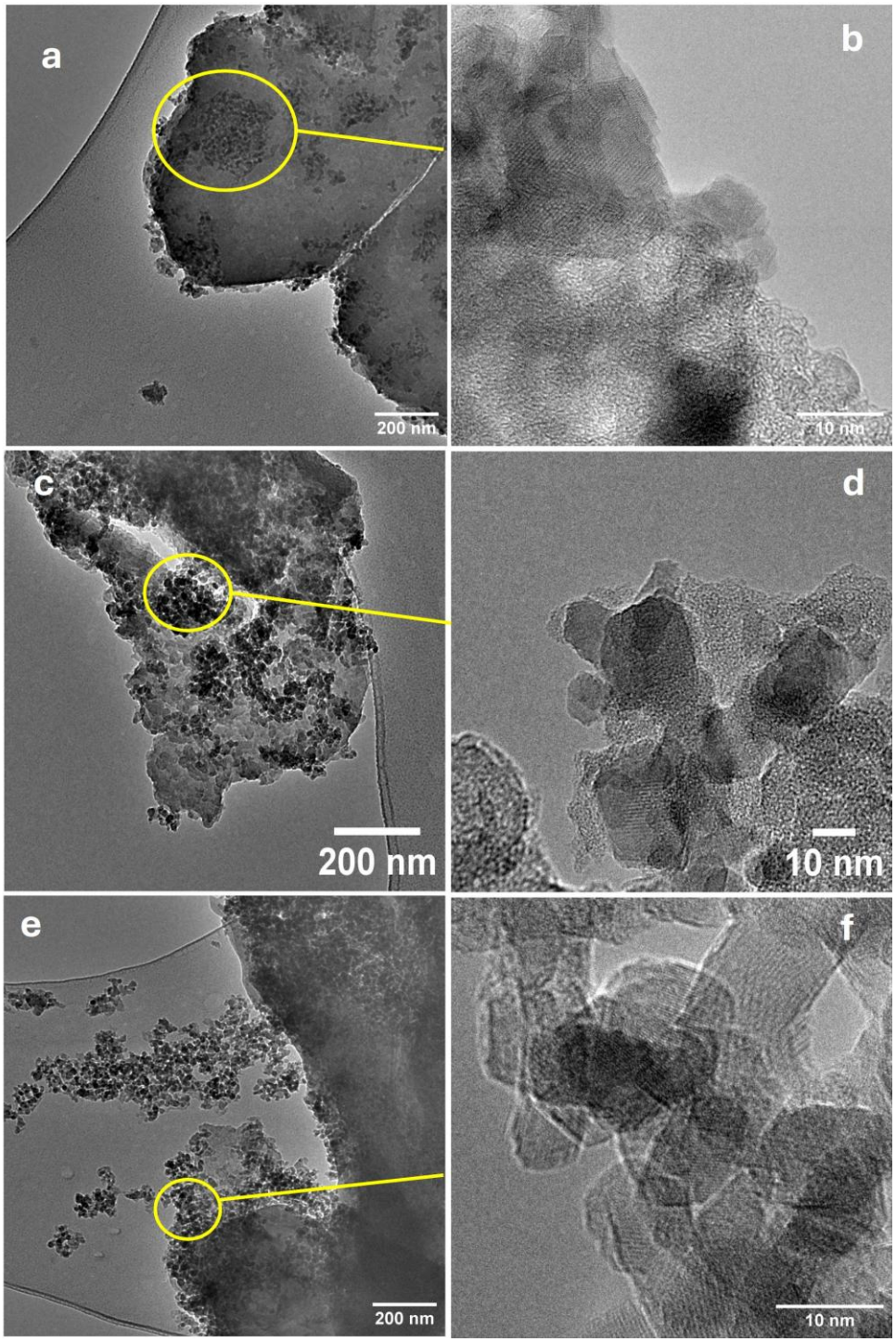

Figure 48. TEM pictures of the films at (a) 20 mV/s with (b) a zoom in the crystalline domains, at (c) 200 mV/s with (d) a zoom in the crystalline domains, and at (e) 1000 mV/s with (f) a zoom in the crystalline domain. Scale bars represent 200 nm (left column) and 10 nm (right column).

While the work on gold electrodes started as an alternative to characterize the 1,8-DHN-based film, a short test with copper was performed on glassy carbon. A co-deposition of

1,8-DHN and $CuSO_4$ (with a 4:1 ratio) via a 25 CV cycles synthesis at 20 mV/s was carried out and the obtained film was placed on a TEM grid. The images captured are shown in Figure 49. The film layers were very different and less homogeneous than without copper. The copper was dispersed in the whole film as small dots of 12 ± 3 nm in diameter.

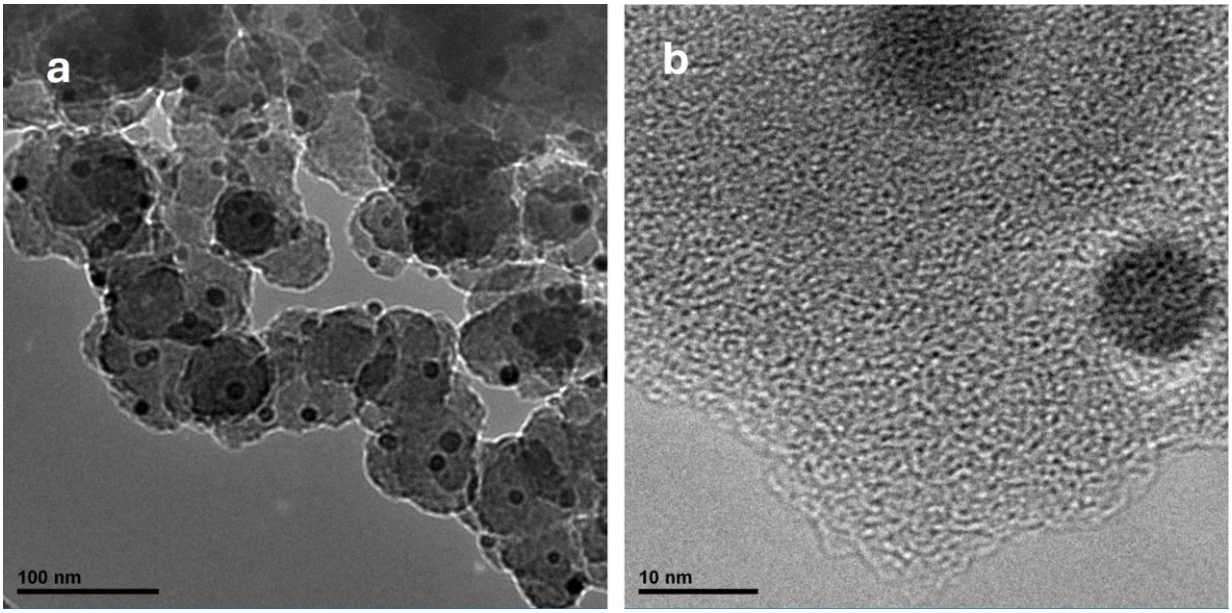

Figure 49. TEM images of (a) the 1,8-DHN film containing Cu with (b) a zoom on the particles observed. 1,8-DHN was co-deposited with $CuSO_4$ with 25 CV cycles at 20 mV/s. Scale bars represent 100 nm (a) and 10 nm (b).

5.2. Electrodeposition of 1,8-DHN on the carbon plate electrode

Later in the project, the plate-shaped electrodes were purchased and used as glassy carbon working electrodes. Their size and shape was similar to those of the gold working electrodes and were suitable for a larger array of characterizations.

The synthesis was kept with the same conditions as before. The films were electrodeposited with 25 CV cycles at 20, 200 and 1000 mV/s. The 1,8-DHN solution was prepared at 1 mg/mL in the sodium acetate buffer and ethanol mixture at pH 5.75.

The CV curves are shown in Figure 50 and Figure 51 shows the pictures of the corresponding films. The 1,8-DHN had a concentration of 1 mg/mL in the same sodium acetate buffer and ethanol mixture described in Chapter 2 with a pH of 5.75. In all cases, oxidation and reduction peaks were observed. As well as with the disc electrodes, the oxidation and peak currents increased after 4-5 cycles until at least 25 cycles. However, the increase in current cycles after cycles seems less marked than on the disc electrodes. The maxima of the first peak are obtained for +0.477 V, +0.682 V and above +1 V (actually around +1.2 V if we increase the upper potential limit of the experiment), respectively for 20 mV/s, 200 mV/s and 1000 mV/s.

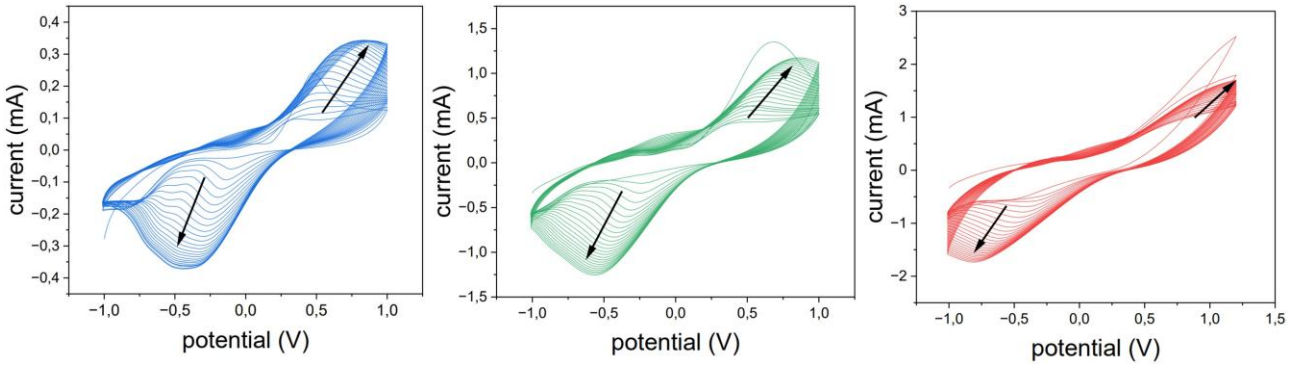

Figure 50. 25 CV cycles with 1,8-DHN (1 mg/mL in sodium acetate buffer and ethanol, pH 5.75) at 20 mV/s (blue), 200 mV/s (green) and 1000 mV/s (red) on the glassy carbon plate electrode. Black arrows indicates the evolution of the peak currents when the number of cycles increases. The potential window of the synthesis of the film at 1000 mV/s was increased with an upper limit set at +1.2 V.

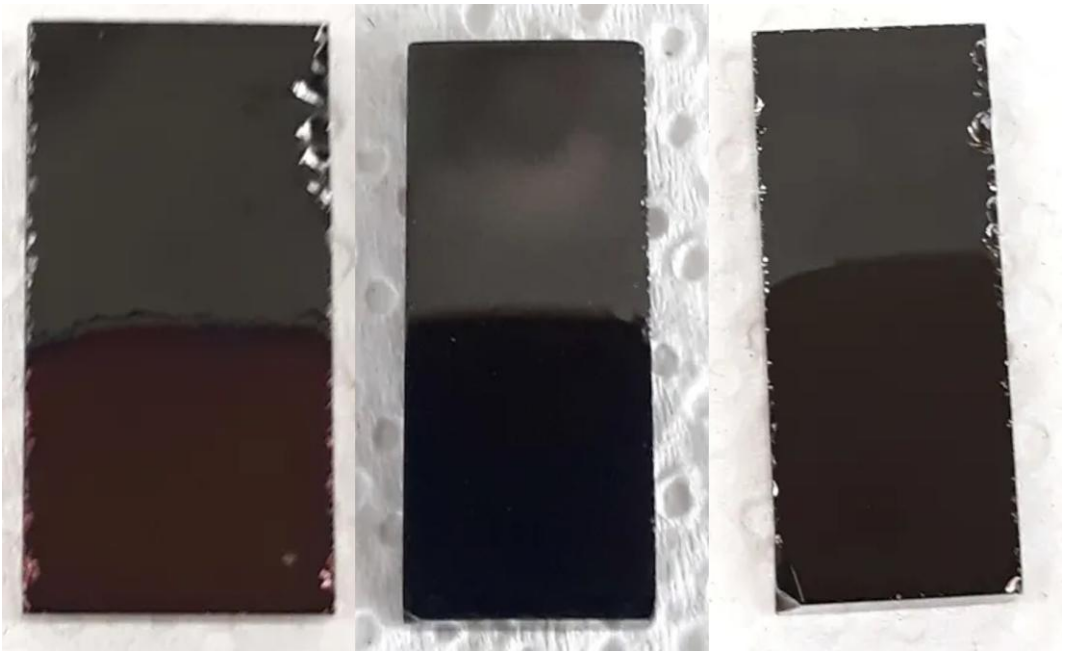

Figure 51. Pictures of the deposited films on carbon plate working electrodes after 25 CV cycles at 20 mV/s (a), 200 mV/s (b) and 1000 mV/s (c)

A significant shift of the oxidation peak potential is observed with the deposition on the plate electrodes, while the reduction peak potential is only slightly decreased. The shifts of the oxidation peak are equal to 193 mV at 20 mV/s, 264 mV at 200 mV/s and 600 mV at 1000 mV/s. The shift is more pronounced with higher scan rates. Furthermore, when the area of the deposition is controlled with a disc of 6 mm in diameter on the plate electrode (one face), the shift is almost not marked compared to the disc electrodes. Therefore, this shift is very unclear. Indeed, to the best of our knowledge, the surface area only impacts the current of the peak, not its potential position. All faces of the plate electrodes were polished and prepared equally, then the deposition should be similar on each face and that should not be the cause of the potential shift observed (from an overall heterogeneous deposition depending on the faces for instance). The geometry of the electrode's surface may have an impact but that is not known to our knowledge to create such huge potential shifts. Our main hypothesis consider effects from the electrical field lines due to the orientation of the working electrode. Figure 52 represents the 2 CV at 1000 mV/s on the

disc electrode (Figure 52a) and on the plate electrode (Figure 52b) and shows how the oxidation peak is shifted to higher potential values in the second case.

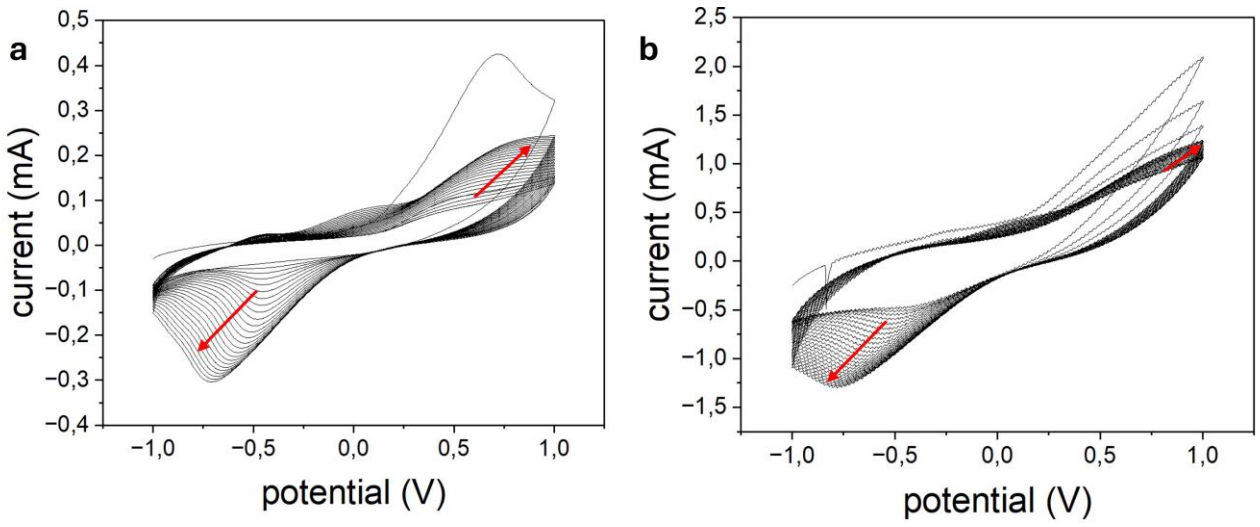

Figure 52. 25 CV cycles of 1,8-DHN at 1000 mV/s on (a) the disc electrode and on (b) the plate electrode. Red arrows indicate the direction of the evolution of the oxidation and reduction peaks.

Despite this unexpected observation, we decided to continue the investigation on the films obtained on the plate electrode and several characterizations were performed.

The TEM images are shown in Figure 53. Both the crystallinity proportion and the surface morphology looked different. None of the films were crystalline. The 3 films were completely amorphous according to the TEM images (Figure 53). This is in great contrast compared to the images obtained on the disc electrodes, where the films were partially crystalline. The surface presented a “grainy” feature, which was also not the case on the disc electrodes.

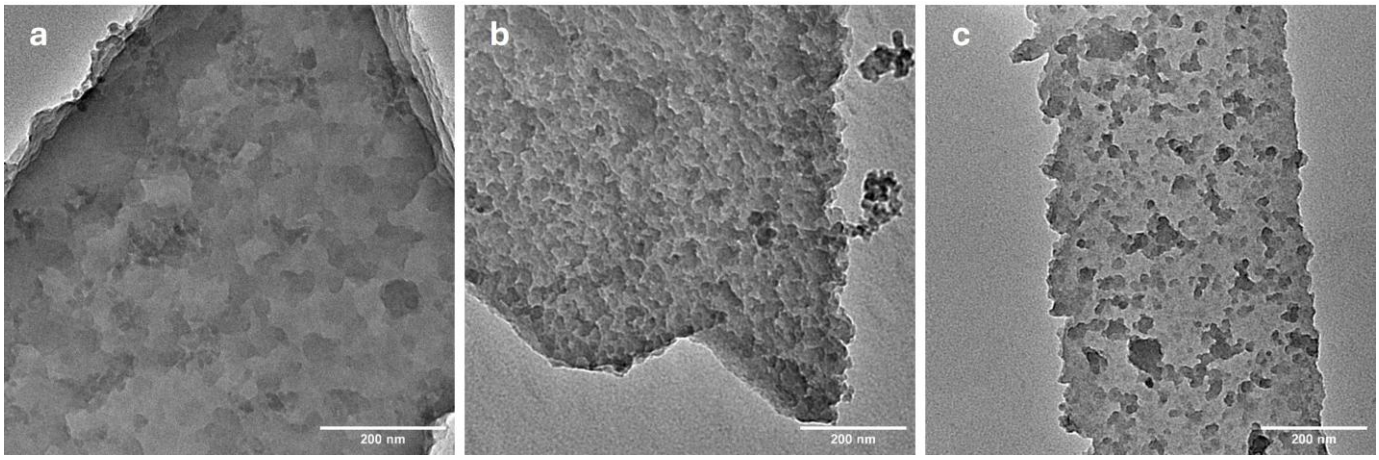

Figure 53. TEM images of the films removed from the plate electrodes after 25 CV cycles performed at (a) 20 mV/s, (b) 200 mV/s, and (c) 1000 mV/s. Scale bars represent 200 nm.

In order to look at the surface morphology and to investigate the thickness and roughness of the films, AFM and SEM measurements were performed. Unfortunately, the AFM machine was broken few days after the first measurement and is still under repairs, then only the measurement with the film prepared with 25 CV cycles at 20 mV/s was carried out. The corresponding AFM image is presented in Figure 54. The grainy appearance was observed again. The RMS roughness was 15 nm. This value is lower than the roughness measured on the film deposited on gold working electrodes. The SEM images (Figure 55) showed the same grainy surface. From the section of the film after a scratch was done, the thicknesses were determined equal to 250 ± 19 nm, 73 ± 9 nm and 43 ± 6 nm, respectively for the films prepared at 20, 200 and 1000 mV/s. The thicknesses obtained on the carbon plate electrodes are then lower than the thicknesses measured on the gold electrodes (Figure 26g). To see if the thickness can be increased by decreasing the scan rate of the electrodeposition (that means increasing the reaction time), a film was prepared with 25 CV cycles but at 5 mV/s. The obtained thickness was 542 ± 18 nm. Thus, confirming that the thickness could be increased by decreasing the scan rate to 5 mV/s.

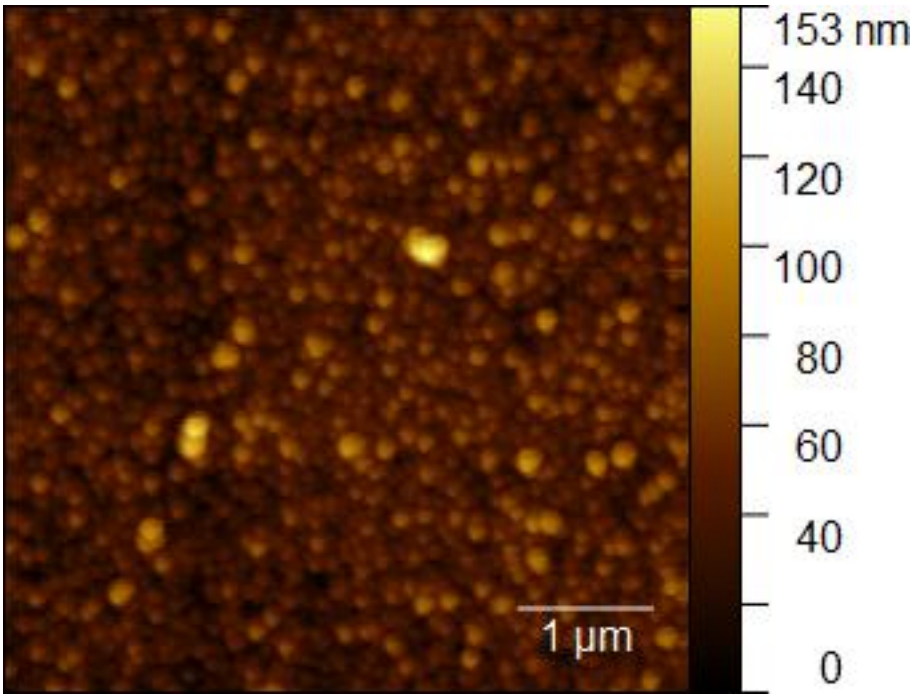

Figure 54. AFM image of the film prepared at 20 mV/s on a glassy carbon plate electrode.

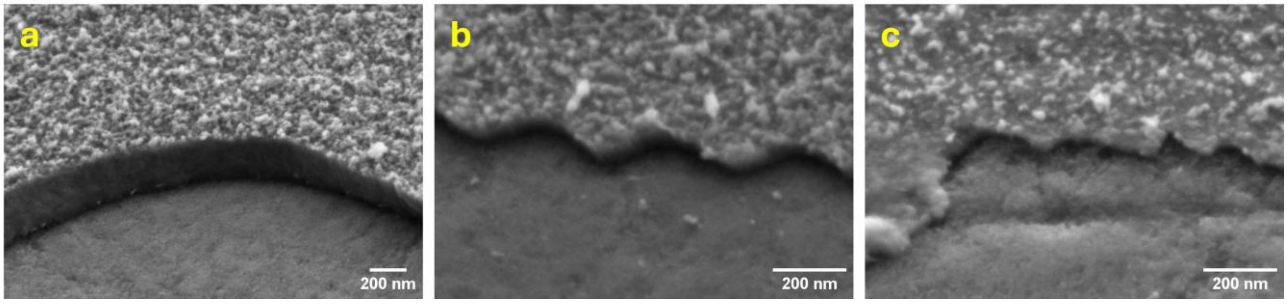

Figure 55. SEM images of the films prepared at (a) 20 mV/s, (b) 200 mV/s and (c) 1000 mV/s on the plate electrodes. Scale bars represent 200 nm.

The wettability of the obtained films was investigated by using a contact angle goniometer (Figure 56). The contact angles measured were similar to those obtained for depositions on gold electrodes. They were equal to 23 ± 1 °, 23 ± 1 ° and 21 ± 1 °, respectively for 20, 200 and 1000 mV/s, while the pristine carbon plate electrode showed an angle of 64 ± 1 °. This values strongly suggest a hydrophilic behavior of the films.

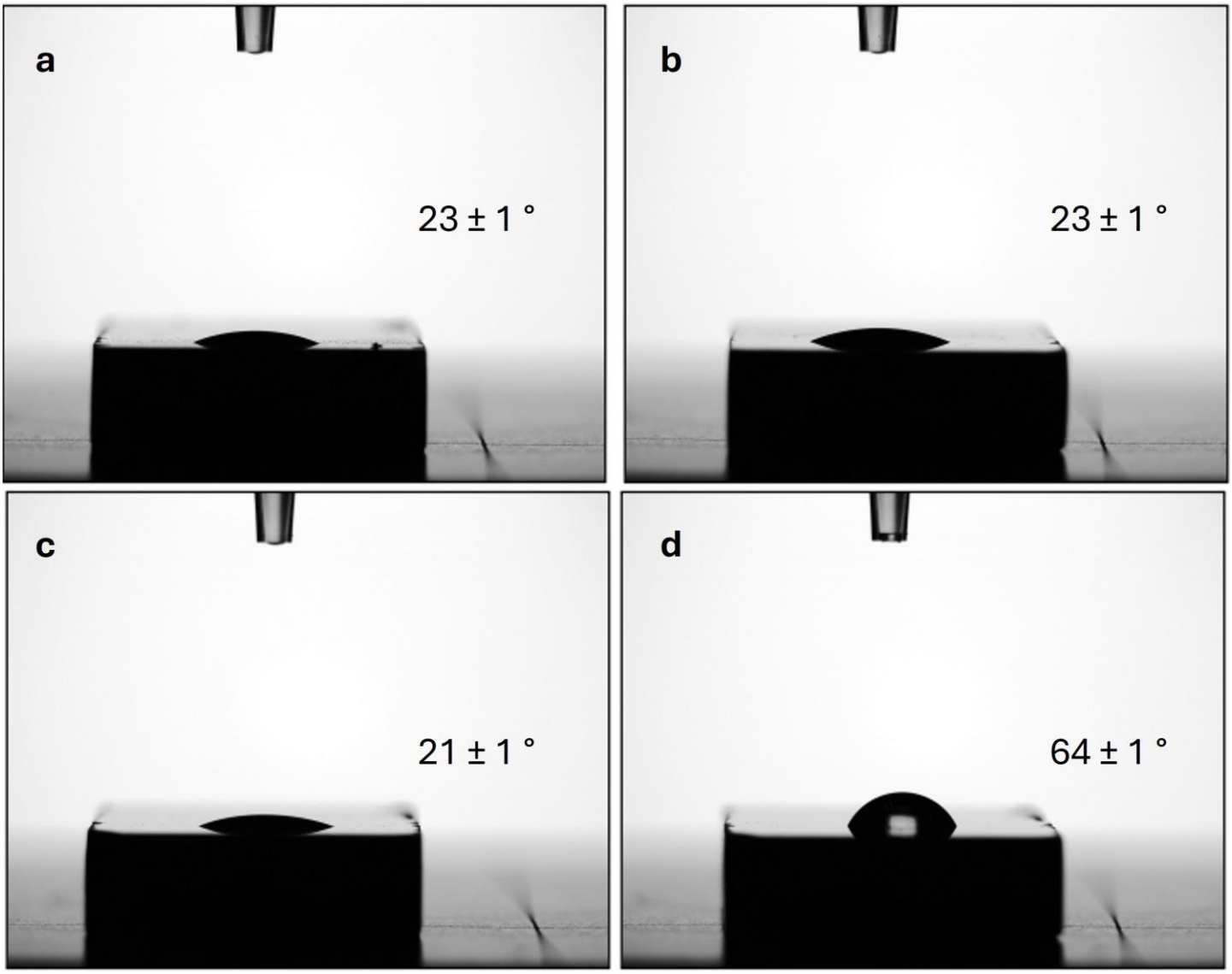

Figure 56. Pictures of water droplets (4µL) at 25 °C on the films deposited after 25 CV cycles at (a) 20 mV/s, (b) 200 mV/s and (c) 1000 mV/s and (d) on a pristine carbon plate electrode.

Raman spectroscopy (Figure 57) and XPS (Figure 58) characterizations were carried out to investigate the chemical composition of the films.

First, a measurement of the Raman spectrum was performed (Figure 57a) to distinguish potential electrode's features on the film's spectra. The electrode was stable enough to use a laser power of 2 mW . However, the films were not stable at all. Indeed, the signal increased significantly over the measurement time as it shown for the film at 1000 mV/s in

Figure 57b. This suggests a heating of the material. The optical binocular coupled with the Raman microscope confirmed the presence of holes where the laser was pointed at. That happened even with the lowest laser power available with this device (0.1 mW). Therefore, it is not surprising that the spectra obtained for the films correspond to the spectrum of the pristine electrode.

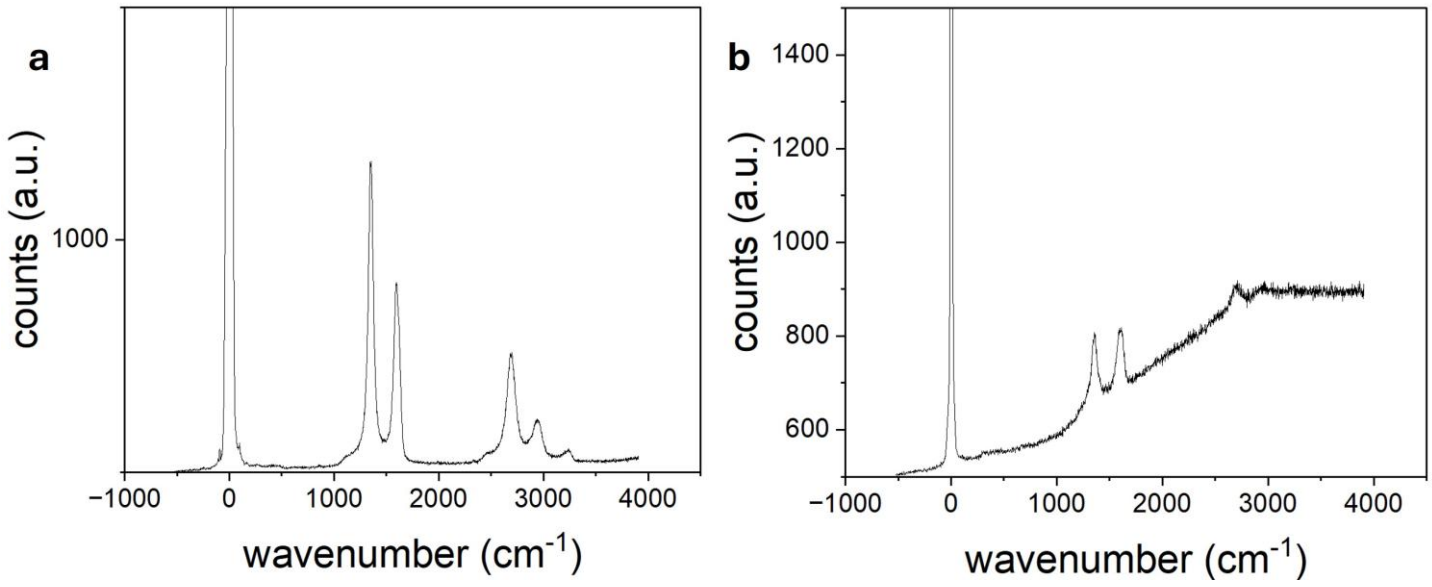

Figure 57. Raman spectra of (a) a pristine glassy carbon plate electrode and of (b) a 1,8-DHN-based film deposited at 1000 mV/s. The laser power was respectively 2 mW and 0.1 mW.

The theoretical C/O ratio of the 1,8-DHN precursor is equal to 5. XPS measurements determined similar ratios of 4.5, 4.4 and 4.3 for the films deposited at 20 mV/s, 200 mV/s, and 1000 mV/s, respectively. These ratios are lower than for the films obtained on gold electrodes. That indicates a slightly higher oxygen content compared to the depositions on gold (~ 5), but also compared to the precursor molecules. C 1s spectra of the three films (Figure 58) show the presence of both C=O groups (288.3 eV) and C-OH groups (286.3 eV). The C-OH/C=O ratio is between 10 and 11 according to the potential sweep rate used for the film deposition. This value is higher to the ratios obtained on gold substrates (~ 3), indicating a lower amount of carbonyl groups. As expected, the C 1s spectra also indicates

the presence of C-C bonds (284.7 eV). The results obtained by XPS indicate the presence of C=O and C-OH bonds and also aromatic rings. No carboxylic acid, ester or ether groups were found. This suggests that the aromatic rings are only connected via C-C bonds as it was observed for the deposition on gold electrodes.

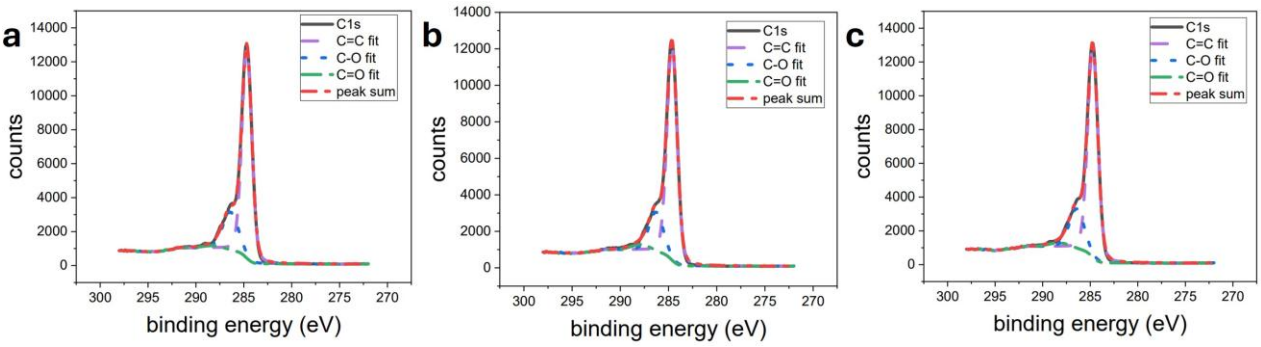

Figure 58. High resolution XPS C 1s spectra of the films deposited after 25 CV cycles (a) C 1s for the film at 20 mV/s, (b) C 1s for the film at 200 mV/s, and (c) C 1s for the film at 1000 mV/s.

The transfer method process used with films deposited on gold electrodes was reused without further modification with the films electrodeposited on the carbon plate electrodes. The transfer worked successfully and can allow applications on different substrates after the film was first deposited on glassy carbon electrodes.

5.3. Hybrid systems of 1,8-DHN and 2,5-DHP

1,8-DHN-based films showed interesting mechanical, biological and catalytic properties when deposited on gold electrodes. Despite it has not yet been confirmed for the deposition on carbon electrode, such promising properties are also expected. DHP-based films' properties were not extensively studied but the films are antioxidant and the N heteroatom in the aromatic ring may enable some catalytic efficiency and be used as metal-free catalysts. In order to study potential synergistic or enhanced behaviors of hybrid

films, few investigations were carried out, mainly to investigate the presence of nitrogen in the obtained material.

To produce these hybrid films from 1,8-DHN and 2,5-DHP, 3 different approaches were performed: the co-deposition of DHN and DHP, the successive deposition of DHN and then DHP, and the successive deposition of DHP and then DHN. In all cases, every precursor was used at 1 mg/mL in sodium acetate buffer and ethanol mixture with 25 CV cycles at 20 mV/s (a scan rate close to the optimal conditions for 2,5-DHP, Figure 11c) on the glassy carbon plate electrodes. A preliminary CV was performed with 2,5-DHP to evaluate the shift in potential on the plate electrodes. The oxidation peak was observed close to +1.2 V, then the potential window used for the hybrids was extended to +1.2 V for the upper limit, while the lower limit was unmodified (-1 V).

Figure 59 shows the CV curves obtained with the 3 different approaches. Figure 59a suggests that the co-deposition turns in favor of the deposition of 1,8-DHN. That is the same effect as observed with the mixtures of DHPs (section 3.5.), where the compound with the lower oxidation potential is predominantly oxidized. Figures 59b, c, d and e suggest different behaviors depending on the first molecule deposited and the second successively. As expected, the CV curves obtained for the first precursor (Figures 59b and d) correspond to the CV already studied for this precursor. However, the CV curves when the DHP is deposited after the DHN (Figure 59c) look like curves for the residual redox activity of the DHN film rather than the deposition curves of 2,5-DHP (Figure 59d). When the DHN is deposited after the DHP (Figure 59e), the CV curves obtained correspond to the curves of a deposition of 1,8-DHN. Therefore, only the CV curves from the third approach (DHP deposited before DHN) can surely suggest the presence of 2,5-DHP-based layers (and then nitrogen heteroatoms) in the hybrids.

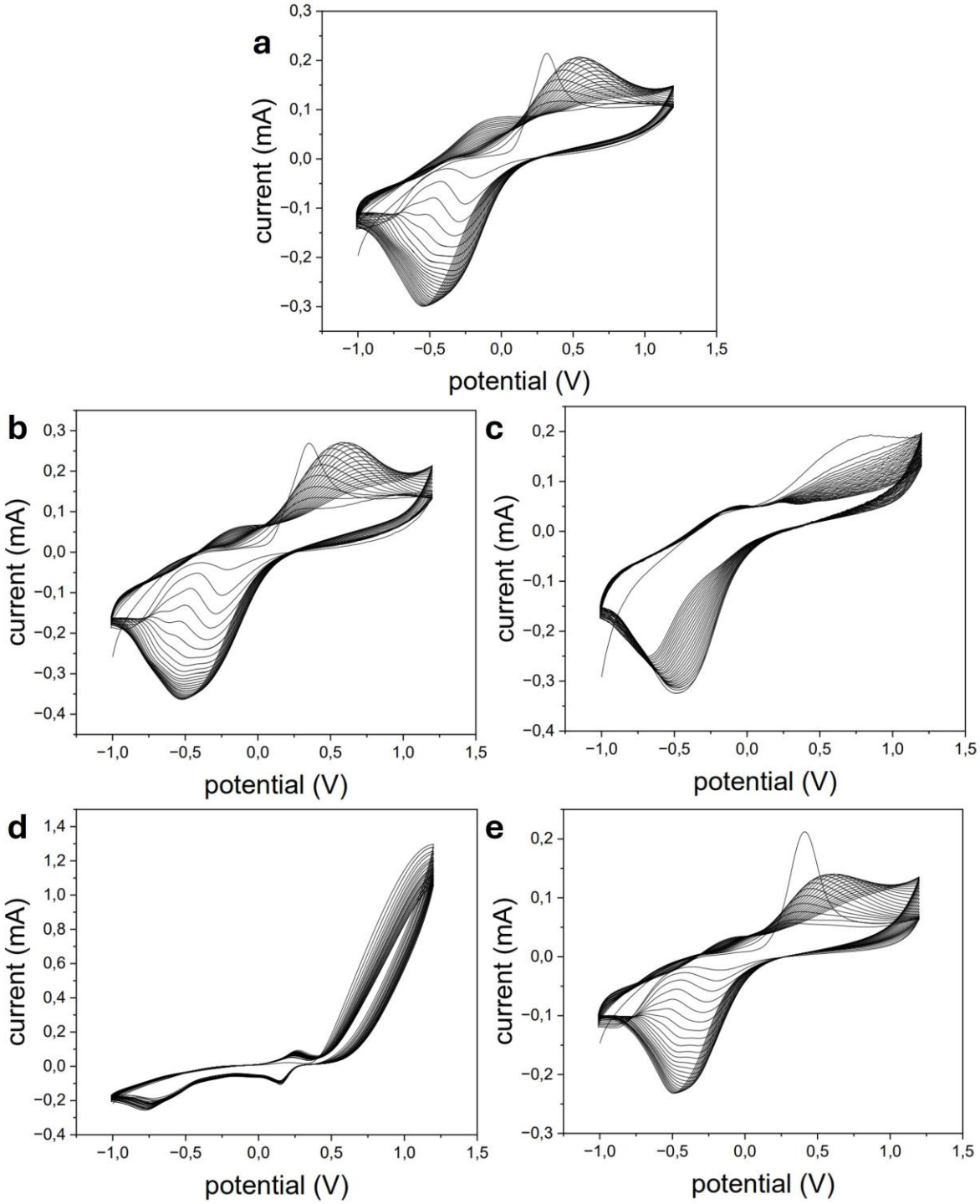

Figure 59. 25 CV cycles at 20 mV/s of (a) co-deposition of 1,8-DHN and 2,5-DHP each at 1 mg/mL, (b) a first deposition of 1,8-DHN at 1 mg/mL followed by (c) a deposition of 2,5-DHP at 1 mg/mL and (d) a first deposition of 2,5-DHP at 1 mg/mL followed by (e) a deposition of 1,8-DHN at 1 mg/mL. Every CV was performed between -1 V and +1.2 V.

SEM measurements were performed to investigate the presence of several layers and to carry out EDX (Energy-Dispersive X-rays spectroscopy, also called EDS) measurements for the detection of nitrogen.

Figure 60 shows the SEM images obtained for the 3 different approaches. None of the 3 hybrids showed distinguishable layers.

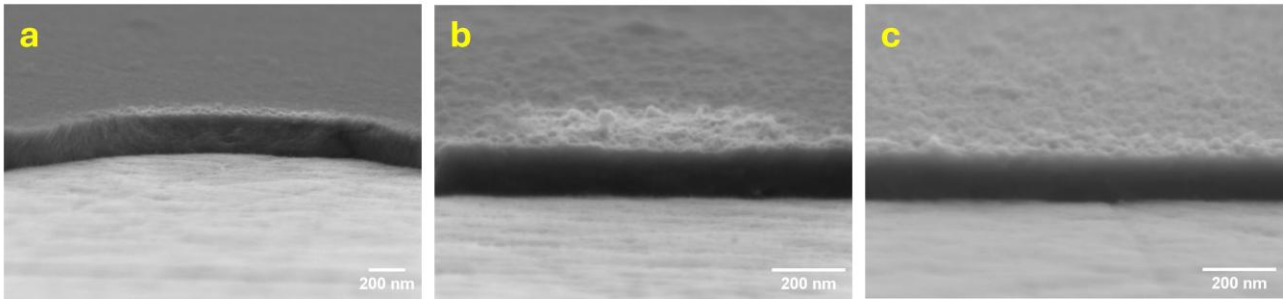

Figure 60. SEM images obtained with the hybrid films prepared via (a) co-deposition of 1,8-DHN and 2,5-DHP, (b) successive deposition of 1,8-DHN then 2,5-DHP and (c) successive deposition of 2,5-DHP then 1,8-DHN. Scale bars represent 200 nm.

Figure 61 presents the corresponding EDX spectra (Figure 61b, c and d) and the spectrum of the pristine carbon electrode (Figure 61a). As expected, the pristine electrode have only a carbon feature with a small oxygen content. For the 3 hybrid films, carbon and oxygen were detected as expected. Despite its maximum height is very close to the noise signal, a small amount of nitrogen was also qualitatively detected compared to the spectrum of the pristine electrode which is nitrogen-free. No quantifications were done, because of the mediocre fit performed by the software.

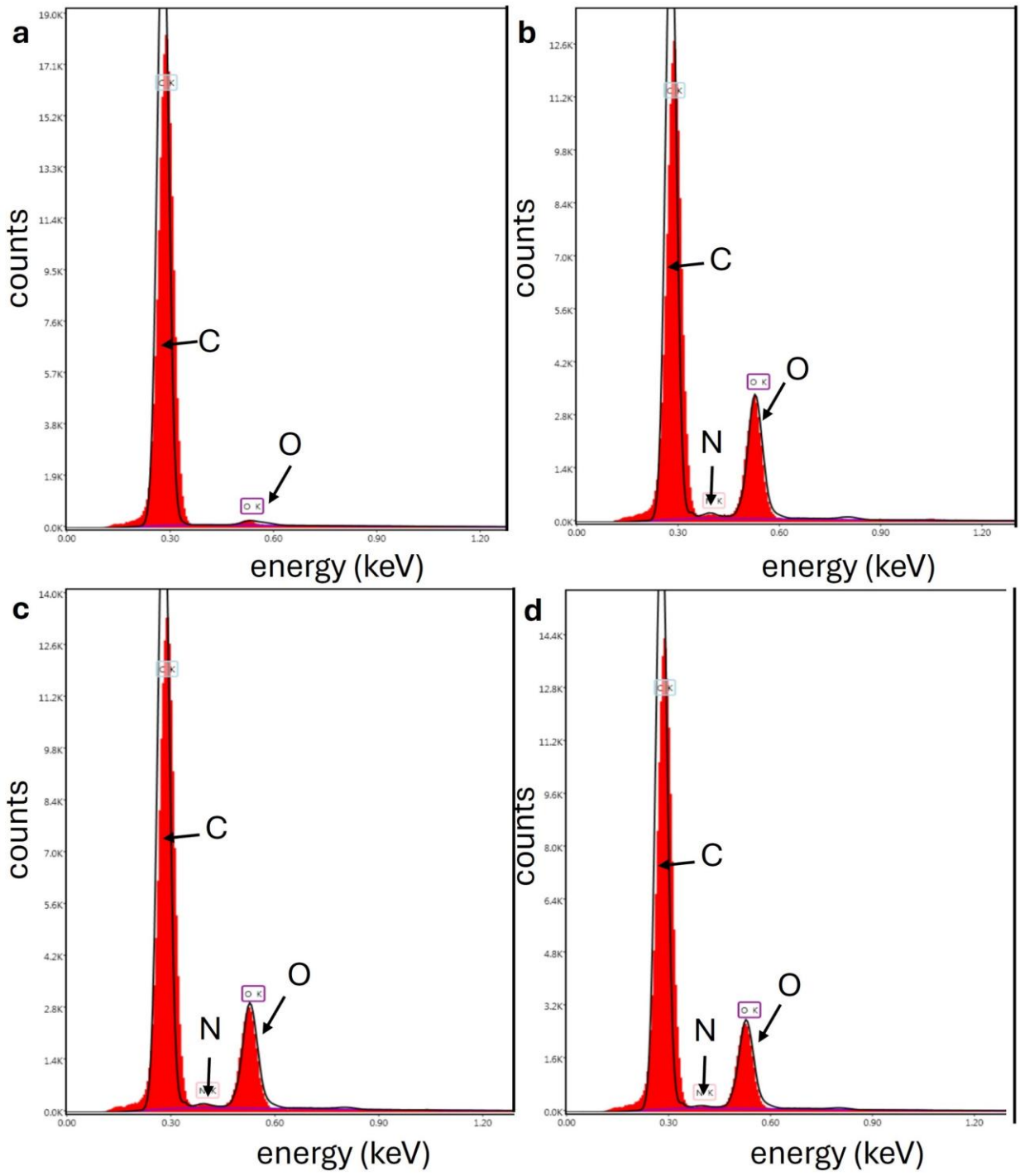

Figure 61. EDX spectra taken at 3 kV and a x500 magnification of (a) a pristine glassy carbon plate electrode, (b) the hybrid film prepared from the co-deposition of 1,8-DHN and 2,5-DHP, (c) the hybrid film prepared from the successive deposition of 1,8-DHN then 2,5-DHP and (d) the hybrid film prepared from the successive deposition of 2,5-DHP then 1,8-DHN.

Discussions

The electrodeposition of dihydroxypyridines and of 1,8-dihydroxynaphthalene led to the formation of films. A wide array of characterizations were performed on the obtained films to understand their structures, their properties and their mechanisms of formation.

Graphene oxide-like materials were obtained from dihydroxypyridines on glassy carbon electrodes. However, the 2,4-DHP did not lead to films in our potential window of experimental conditions. The crystallinity of the films is isomer- and scan rate-dependent. 2,3-DHP and 2,5-DHP films have lattice spacings close to the graphite, while 2,6-DHP is completely amorphous. The 3 films present an antioxidant activity, but their properties and potential applications must be studied in more detail in the future. For catalytic applications, N-doped materials are of high interest as metal-free catalysts[113] to replace transitions metals that are the standard materials currently but can present risks for the environment or human health.

The 1,8-DHN deposition on gold electrodes was intensively studied in this PhD work. The obtained materials are similar to polymers. They are amorphous and can swell. The thickness can be easily controlled by changing the scan rate, while their properties are relatively unmodified. The deposition by chronoamperometry has been a little studied as a first comparison to the CV method but will need a more detailed work in the future. To the best of our knowledge, the report of materials able to exhibit antioxidant properties not only at their surface but also in bulk is an unprecedented result. The combined antioxidant activity, antibacterial activity, mechanical properties, and high stability in many conditions suggest promising applications in biomedicine such as wound healing patches or protheses coatings. It is of great importance to investigate a potential anticorrosion activity in the future.

It is possible to include copper in the films. A great change in the electrochemical performances was observed and suggested that these materials are promising candidates for CO_2RR. However, their stability are greatly affected when copper is included. Further studies will be conducted in the future to improve the stability of these films. Only the co-deposition was tested. The deposition of the DHN-based film in a first time, followed by the deposition of copper (by CV or CA) in a second time, is an alternative method to achieve to deposit potentially more stable films including copper.

The 1,8-DHN deposited on glassy carbon shows surprising features, in particular the oxidation current evolution cycles after cycles. However, depending on the type of glassy carbon electrodes, the results were significantly different. This phenomenon will need further investigations in the future because it is not yet clear. The possibility to include copper nicely dispersed has been demonstrated but further catalytic assays will need to be performed. Investigations of properties for biomedical applications are also of great interest in the future, particularly if they differ from the deposition on gold substrates.

Despite the properties were widely studied, it is very unclear how the films grow and via which mechanism. These 2 pieces of information are the most important lacking elements of the work presented here. Despite the good estimation of the chemical composition of the films, the final chemical structure of the films is also relatively unknown. These lacking data are the most relevant investigations to perform in the future and will be the focus of another project.

The following measurements are ideas of perspectives to achieve some of the above future investigations. The ToF-SIMS measurement can be replaced with a MALDI-ToF measurement which causes less fragmentation and then can lead to a good identification of the chemical structure. *In situ* measurements can help to understand the growth of the

films. For instance, *in* situ TEM in an electrochemical cell, *in situ* Raman or infrared spectroscopies coupled with electrochemistry to follow the different steps of the synthesis, and particularly after the first CV cycles. Computational simulations (such as DFT – Density Functional Theory) are also of great interest to confirm our results and assumptions on the obtained materials and mechanisms.

General conclusions

Carbon-based films were obtained through an electrodeposition of polyphenol-related biogenic monomers using cyclic voltammetry.

The technique of cyclic voltammetry allows a reproducible film synthesis and a great control of the thickness of the obtained material. The working conditions in aqueous media, with relatively low potential range and biogenic monomers make this project of great interest to work in “green chemistry” conditions to reduce the impact on the environment.

The electrodeposition of dihydroxypyridines was successful. Like a previous study on pyrocatechol, the deposition into graphene oxide-like materials on glassy carbon electrodes was achieved. The influence of the isomer used as well as the influence of the scan rate chosen were demonstrated.

The electrodeposition of dihydroxynaphthalene was successful on both gold and glassy carbon electrodes. While the scan rate is not very impactful on the deposition on gold electrodes, it has a significant effect on the deposition on the glassy carbon disc electrodes. We demonstrated that the obtained films on gold have promising properties for biomedical and electrocatalysis applications for instance, while the films on glassy carbon still need some additional studies.

However, the mechanisms of these electrodepositions is still not yet clear. Further investigations will be performed in the future to increase the understanding of these film formations and the chemical structure of the obtained materials.

All the films presented antioxidant properties. The films based on 1,8-DHN also has promising mechanical properties and an antibacterial activity. The presence of nitrogen or

copper complexes may enable catalytic properties in CO_2RR. The applications for such materials include different scientific fields such as biomedicine, energy storage or electrocatalysis. Their ability to get transferred to different substrates allows broader perspectives.

References

(1) Eftekhari, A.; Jafarkhani, P. Polymerization of Aniline through Simultaneous Chemical and Electrochemical Routes. *Polymer J.*, **2006**, 38, 651-658.

(2) Musiani, M. M.; Mengoli, G.; Furlanetto, F. Improved Polyaniline Coatings by In Situ Electropolymerization. *Journal of Applied Polymer Science*, **1984**, 29, 4433-4438.

(3) Saidman, S. B.; Vela, M. E. Electropolymerization of Pyrrole onto Aluminium from Alkaline Solutions Containing a Surfactant. *Thin Solid Films*, **2005**, 493, 96-103.

(4) Ryan, E. M.; Breslin, C. B.; Moulton, S. E.; Wallace, G. G. The Effect of Dopant pK_a and the Solubility of Corresponding Acid on the Electropolymerisation of Pyrrole. *Electrochimica Acta*, **2013**, 92, 276-284.

(5) Wang, X.; Shi, G.; Liang, Y. Low Potential Electropolymerization of Thiophene at a Copper Oxide Electrode. *Electrochem. Comm.*, **1999**, 1, 536-539.

(6) Krische, B.; Zagorska, M. Polythiophene Synthesis by Electropolymerization of Thiophene and Bithiophene. *Synthetic Metals*, **1989**, 33, 257-267.

(7) Diaz, A. F.; Logan, J. A. Electroactive Polyaniline Films. *J. Electroanal. Chem.*, **1980**, 111, 111-114.

(8) Chiang, J. C.; MacDiarmid, A. G. 'Polyaniline': Protonic Acid Doping of the Emeraldine Form to the Metallic Regime. *Synth. Met.*, **1986**, 13, 193-205.

(9) Xia, Y. N.; Wiesinger, J. M.; MacDiarmid, A. G.; Epstein, A. J. Camphorsulfonic Acid Fully Doped Polyaniline Emeraldine Salt: Conformations in Different Solvents Studied by

an Ultraviolet/Visible/Near-Infrared Spectroscopic Method. *Chem. Mater.*, **1995**, 7, 443-445.

(10) Levi, M. D.; Lopez, C.; Vieil, E.; Vorotyntsev, M. A. Influence of Ionic Size on the Mechanism of Electrochemical Doping of Polypyrrole Films Studied by Cyclic Voltammetry. *Electrochimica Acta*, **1997**, 42, 757.

(11) Gileadi, E. *Physical Electrochemistry. Fundamentals, techniques and applications.* Wiley-VCH, **2011**, chapter 4.

(12) Van Benschoten, J. J.; Lewis, J. Y.; Heineman, W. R.; Roston, D. A.; Kissinger, P. T. Cyclic Voltammetry Experiment. *J. Chem. Educ.*, **1783**, 60, 772.

(13) Ball, V. *Self-Assembly Processes at Interfaces: Multiscale Phenomena*. Interface Science and Technology, Elsevier, **2017**, chapter 3.

(14) Kissinger, P. T.; Heineman, W. R. Cyclic Voltammetry. *J. Chem. Educ.*, **1783**, 60, 702.

(15) Elgrishi, N.; Rountree, K. J.; McCarthy, B. D.; Rountree, E. S.; Eisenhart, T. T.; Dempsey, J. L. A Practical Beginner's Guide to Cyclic Voltammetry. *J. Chem. Educ.*, **2018**, 95, 197-206.

(16) Gileadi, E. *Physical Electrochemistry. Fundamentals, Techniques and Applications.* Wiley-VCH, **2011**, chapter 15.

(17) Terranova, M. L.; Tamburri, E. Understanding the Way Eumelanin Works: A Unique Example of Properties and Skills Driven by Molecular Heterogeneity. *Polymer*, **2021**, 229, 123952.

(18) Pezella, A.; Crescenzi, O.; Panzella, L.; Napolitano, A.; Land, E. J.; Barone, V.; d'Ischia, M. Free Radical Coupling of *o*-Semiquinones Uncovered. *J. Am. Chem. Soc.*, **2013**, 135, 12142-12149.

(19) Voisin, E.; Williams, V. E. Do Catechol Derivatives Polymerize? *Macromolecules*, **2008**, 41, 2994-2997.

(20) Quynh, B. T. P.; Byun, J. Y.; Kim, S. H. Electrochemical Behavior of Aromatic Compounds on Nanoporous Gold Electrode. *Journal of the Electrochemical Society*, **2018**, 165, B414-B421.

(21) Saito, K.; Sun, G.; Nishide, H. Green Synthesis of Soluble Polyphenol: Oxidative Polymerization of Phenol in Water. *Green Chemistry Letters and Reviews*, **2007**, 1, 47-51.

(22) Iotov, P. I.; Kalcheva, S. V. Mechanistic Approach to the Oxidation of Phenol at a Platinum/Gold Electrode in an Acid Medium. *Journal of Electroanalytical Chemistry*, **1998**, 442, 19-26.

(23) Mosa, J.; Fontaine, O.; Ferreira, P.; Borges, R. P.; Vivier, V.; Grosso, D.; Laberty-Robert, C.; Sanchez, C. Synthesis of Poly(Phenylene Oxide)-Based Fluoro-Tin-Oxide/ZrO_2 Nanoelectrode Arrays by Hybrid organic/inorganic Approach. *Electrochimica Acta*, **2011**, 56, 7155-7162.

(24) Szewczyk, J.; Aguilar-Ferrer, D.; Coy, E. Polydopamine Films: Electrochemical Growth and Sensing Applications. *Eur. Polym. J.*, **2022**, 174, 111346.

(25) Wang, Y.; Wang, J.; Jiao, Y.; Chen, K.; Chen, T.; Wu, X.; Jiang, X.; Bu, W.; Liu, C.; Qu, X. Redox-Active Polyphenol Nanoparticles Deprive Endogenous Glutathione of

Electrons for ROS Generation and Tumor Chemodynamic Therapy. *Acta Biomaterialia*, **2023**, 172, 423-440.

(26) United States Environmental Protection Agency, https://www.epa.gov/greenchemistry/basics-green-chemistry, (accessed January 2024).

(27) Karapinar D.; Creissen, C. E.; Rivera de la Cruz, J. G.; Schreiber, M. W.; Fontecave, M. Electrochemical CO_2 Reduction to Ethanol with Copper-Based Catalysts. *ACS Energy Lett.*, **2021**, 6, 694-706.

(28) Soriaga, M. P.; Stickney, J. L.; Hubbard, A. T. Electrochemical Oxidation of Aromatic Compounds Adsorbed on Platinum Electrodes. *J. Electroanal. Chem.*, **1983**, 144, 207-215.

(29) Varmaghani, F.; Nematollahi, D. Electrochemically Induced Oxidative Cyclization of 2,3-dihydroxypyridine. Synthesis of a Novel Highly Oxygenated Heterocyclic Compound. *J. Phys. Org. Chem.*, **2012**, 25, 511-514.

(30) Curtis, K. E.; Atkinson, G. F. Equilibrium Constants for 2,3-dihydroxypyridine and its Complex with Iron(III) in 1M Hydrochloric Acid. *Can. J. Chem.*, **1972**, 50, 1649-1654

(31) Spinner, E.; White, J. C. B. Spectral and Ionisation Constant Studies of Substituted 2-hydroxypyridines (1,2-dihydro-2-oxopyridines). *J. Chem. Soc. B*, **1966**, 991-995.

(32) Lino, L.; Manini, P. Dihydroxynaphthalene-Based Allomelanins: A Source of Inspiration for Innovative Technological Materials. *ACS Omega*, **2022**, 7, 15308-15314

(33) Mavridi-Printezi, A.; Mollica, F.; Lucernati, R.; Montalti, M.; Amorati, R. Insight into the Antioxidant Activity of 1,8-Dihydroxynaphthalene Allomelanin Nanoparticles. *Antioxidants*, **2023**, 12, 1511.

(34) Manini, P.; Lino, V.; D'Errico, G.; Reale, S.; Napolitano, A.; De Angelis, F.; d'Ischia, M. "Blackness" is an Index of Redox Complexity in Melanin Polymers. *Polym. Chem.*, **2020**, 11, 5005.

(35) Svoboda, J.; Král, M.; Dendisová, M.; Matějka, P.; Pop-Georgievski, O. Unraveling the Influence of Substrate on the Growth Rate, Morphology and Covalent Structure of Surface Adherent Polydopamine Films. *Colloids and Surfaces B: Biointerfaces*, **2021**, 205, 111897.

(36) Bejerano, T.; Forgacs, Ch.; Gileadi, E. Selective Inhibition of Electrode Reactions by Organic Compounds: I. The Inhibition of Br_2 and I_2 Evolution on Platinum by Phenol. *Electroanal. Chem. Interf. Electrochem.*, **1970**, 27, 69-79.

(37) Eom, T.; Lee, J.; Lee, S.; Ozlu, B.; Kim, S.; Matin, D. C.; Shim, B. S. Highly Conductive Polydopamine Coatings by Direct Electrochemical Synthesis on Au. *ACS Appl. Polym. Mater.*, **2022**, 4, 5319-5329.

(38) Li, S.; Wang, H.; Young, M.; Xu, F.; Cheng, G.; Cong, H. Properties of Electropolymerized Dopamine and its Analogues. *Langmuir*, **2019**, 35, 1119-1125.

(39) Vatrál, J.; Boča, R.; Linert, W. Oxidation Properties of Dopamine At and Near Physiological Conditions. *Monatschefte für Chemie – Chemical Monthly*, **2015**, 146, 1799-1805.

(40) Stöckle, B.; Ng, D. Y. W.; Meier, C.; Paust, T.; Bischoff, F.; Diemant, T.; Behm, R. J.; Gottschalk, K. E.; Ziener, U.; Weil, T. Precise Control of Polydopamine Film Formation by Electropolymerization. *Macromol. Symp.*, **2014**, 346, 73.

(41) Bernsmann, F.; Voegel, J.-C.; Ball, V. Different Synthesis Methods Allow to Tune the Permeability and Permselectivity of Dopamine-Melanin Films to Electrochemical Probes. *Electrochimica Acta*, **2011**, 56, 3914-3919.

(42) Li, Y.; Liu, M.; Xiang, C.; Xie, Q.; Yao, S. Electrochemical Quartz Crystal Microbalance Study on Growth and Property of the Polymer Deposit at Gold Electrodes During Oxidation of Dopamine in Aqueous Solutions. *Thin Solid Films*, **2006**, 497, 270-278.

(43) Ball, V. Electrodeposition of Pyrocatechol Based Films: Influence of Potential Scan Rate, Pyrocatechol Concentration and pH. *Colloids & Surf. A: Physicochem. Eng. Aspects*, **2017**, 518, 109-115.

(44) In Gyun, K.; Nam, Y. J.; Ahn, H. J.; Jung, D.-Y. Electrochemical Growth of Synthetic Melanin Thin Films by Constant Potential Methods. *Electrochimica Acta*, **2011**, 56, 2954-2959.

(45) González Orive, A.; Gimeno, Y.; Hernández Creus, A.; Grumelli, D.; Vericat, C.; Benitez, G.; Salvarezza, R. C. Electrochemical Preparation of Metal-Melanin Functionalized Graphite Surfaces. *Electrochimica Acta*, **2009**, 54, 1589-1596.

(46) Ball, V.; Alfieri, M. L.; Ziegler, K.; Arntz, Y.; d'Ischia, M. Structure-Controlled Electrodeposition and Electrochemical Behavior of Films from Isomeric Diphenols at the Solid-Liquid Interface. *Surf. & Interf.*, **2022**, 30, 101841.

(47) Ortiz Peña, N.; Ihiawakrim, D.; Ball, V.; Stanescu, S.; Rastei, M.; Sanchez, C.; Portehault D.; Ersen, O. Correlative Microscopy Insight on Electrodeposited Ultrathin Graphite Oxide Films. *J. Phys. Chem. Lett.*, **2020**, 11, 9117-9122.

(48) Ngamchuea, K.; Tharat, B.; Hirunsit, P.; Suthirakun, S. Electrochemical Oxidation of Resorcinol: Mechanistic Insights from Experimental and Computational Studies. *RSC Advances*, **2020**, 10, 28454-28463.

(49) Pourghobadi, R.; Nematollahi, D.; Reza Baezzat, M.; Alizadeh, S.; Goljani, H. Electropolymerization of Catechol on Wireless Graphite Electrode. Unusual Cathodic Pyrocatechol Formation. *J. Electroanal. Chem.*, **2020**, 866, 114180.

(50) Lopes da Silva, A. R.; dos Santos, A. J.; Martínez-Huitle, C. A. Electrochemical Measurements and Theoretical Studies for Understanding the Behavior of Catechol, Resorcinol on the Boron Doped Diamand Surface. *RSC Adv.*, **2018**, 8, 3483-3492.

(51) Huynh, M. T.; Anson, C. W.; Cavell, A.C.; Stahl, S. S.; Hammes-Schiffer, S. Quinone 1e- and 2e-/2H+ Reduction Potentials: Identification and Analysis of Deviations from Systematic Scaling Relationships. *J. Amer. Chem. Soc.*, **2016**, 138, 15903-15910.

(52) Barham, A. S.; Kennedy, B. M.; Cunnane, V. J.; Daous, M. A. The Electrochemical Polymerisation of 1,2-dihydroxybenzene and 2-hydroxybenzyl alcohol Prepared in Different Solutions Media. *Electrochimica Acta*, **2014**, 147, 19-24.

(53) Enache, T. A.; Oliveira-Brett, A. M. Phenol and *para*-Substituted Phenols Electrochemical Oxidation Pathways. *J. Electroanal. Chem.*, **2011**, 655, 9-16.

(54) Antonietti, M.; Oschatz, M. The Concept of “Noble, Heteroatom-Doped Carbons,” Their Directed Synthesis by Electronic Band Control of Carbonization, and Applications in Catalysis and Energy Materials. *Adv. Mater.*, **2018**, 30, 1706836.

(55) Gui, J. Y.; Stern, D. A.; Lin, C.-H.; Cao, P.; Hubbard, A. T. Potential Dependent Surface Chemistry of Hydroxypyridines Adsorbed at a Pt(111) Electrode Studied by

Electron Energy Loss Spectroscopy, Low Energy Electron Diffraction, Auger Electron Spectroscopy, and Electrochemistry. *Langmuir*, **1991**, 7, 3183-3189.

(56) Soriaga, M. P.; Hubbard, A. T. Determination of the Orientation of Adsorbed Molecules at Solid-Liquid Interfaces by Thin Layer Electrochemistry: Aromatic Compounds at Platinum Electrodes. *J. Amer. Chem. Soc.*, **1982**, 104, 2735-2742.

(57) Nakano, H.; Wieser, M.; Burt, B.; Kawai, T.; Yoshida, T.; Nagasawa, T. Purification, Characterization and Gene Cloning of 6-hydroxynicotinate-3-monooxygenase from Pseudomonas Fluorescens TN5. *Eur. J. Beachem.*, **1999**, 260, 120-126.

(58) Blois, M. S. Antioxidant Determinations by the Use of a Stable Free Radical. *Nature*, **1958**, 1199-1200.

(59) Gileadi, E. *Physical Electrochemistry. Fundamentals, Techniques and Applications*. Wiley-VCH, Weinheim, **2011**, chapter 16.

(60) Zubavichus, Y.; Zharnikov, M.; Yang, Y.; Fuchs, O.; Umbach, E.; Heske, C.; Ulman, A.; Grunze, M. X-ray-photoelectron Spectroscopy and Near-Edge X-ray Absorption Fine Structure Study of Water Absorption on Pyridine-terminated Thiolate Self-assembled Monolayers. *Langmuir*, **2004**, 20, 11022-11029.

(61) Alfieri, M. L.; Micillo, R.; Panzella, L.; Crescenzi, O.; Oscurato, S. L.; Maddalena, P.; Napolitano, A.; Ball, V.; d'Ischia, M. Structural Basis of Polydopamine Film Formation: Probing 5,6-Dihydroxyindole-Based Eumelanin Type Units and the Porphyrin Issue. *ACS Appl. Mater. Interf.*, **2018**, 10, 7670-7680.

(62) Dangles, O. Antioxidant Activity of Plant Phenols: Chemical Mechanisms and Biological Significance. *Curr. Org. Chem.*, **2012**, 16, 692-714.

(63) Almeida, L. C.; Correia, J. P.; Viana, A. S. Electrochemical and Optical Characterization of Thin Polydopamine Films on Carbon Surfaces for Enzymatic Sensors. *Electrochim. Acta*, **2018**, 263, 480-489.

(64) Cecchini, M. M.; Reale, S.; Manini, P.; d'Ischia, M.; De Angelis, F. Modeling Fungal Melanin Buildup: Biomimetic Polymerization of 1,8-Dihydroxynaphthalene Mapped by Mass Spectroscopy. *Chem. Eur. J.*, **2017**, 23, 8092-8098.

(65) Liu, Y.; Ai, K.; Lu, L. Polydopamine and Its Derivative Materials: Synthesis and Promising Applications in Energy, Environmental, and Biomedical Fields. *Chem. Rev.*, **2014**, 114, 5057-5115.

(66) Lopes, R. C.F.G.; Rocha, B. G.M.; Maçôas, E. M.S.; Marques, E. F.; Martinho, J. M.G. Combining Metal Nanoclusters and Carbon Nanomaterials: Opportunities and Challenges in Advanced Nanohybrids. *Adv. Colloid Interf. Sci.*, **2022**, 304, 102667.

(67) Vecchia, N. F. D.; Luchini, A.; Napolitano, A.; D'Errico, G.; Vitiello, G.; Szekely, N.: d'Ischia, M.; Paduano, L. Tris Buffer Modulates Polydopamine Growth, Aggregation, and Paramagnetic Properties. *Langmuir*, **2014**, 30, 9811-9818.

(68) Pezella, A.; Barra, M.; Musto, A.; Navarra, A.; Alfè, M.; Manini, P.; Parisi, S.; Cassinese, A., Criscuolo V. and d'Ischia M. Stem Cell-Compatible Eumelanin Biointerface Fabricated by Chemically Controlled Solid State Polymerization. *Mater. Horiz.*, **2015**, 2, 212.

(69) Bogeat, A. B. Understanding and Tuning the Electrical Conductivity of Activated Carbon: A State-of-the-Art Review. *Crit. Rev. Solid. State Mater Sci.*, **2021**, 46, 1-37.

(70) Jerigová, M.; Odziomek, M.; López-Salas, N. “We are here!” Oxygen Functional Groups in Carbons for Electrochemical Applications. *ACS Omega,* **2022**, 7, 11544-11554.

(71) Al-Gaashani, R.; Najjar, A.; Zakaria, Y.; Mansour, S.; Atieh, M. A. XPS and Structural Studies of High Quality Graphene Oxide and Reduced Graphene Oxide Prepared by Different Chemical Oxidation Methods. *Ceramics Intern.*, **2019**, 45, 14439-14448.

(72) Coskun, H.; Aljabour, A.; De Luna, P.; Farka, D.; Greunz, T.; Stifter, D.; Kus, M.; Zheng, X.; Liu, M.; Stadler, P. *et al*. Biofunctionalized Conductive Polymers Enable Efficient CO_2 Electroreduction. *Sci. Adv.*, **2017**, 3, e1700686.

(73) Kennedy, B.; Glidle, A.; Cunnane, V. J. A Study of the Oxidation and Polymerisation of Meta Substituted Phenol and Aniline Derivatives. *J. Electroanal. Chem.,* **2007**, 608, 22-30.

(74) Coskun, H.; Aljabour, A.; Uiberlacker, L.; Strobel, M.; Hild, S.; Cobet, C.; Farka, D.; Stadler, P.; Sariciftci, N. S. Chemical Vapor Deposition-Based Synthesis of Conductive Polydopamine Thin-Films. *Thin Solid Films*, **2018**, 645, 320-325.

(75) Kim, I. G.; Nam, H. J.; Ahn, H. J.; Jung, D.-Y. Electrochemical Growth of Synthetic Melanin Thin Films by Constant Potential Methods. *Electrochim. Acta,* **2011**, 56, 2954-2959.

(76) Alfieri, M. L.; Panzella, L.; Arntz, Y.; Napolitano, A.; Ball, V.; d’Ischia, M. A Clean and Tunable Mussel-Inspired Coating Technology by Enzymatic Deposition of Pseudo-Polydopamine (Ψ-PDA) Thin Films from Tyramine. *Int. J. Mol. Sci.*, **2020**, 21, 4873.

(77) Zhou, X.; McCallum, N. C.; Hu, Z.; Cao, W.; Gnanasekaran, K.; Feng, Y.; Stoddart, J. F.; Wang, Z.; Gianneschi, N. C. Artificial Allomelanin Nanoparticles. *ACS Nano*, **2019**, 13, 10980-10990.

(78) McCallum, N. C.; Son, F. A.; Clemons, T. D.; Weigand, S. J.; Gnanasekaran, K.; Battistella, C.; Barnes, B. E.; Abeyratne-Perera, H.; Siwicka, Z. E.; Gianneschi, N. C. *et al*. Allomelanin: A Biopolymer of Intrinsic Microporosity. *J. Am. Chem. Soc.*, **2021**, 143, 4005-4016.

(79) United Nations – Regional Information Centre For Western Europe, https://unric.org/en/sdg12/#:~:text=Goal%2012%3A%20Ensure%20sustainable%20consumption,destructive%20impacts%20on%20the%20planet., (accessed January 2024).

(80) Manini, P.; Bietti, M.; Galeotti, M.; Salamone, M.; Lanzalunga, P.; Cecchini, M. M.; Reale, S.; Crescenzi, O.; Napolitano, A.; D'Ischia, M. *et al*. Characterization and fate of Hydrogen-Bonded Free-Radical Intermediates and Their Coupling Products from the Hydrogen Atom Transfer Agent 1,8-Naphthalenediol. *ACS Omega*, **2018**, 3, 3918-3927.

(81) Manini, P.; Lucci, V.; Lino, V.; Sartini, S.; Rossella, F.; Falco, G.; Chiappe, C.; d'Ischia, M. Synthetic Mycomelanin Thin Films as Emergent Bio-Inspired Interfaces Controlling the Fate of Embryonic Stem Cells. *J. Mater. Chem. B*, **2020**, 8, 4412.

(82) El Yakhlifi, S.; Alfieri, M. L.; Arntz, Y.; Eredia, M.; Ciesielski, A.; Samorì, P.; d'Ischia, M.; Ball, V. Oxidant-Dependent Antioxidant Activity of Polydopamine Films: The Chemistry-Morphology Interplay. *Colloids & Surf. A: Physicochem. Eng. Aspects*, **2021**, 614, 126134.

(83) Stover, C. K.; Pham, X. Q.; Erwin, A. L.; Mizoguchi, S. D.; Warrener, P.; Hickey, M. J.; Brinkman, F. S. L.; Hufnagle, W. O.; Kowalik, D. J.; Olson, M. V. *et al*. Complete Genome

Sequence of *Pseudomonas aeruginosa* PAO1, an Opportunistic Pathogen. *Nature*, **2000**, 406, 959-964.

(84) He, J.; Baldini, R. L.; Déziel, E.; Saucier, M.; Zhang, Q.; Liberati, N. T.; Lee, D.; Urbach, J.; Goodman, H. M.; Rahme, L. G. The Broad Host Range Pathogen *Pseudomonas aeruginosa* Strain PA14 Carries Two Pathogenicity Islands Harboring Plant and Animal Virulence Genes. *PNAS*, **2004**, 101, 2530-2535.

(85) O'Toole, G. A. Microtiter Dish Biofilm Formation Assay. *J. Vis. Exp.* **2011**, 47, e2437.

(86) Polash, S. A.; Hamza, A.; Hossain, M.; Dekiwadia, C.; Saha, T.; Shukla, R.; Bansal, V.; Sarker, S. R. Lactoferrin Functionalized Concave Cube Au Nanoparticles as Biocompatible Antibacterial Agent. *OpenNano*, **2023**, 12, 100163.

(87) Sarker, S. R.; Polash, S. A.; Karim, N.; Saha, T.; Dekiwadia, C.; Bansal, V.; Sabri, Y.; Kandjani, A. E.; Bhargava, S. K. Functionalized Concave Cube Gold Nanoparticles as Potent Antimicrobial Agents against Pathogenic Bacteria. *ACS Appl. Bio Mater.*, **2022**, 5, 492-503.

(88) Marchesi D'Alvise, T.; Harvey, S.; Hueske, L.; Szelwicka, J.; Veith, L.; Knowles, T. P. J.; Kubiczek, D.; Flaig, C.; Port, F.; Weil, T. *et al*. Ultrathin Polydopamine Films with Phospholipid Nanodiscs Containing a Glycophorin A Domain. *Adv. Funct. Mater.*, **2020**, 30, 2000378.

(89) Stafford, C. M.; Harrison, C.; Beers, K. L.; Karim, A.; Amis, E. J.; Vanlandingham, M. R.; Kim, H.-C.; Volksen, W.; Miller, R. D.; Simonyi, E. E. A Buckling-Based Metrology for Measuring the Elastic Moduli of Polymeric Thin Films. *Nat. Mater.*, **2004**, 3, 545-550.

(90) Ball, V. Electrodeposition of Pyrogallol Versus Pyrocatechol Using Cyclic Voltammetry and Chronoamperometry. *J. Electroanal. Chem.*, **2022**, 909, 116142.

(91) Nady, H.; El-Rabiei, M. M.; Abd El-Hafez, G. M. Electrochemical Oxidation Behavior of Some Hazardous Phenolic Compounds in Acidic Solution. *Egypt. J. Petrol.*, **2017**, 26, 669-678.

(92) Gileadi, E. *Physical Electrochemistry. Fundamentals, techniques and applications.* Wiley-VCH, **2011**, chapters 15 and 16.

(93) Bard, A. J.; Faulkner, L. R. *Electrochemical methods: Fundamentals and Applications, 2nd Edition.* Wiley-VCH, **2000**.

(94) Varol, H. S.; Herberger, T.; Kirsch, M.; Mikolei, J.; Veith, L.; Kannan-Sampathkumar, V.; Brand, R. D.; Synatschke, C. V.; Weil, T.; Andrieu-Brunsen, A. Electropolymerization of Polydopamine at Electrode-Supported Insulating Mesoporous Films. *Chem. Mater.*, **2023**, 35, 9192-9207.

(95) DiTucci, M. J.; Williams, E. R. Nanometer Patterning of Water by Tetraanionic Ferrocyanide Stabilized in Aqueous Nanodrops. *Chem. Sci.*, **2017**, 8, 1391.

(96) Lavallee, C.; Lavallee, D. K. Kinetic and Equilibrium Parameters for the Reaction of Neptunium(III) with tris(ethyldiamine)ruthenium(III). *Inorg. Chem.*, **1977**, 16, 2601-2605.

(97) Walters, C. C.; Kliewer, C. E.; Awwiller, D. N.; Rudnicki, M. D.; Passey, Q. R.; Lin, M. W. Influence of Turbostratic Carbon Nanostructures on Electrical Conductivity in Shales. *Int. J. Coal Geol.*, **2014**, 122, 105-109.

(98) Schöche, S.; Hong, N.; Khorasaninejad, M.; Ambrosio, A.; Orabona, E.; Maddalena, P.; Capasso, F. Optical Properties of Graphene Oxide and Reduced Graphene Oxide Determined by Spectroscopic Ellipsometry. *Appl. Surf. Sci.*, **2017**, 421, 778-782.

(99) Szewczyk, J.; Babacic, V.; Krysztofik, A.; Ivashchenko, O.; Pochylski, M.; Pietrzak, R.; Gapiński, J.; Graczykowski, B.; Bechelany, M.; Coy, E. Control of Intermolecular Interactions toward the production of Free-Standing Interfacial Polydopamine Films. *ACS Appl. Mater. Interfaces*, **2023**, 15, 36922-36935.

(100) Liu, H.; Qu, X.; Tan, H.; Song, J.; Lei, M.; Kim, E.; Payne, G. F.; Liu, C. Role of Polydopamine's Redox-Activity on its Pro-Oxidant, Radical-Scavenging, and Antimicrobial Activities. *Acta Biomaterialia*, **2019**, 88, 181-196.

(101) Zangmeister, R. A.; Morris, T. A.; Tarlov, M. J. Characterization of Polydopamine Thin Films Deposited at Short Times by Autoxidation of Dopamine. *Langmuir*, **2013**, 29, 8619-8628.

(102) Slitikov, P. V.; Rasadkina, E. N.; Vasyanina, L. K.; Nifant'ev, E. E. Cyclic Bis-amidophosphites Based on 1,6-Dihydroxynaphthalene. *Russ. Chem. Bull., Int. Ed.*, **2013**, 62, 2023-2031.

(103) Goupy, P.; Dufour, C.; Loonis, M.; Dangles, O. Quantitative Kinetic Analysis of Hydrogen Transfer Reactions from Dietary Polyphenols to the DPPH Radical. *J. Agric. Food Chem.*, **2003**, 51, 615-622.

(104) Foti, M. C.; Johnson, E. R.; Vinqvist, M. R.; Wright, J. S.; Barclay, L. R. C.; Ingold, K. U. Naphthalene Diols: A New Class of Antioxidants Intramolecular Hydrogen Bonding in Catechols, Naphthalene Diols, and Their Aryloxyl Radicals. *J. Org. Chem.*, **2002**, 67, 5190-5196.

(105) Liu, H.; Qu, X.; Kim, E.; Lei, M.; Dai, K.; Tan, X.; Xu, M.; Li, J.; Liu, Y.; Shi, X.; Li, P.; Payne, G. F.; Liu, C. Bio-Inspired Redox-Cycling Antimicrobial Film for Sustained Generation of Reactive Oxygen Species. *Biomaterials*, **2018**, 162, 109-122.

(106) De Freitas, L. C. Global Priority List of Antibiotic Resistant Bacteria to Guide Research, Discovery, and Development of New Antibiotics. *Cad. Pesqui.*, **2013**, 43, 348-365.

(107) Allegranzi, B.; Nejad, S. B.; Combescure, C.; Graafmans, W.; Attar, H.; Donaldson, L.; Pittet, D. Burden of Endemic Health-Care-Associated Infection in Developing Countries: Systematic Review and Meta-Analysis. *Lancet*, **2011**, 377, 228-241.

(108) Khoubnasabjafari, M.; Ansarin, K.; Jouyban, A. Reliability of Malondialdehyde as a Biomarker of Oxidative Stress in psychological disorders. *Bioimpacts*, **2015**, 5, 123-127.

(109) Xin, Z.; Liu, J.; Wang, X.; Shen, K.; Yuan, Z.; Chen, Y.; Lan, Y.-Q. Implanting Polypyrrole in Metal-Porphyrin MOFs: Enhanced Electrocatalytic Performance for CO_2RR. *ACS Appl. Mater. Interf*., **2021**, 13, 54959-54966.

(110) United States National Institute of Standards and Technology, https://srdata.nist.gov/xps/XPSDetailPage/25830, (accessed July 2024).

(111) Das Periodensystem der Elemente online, https://www.periodensystem-online.de/index.php?el=29&id=redox, (accessed July 2024).

(112) Panzella, L.; Gentile, G.; D'Errico, G.; Vecchia, N. F. D.; Errico, M. E.; Napolitano, A.; Carfagna, C.; d'Ischia, M. Atypical Structural and π-Electron Features of a Melanin Polymer That Lead to Superior Free-Radical-Scavenging Properties. *Angew. Chem.*, **2013**, 52, 12684-12687.

(113) Adegoke, K. A.; Maxakato, N. W. Electrochemical CO_2 Conversion to Fuels on Metal-Free N-Doped Carbon-Based Materials: Functionalities, Mechanistic, and Technoeconomic Aspects. *Materials Today Chemistry*, **2022**, 24, 100838.

Supporting information

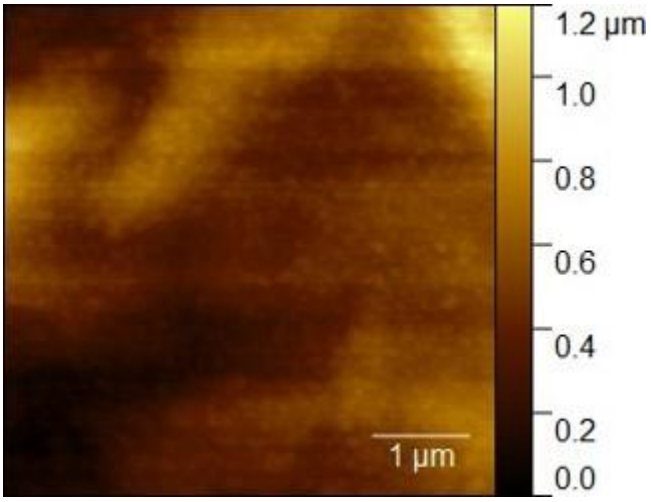

Figure S1. Liquid-AFM surface topography of the film deposited after 25 CV cycles at 200 mV/s.

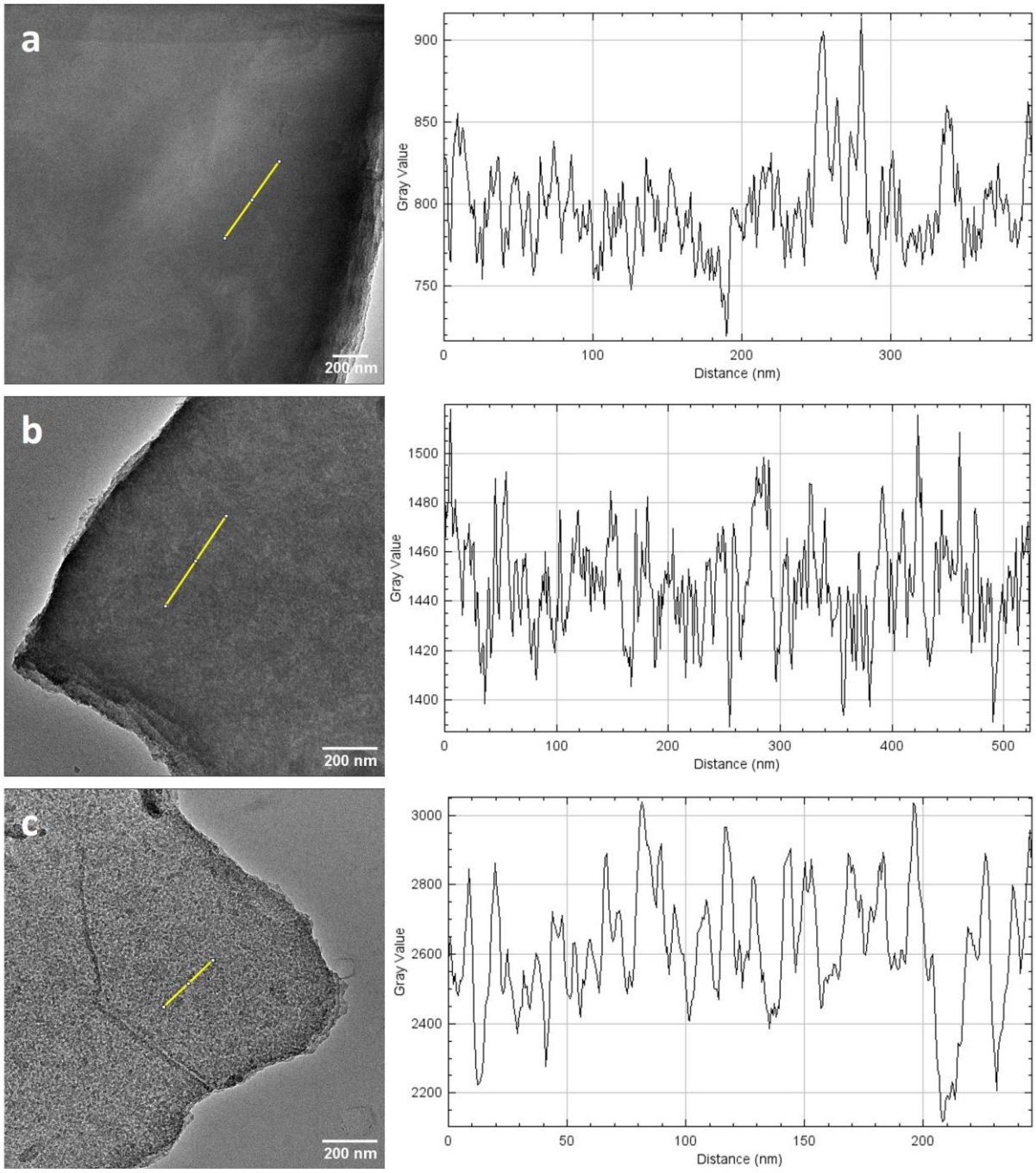

Figure S2. Grey scale analysis on the TEM images of the films removed from the gold electrodes after 25 CV cycles performed at (a) 20 mV/s, (b) 200 mV/s and (c) 1000 mV/s. The yellow segments indicates the part used for the grey scale panels shown on the right side.

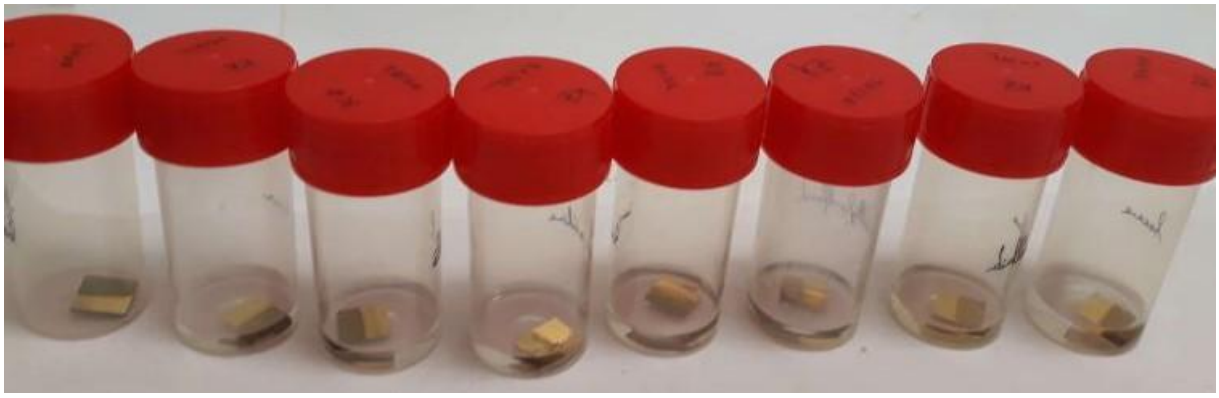

Figure S3. Picture of films prepared after 25 CV cycles at 200 mV/s and placed in different tubes containing solvents to test the stability of the film. From left to right: no solvent, water, ethanol, acetone, isopropanol, dimethylsulfoxide, dichloromethane and hexane. This picture was taken after 7 days of immersion. The 1,8-DHN based film appears black and the uncoated part of the gold electrode covers about half of the substrate.

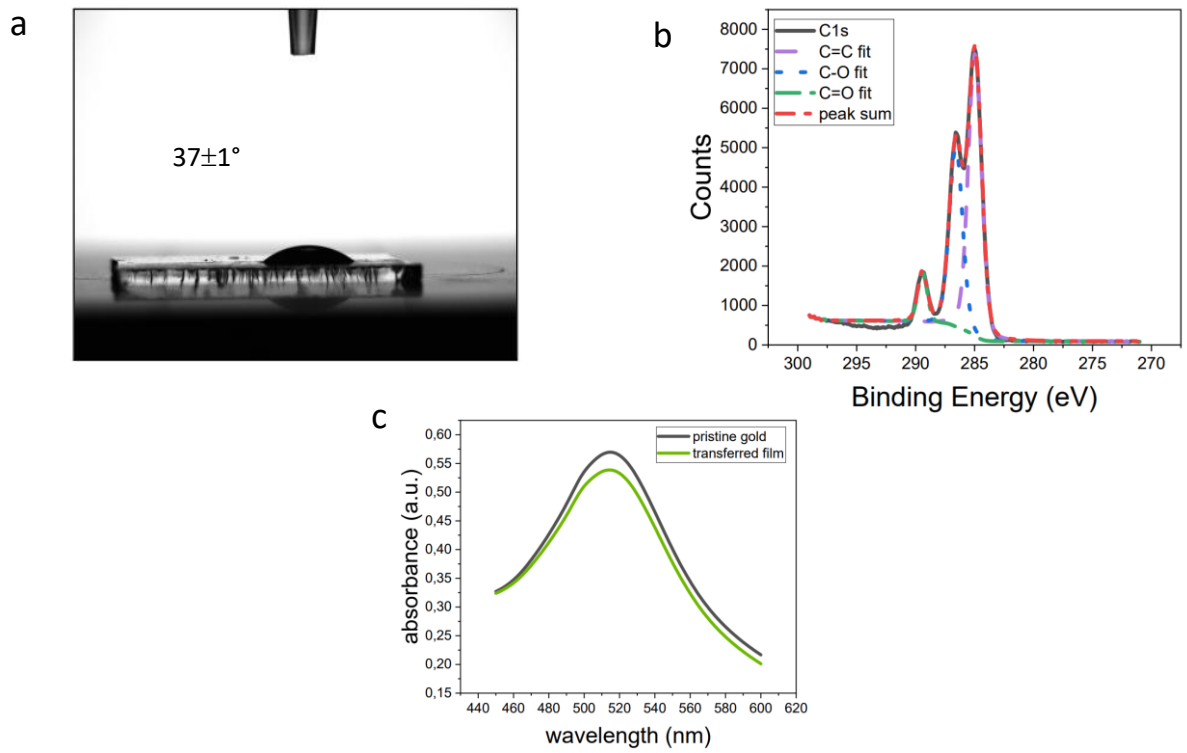

Figure S4. Static water contact angle measurement on the free-standing membrane after its detachment from the gold electrode (25 CV cycles at 200 mV/s) (a), high resolution C1s XPS spectrum thereof (b) and DPPH scavenging assay (c).

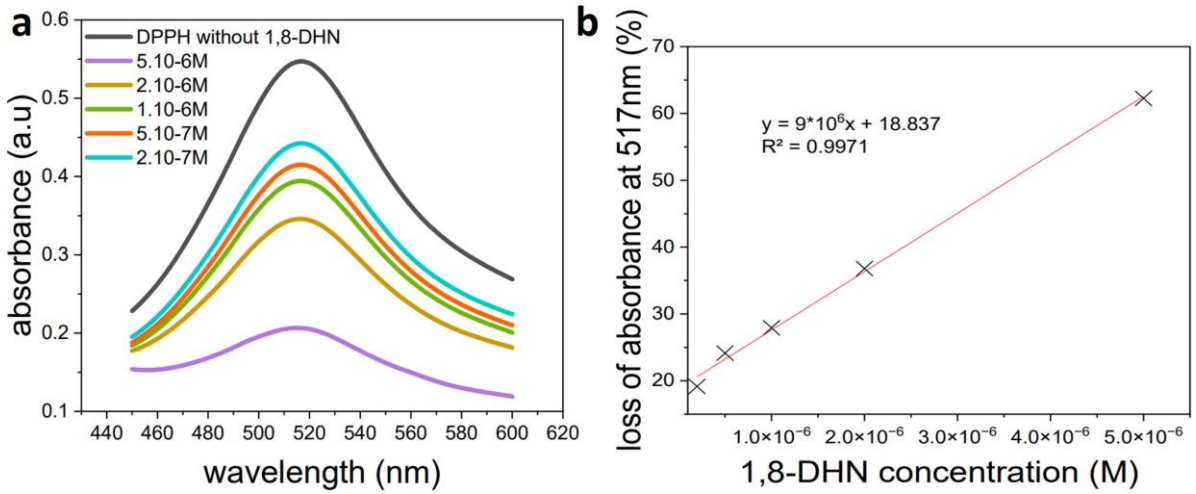

Figure S5. (a) UV-visible spectra between 450 and 600 nm for a DPPH 10^{-4} M solution alone (black) and mixed 20 minutes with different concentrations of the precursor solutions (colors) with respect to an absolute ethanol solution as reference. (b) Calibration curve to determine the equivalent precursor concentration of the radical scavenging activity of the films.

Long résumé en français

1. Introduction

1.1. Importance et place de ce travail dans la recherche

Les routes chimiques et électrochimiques de polymérisation de monomères ont toutes deux été largement étudiées dans le passé. La polymérisation par voie chimique induit des espèces rédox, tandis que la polymérisation par voie électrochimique implique des charges électriques et n'est pas utilisable pour tous les monomères.[1] La déposition électrochimique émerge parmi les techniques à faible empreinte carbone. La méthode permet également de former des films en couche mince, car la déposition se fait sur un substrat. Par conséquent c'est une technique de grand intérêt pour des technologies avancées impliquant des matériaux sous forme de film.

Parmi les monomères déjà étudiés, les polymères conducteurs comme la polyaniline, le polypyrrole et le polythiophene[1-6] sont les plus intensivement étudiés en raison de leur nombreuses propriétés dans des applications très variées.[1]

La polyaniline est un polymère conducteur typique et fût l'un des premiers polymères synthétisés par électrochimie.[7] Ce polymère a été également grandement étudié pour des applications optiques et électriques, par la présence d'une grande stabilité et des propriétés optiques et électriques modulables.[8,9] La deposition de films de polyaniline a été reportée par Eftekhari et Jafarkhani[1] et Musiani et al.[2] par exemple.

Le polypyrrole est quand à lui de loin le polymère conducteur le plus étudié.[4] Cela est notamment dû à sa solubilité dans l'eau, à de bonnes propriétés rédox et à sa capacité à donner de bonnes conductivités électriques.[4] On peut par exemple citer Saidman et Vela[3]

pour le dépôt sur aluminium et Ryan et al.[4] pour le dépôt sur des électrodes disque d'or et de platine.

Malgré la possibilité de produire des films à partir de monomères prometteurs, certaines conditions apportent leurs lots d'inconvénients. En effet, Les solvants utilisés sont parfois toxiques pour l'Homme ou l'environnement. Dans certains cas, des surfactants peuvent être nécessaires et ceux-ci peuvent s'incorporer dans les matériaux finaux,[3] de même que les ions présents dans les électrolytes,[10] alors qu'ils peuvent être nocifs. La polyaniline elle-même est un matériau nocif.

Il est donc important de trouver des alternatives. Il est notamment intéressant d'utiliser des précurseurs naturels à faible empreinte carbone, mais aussi de travail dans des conditions plus douces, comme à température ambiante et en solution aqueuse pour réduire l'impact sur l'environnement et la consommation énergétique.

1.2. Principe de la voltammétrie cyclique

L'électrochimie est une technique basée sur la dépendance courant-potentiel et sur des réactions impliquant des transferts d'électrons.

Les expériences peuvent être menées soit en contrôlé le courant et en mesurant le potential soit l'inverse. Le premier cas est appelé mesure galvanostatique et la seconde potentiostatique. Les galvanostats sont plus simples que les potentiostats d'un point de vue de coûts, mais aussi de performance. Des galvanostats avec des courants contrôlable de l'ordre de centaines d'ampères sont disponibles et sont plus adaptés pour les procédés industriels, tandis que les potentiostats sont devenus disponible commercialement qu'après les années 1950. C'était notamment vrai le siècle dernier mais aujourd'hui, avec les composants électroniques du présent, ces limitations n'existent presque plus.[11] Dans

ce travail, toutes les mesures électrochimiques sont réalisées avec des potentiostats et un système à 3 électrodes.

Comme montré dans la Figure 1, le système à 3 électrodes standard est composé d'une électrode de travail, d'une électrode de référence et d'une contre-électrode (aussi appelée électrode auxiliaire).[12,13] Le potential de l'électrode de travail est contrôlé par rapport à l'électrode de référence. L'électrode de référence a un potential bien connu et très stable (par rapport à l'électrode de référence à hydrogène standard).L'électrode de travail est le lieu où la réaction d'intérêt va avoir lieu. La contre-électrode permet de fermer le circuit électrique et le courant se déplace entre l'électrode de travail et la contre-électrode.[14,15] En solution, le courant est assuré par la migration de l'électrolyte dissous. Dans cette étude, l'électrode de travail est une électrode de carbone vitreux ou une électrode d'or et la contre-électrode est un fil de platine. La reference est une électrode Ag/AgCl. Ainsi, tous les potentiels donnés seront par rapport à Ag/AgCl.

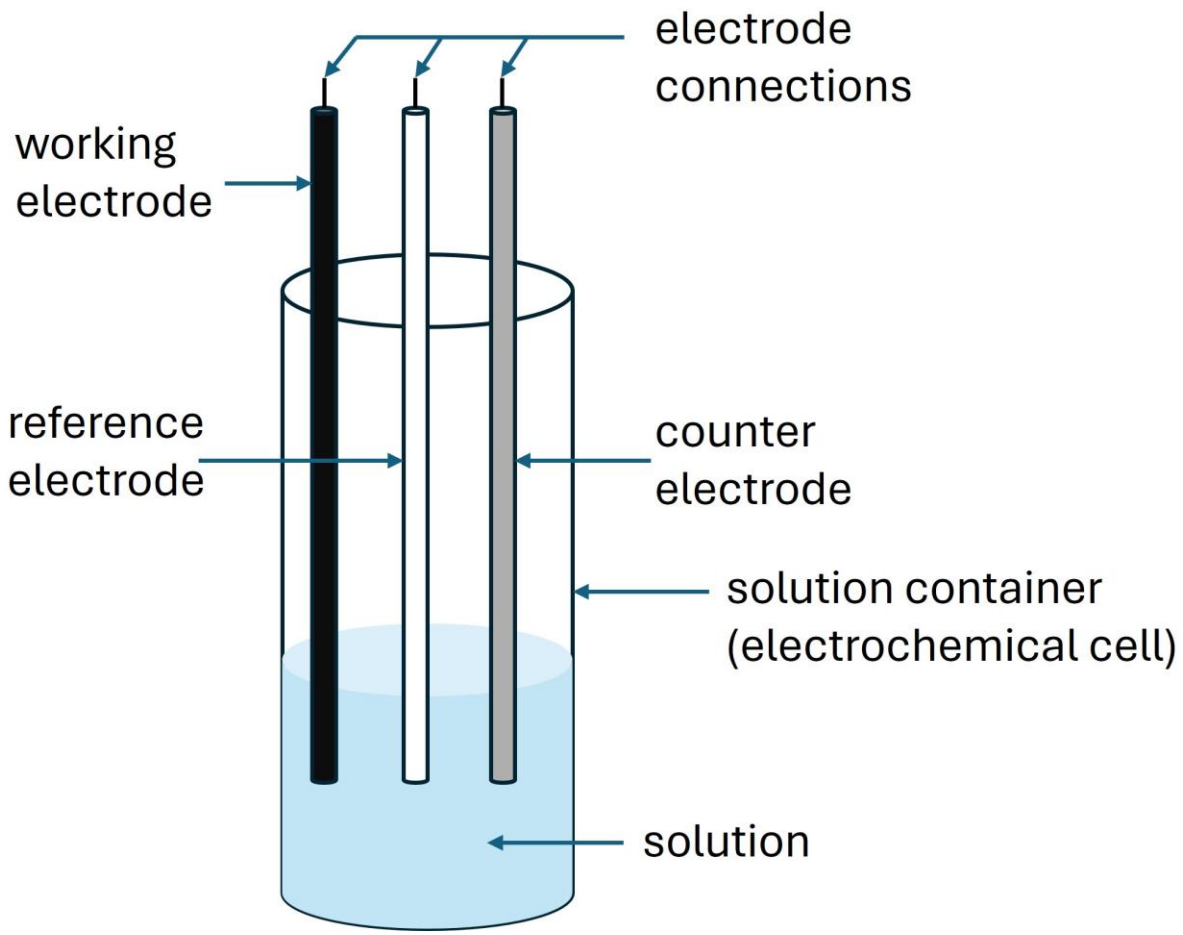

Figure 1. Représentation schématique d'une cellule électrochimique à 3 électrodes.

La voltammétrie cyclique est souvent la première méthode employée dans une étude électrochimique d'un composé, d'un matériau biologique ou de la surface d'une électrode. Sa versatilité combinée à sa facilité d'utilisation en a fait une technique répandue.[14] Avec la voltammétrie cyclique, le potential évolue linéairement avec le temps (ce paramètre est appelé vitesse de balayage) entre deux limites définies et un nombre de cycles déterminé. Souvent, le courant obtenu lors du premier cycle est très different de celui d'après, mais après 5-10 cycles le système se stabilise généralement et le courant finit par tracer le même signal comme une fonction du potential, indépendamment du nombre de cycles. Cela est extrêmement bien reproductible et le voltammogramme obtenu est indépendant du temps.[16]

1.3. Molécules polyphénoliques

Les phénols, polyphénols et molecules dérivées ont été étudié depuis des décennies et sont désormais des précurseurs bien connus pour des objectifs en chimie, électrochimie ou biologie. La presence de plusieurs groupes hydroxyle permet des réactions chimiques et redox mais aussi une future fonctionnalisation du matériau obtenu.

Durant la dernière décennie, ce type de molecules et en particulier les eumélanines (pigments noirs/bruns foncés)[17] ont attiré tout particulière l'intérêt de la communauté scientifique grâce à leurs propriétés uniques et les applications prometteuses qui en découlent en sciences des matériaux.[18]

Pour ne nommer que quelques études électrochimiques, Voisin et al.[19] ont étudié l'oxidation du catéchol et démontré que le matériau obtenu ressemble davantage à un dérivé du triphénylène plutôt qu'un matériau polymère. Quynh et al.[20] ont présenté leur étude sur le comportement électrochimique de composés aromatiques (benzène, phénol, hydroquinone, catéchol, 2-aminophénol et 2-chlorophénol) sur des électrodes d'or. Saito et al.[21] ont synthétisé un polyphénol soluble en travaillant en solution aqueuse. Iotov et al.[22] ont suggéré une approche mécanistique de l'oxydation du phénol sur une électrode or/platine. Mosa et al.[23] ont utilisé une combinaison de méthodes d'électrodéposition et sol-gel pour assembler une électrode poreuse basée sur le poly(phénylène oxyde) pour des senseurs électrochimiques et du stockage de l'énergie.

Récemment, des matériaux à base de polydopamine, obtenu via l'oxydation de la dopamine ou de dérivés catécholamines, ont été le centre d'une recherche accrue.[24] Malgré une étude relativement large de ces molecules polyphénoliques, il y a toujours un vaste potentiel d'investigation à réaliser pour comprendre leurs complexes mécanismes de déposition sur la surface d'électrodes.

Ces molecules ont souvent des propriétés redox : ils peuvent être réduits ou oxydés, mais présentent aussi une activité rédox résiduelle dans le matériau final.[25] Leur origine naturelle les rend prometteurs comme candidats en tant que précurseurs pour des études électrochimiques, comme pour la synthèse et le dépôt de films par voltammétrie cyclique avec de faibles potentiels appliqués et des solvants non toxiques pour travailler dans des conditions en accord avec le 12ème objectif des Nations Unies dans le but de réduire les dangers, la pollution et les impacts sur l'environnement et la santé humaine.[26]

1.4. Dihydroxypyridines

La 2,3-dihydroxypyridine a une structure similaire à celle du catéchol, mais un carbone en position *ortho* (adjacent à un groupe hydroxyle) du cycle aromatique est remplacé par un atome d'azote (Schéma 1). Cette difference induit une densité électronique différente au sein du cycle aromatique. Cela peut modifier le mécanisme réactionnel de l'oxydation lors de l'électropolymérisation mais aussi les propriétés finales du matériau obtenu. La presence d'azone dans le film permettrait également de catalyser l'électroréduction du CO_2, et probablement avec une certaine sélectivité.[27]

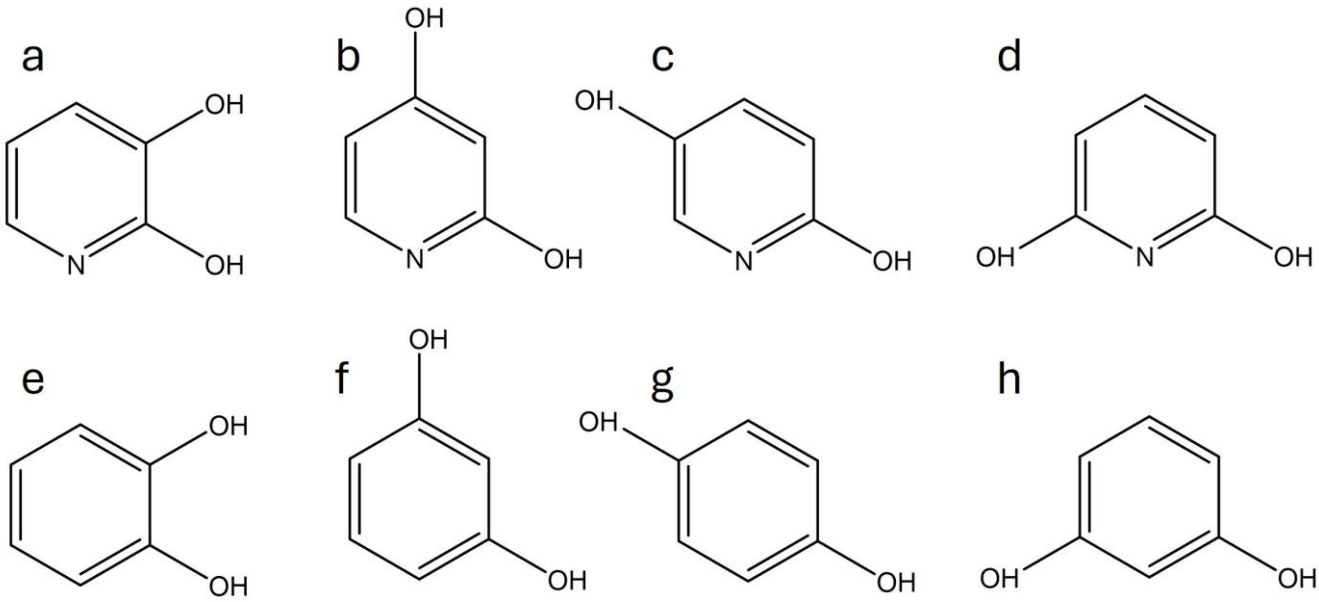

Schéma 1. Structures des isomers de la dihydroxypyridine (en haut) et de leurs analogues sans azote (en bas): (a) 2,3-dihydroxypyridine, (b) 2,4-dihydroxypyridine, (c) 2,5-dihydroxypyridine, (d) 2,6-dihydroxypyridine, (e) catéchol, (f) résorcinol, (g) hydroquinone et (h) résorcinol à nouveau.

Au meilleur de notre connaissance, la molécule de 2,3-dihydroxypyridine n'a jamais été intensivement étudiée d'après la littérature, que ce soit pour des objectifs chimiques ou électrochimiques. Soriaga et al.[28] ont reporté l'oxydation électrochimique de composés aromatiques sur des électrodes de platine. Ils ont inclu la 2,3-dihydroxypyridine dans leur étude et leur travail est basé sur l'influence de l'orientation d'adsorption de ces molécules. Du mieux que nous connaissons, seulement le travail de Varmaghani et al.[29] décrit la déposition d'un film de 2,3-dihydroxypyridine en utilisant la voltammétrie cyclique. Cependant les films obtenus n'ont que peu été caractérisés.

Les autres isomers de la dihydroxypyridine (Schéma 1) sont encore moins présents dans la littérature. Par exemple, même le pK_a des 2,3-dihydroxypyridine, 2,4-dihydroxypyridine, 2,5-dihydroxypyridine and 2,6-dihydroxypyridine sont partiellement fournis dans la littérature.[30,31]

1.5. 1,8-dihydroxynaphtalène

Le 1,8-dihydroxynaphtalène est un précurseur de type mélanine qui ne contient pas d'azote (appelée classe allomélanine) et est composée de 2 cycles aromatiques ainsi que de 2 groupes hydroxyle, chacun sur un cycle différent (Schéma 2). Cette molecule se trouve dans des espèces de champignons[32] et a été davantage étudiée que les dihydroxypyridines d'après les travaux trouvés dans la littérature. La molecule est aussi connue pour avoir une activité antioxydante.[33]

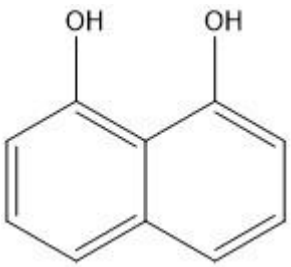

Schéma 2. Structure chimique du 1,8-dihydroxynaphtalène.

Des études chimiques et électrochimiques ont été réalisées avec le 1,8-dihydroxynaphtalène en tant que précurseur; généralement pour produire des nanoparticules mais aussi parfois des films en couche mince.[34] Cependant, aucun travail concernant le dépôt de films à base de 1,8-dihydroxynaphtalène par voltammétrie cyclique n'a été trouvé.

Pour ne citer que quelques exemples, il y a eu des études sur la formation de nanoparticules ou de précipités comme l'étude réalisée par Mavridi-Printezi et al.[33] Manini et al.[34] ont reporté la formation d'un film par oxydation chimique.

1.6. Organisation du manuscrit

Ce travail peut être séparé en 3 grands axes. Ces 3 axes sont décrits dans ce manuscript sous la forme de 3 chapitres.

Tout d’abord, un premier chapitre est dédié à l’électrodéposition des isomères de la dihydroxypyridine. Cette étude montre les différences obtenues en changeant la position d’un des groupes hydroxyle du précurseur, mais aussi de l’influence de la vitesse de balayage sur le matériau obtenu.

Le deuxième chapitre correspond à l’électrodéposition du 1,8-dihydroxynaphtalène sur des électrodes d’or. Ce travail présente les caractéristiques principales, les propriétés prometteuses et une tentative d’explication du mécanisme réactionnel des films obtenus.

Le troisième et dernier chapitre décrit les résultats du 1,8-dihydroxynaphtalène sur carbone vitreux. De plus, des systems hybrids de dihydroxypyridines et de 1,8-dihydroxynaphtalène ont été préparés.

2. Electrodéposition de films à partir des dihydroxypyridines

Les monomères de 2,3-DHP, 2,4-DHP, 2,5-DHP et 2,6-DHP ont été utilisés pour déposer des films en couche mince. Les films ont été déposés sur du carbone vitreux avec 5 cycles successifs de CV entre -1 V et +1 V avec une vitesse de balayage de 10 mV/s (Figure 2) et 100 mV/s.

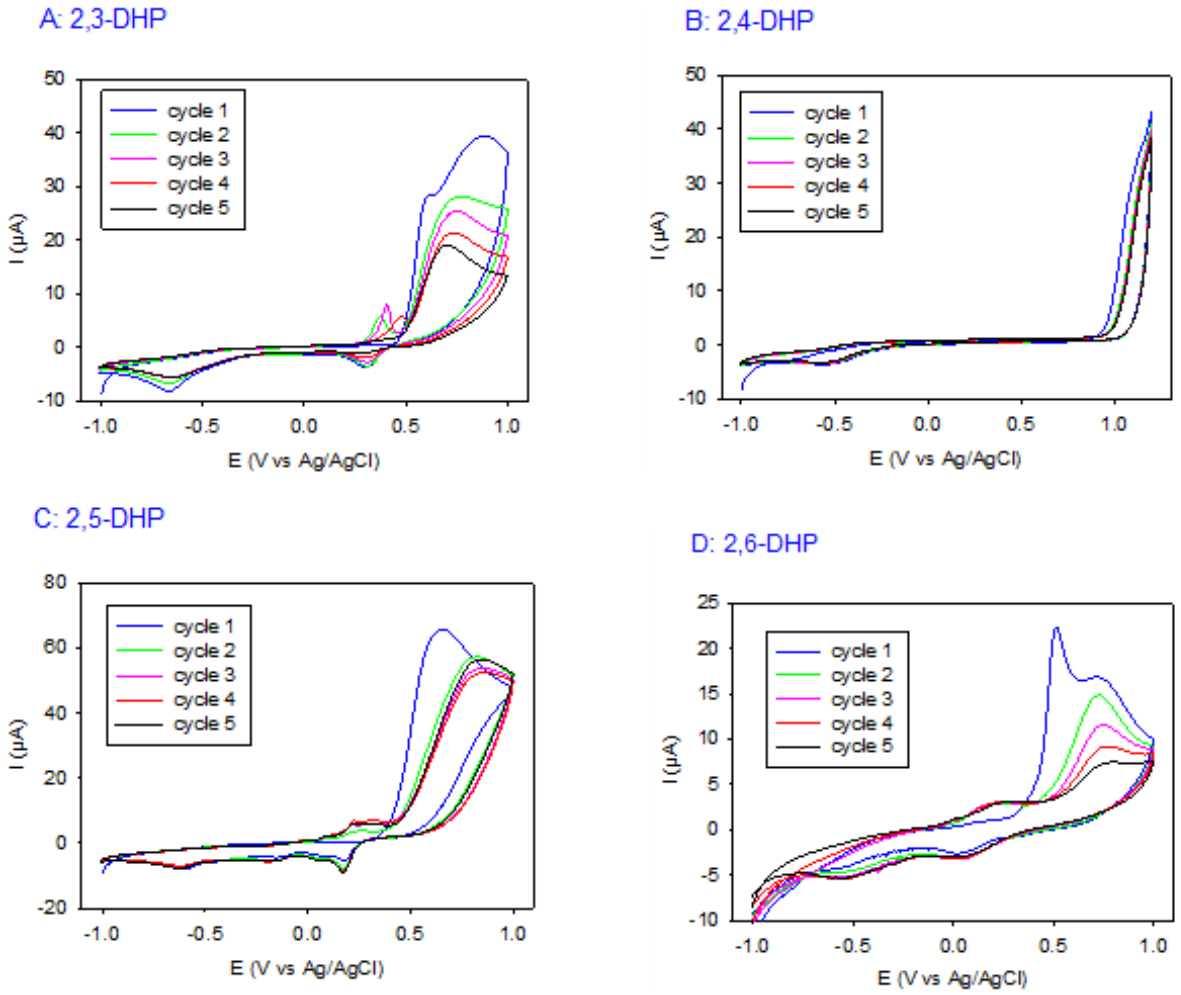

Figure 2. 5 cycles successifs de CV avec une vitesse de balayage de 10 mV/s de la 2,3-DHP (panel A), 2,4-DHP (panel B), 2,5-DHP (panel C) et 2,6-DHP (panel D) dissoute à 1 mg/mL dans une solution tampon de 50 mM d'acétate de sodium (pH = 5.0) sur des électrodes de travail de carbone vitreux.

La 2,4-DHP n'a pas conduit à un dépôt. En effet, son oxydation semble apparaître à un potentiel supérieur à +1 V, donc hors de nos conditions expérimentales (il a été souhaité d'éviter l'oxydation de l'eau qui apparaît également vers +1,2 V).

En fonction de l'isomère utilisé, des différences sont apparues. Non seulement les cycles de CV sont différents mais aussi les spectres d'impédance et les perméabilités à des espèces rédox (tel que l'hexacyanoferrate de potassium). Le spectre d'impédance de la 2,5-DHP laisse suggérer un caractère conducteur du film contrairement aux deux autres films avec la 2,3-DHP et la 2,6-DHP. Cela a également été observé lors des mesures ellipsométriques. De plus, avec une vitesse de balayage de 10 mV/s, la 2,5-DHP diffère à nouveau des deux autres avec un film perméable à la sonde rédox tandis que les deux autres films sont imperméables. En revanche, lorsque la vitesse de balayage est augmentée à 100 mV/s, les films deviennent davantage perméables.

D'autres différences ont été observées en fonction de l'isomère et de la vitesse de balayage choisis. Notamment la morphologie des films et leur porosité (Figure 11). En effet, les films formés à partir des 2,3- et 2,5-DHP à 10 mV/s présentent une cristallinité partielle et des traces de graphitisation (Figure 11A et C). Tandis que les films de 2,6-DHP sont complètement amorphes (Figure 11D). Lorsque la vitesse de balayage est augmentée à 100 mV/s, la cristallinité disparaît. De plus, une certaine porosité apparaît à 100 mV/s (Figure 11B).

Les angles de contact avec des gouttes d'eau sont très différents d'un isomère à l'autre. Les films de 2,3-DHP ont un angle de contact de 32 °, ceux à base de la 2,5-DHP de 53 ° et ceux à partir de la 2,6-DHP ont un angle de 5 °. Ainsi certains films sont davantage hydrophiles (faible angle de contact) que d'autres.

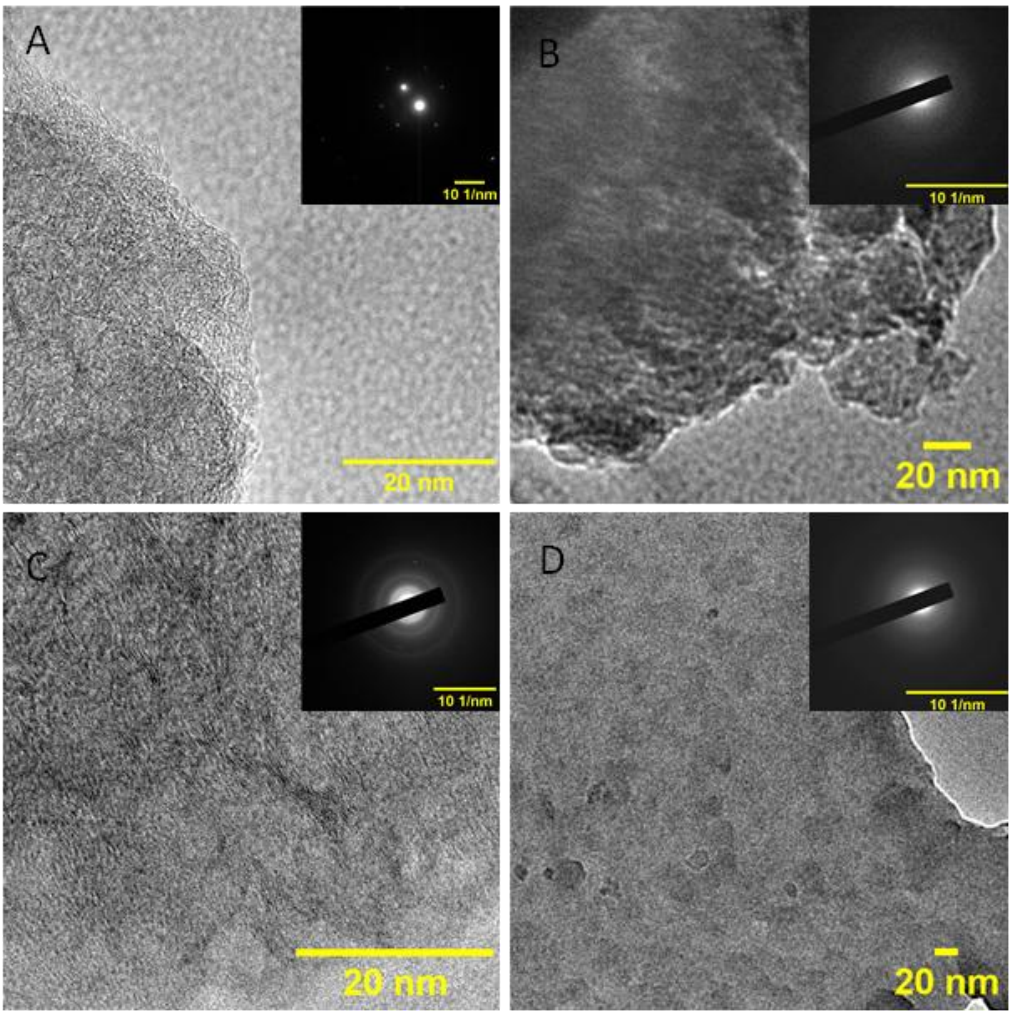

Figure 11. Images obtenues par microscopie électronique en transmission et diffractions électroniques (dans les inserts) des films obtenus après 5 cycles de CV sur des électrodes de carbone vitreux avec A: 2,3-DHP à 10 mV/s; B: 2,3-DHP à 100 mV/s; C: 2,5-DHP à 10 mV/s et D: 2,6-DHP à 10 mV/s.

Les analyses XPS montrent également des différences sur la composition chimiques des 3 films obtenus. Bien que tous les films présentent des liaisons C=O (groupes cétones), C-O (groupes alcool) et C-N (dû à l'azote dans le cycle), les films à partir de la 2,5-DHP présentent un taux d'azote plus faible, suggérant un départ d'azote dans le mécanisme réactionnel.

Enfin, des test d'activité antioxydante ont été réalisés avec le DPPH dissous dans de l'éthanol absolu. Tous les films présentent une activité antioxydante, ouvrant la voie à des

applications en biomédical par exemple où cela permettrait de réduire des effets inflammatoires. L'activité antioxydante est identique quel que soit l'isomère utilisé.

3. Electrodéposition du 1,8-dihydroxynaphtalène sur l'or

Après le succès de dépôt de films de type oxydes de graphène avec certains isomères de DHP, il a été envisagé d'utiliser des molécules présentant déjà un ordre plus grand (plusieurs cycles aromatiques collés) pour comparer les matériaux obtenus et notamment si la cristallinité pouvait être améliorée. Comme cela est décrit en détails dans le chapitre 3, les dépôts sur carbone ont grandement limités les techniques de caractérisation utilisables. Les dépôts à partir du 1,8-DHN ont donc majoritairement été réalisés sur des électrodes d'or.

Le 1,8-DHN a été déposé sur les électrodes d'or avec 25 cycles de CV à 20, 200 et 1000 mV/s entre -1 V et +1 V (Figure 20). Les cycles successifs ne montrent pas de diminution drastique du courant d'oxydation comme cela est le cas en général avec des matériaux isolants. Cela suggère donc la présence d'une conductivité du film formé ou d'une porosité (dû à des pores formés lors de la synthèse ou à un gonflement du film). Même après 100 cycles on peut toujours observer un dépôt aux différentes vitesses de balayage. Les films obtenus présentent également une activité rédox résiduelle. La spectroscopie d'impédance électrochimique révèle plutôt un caractère isolant des films.

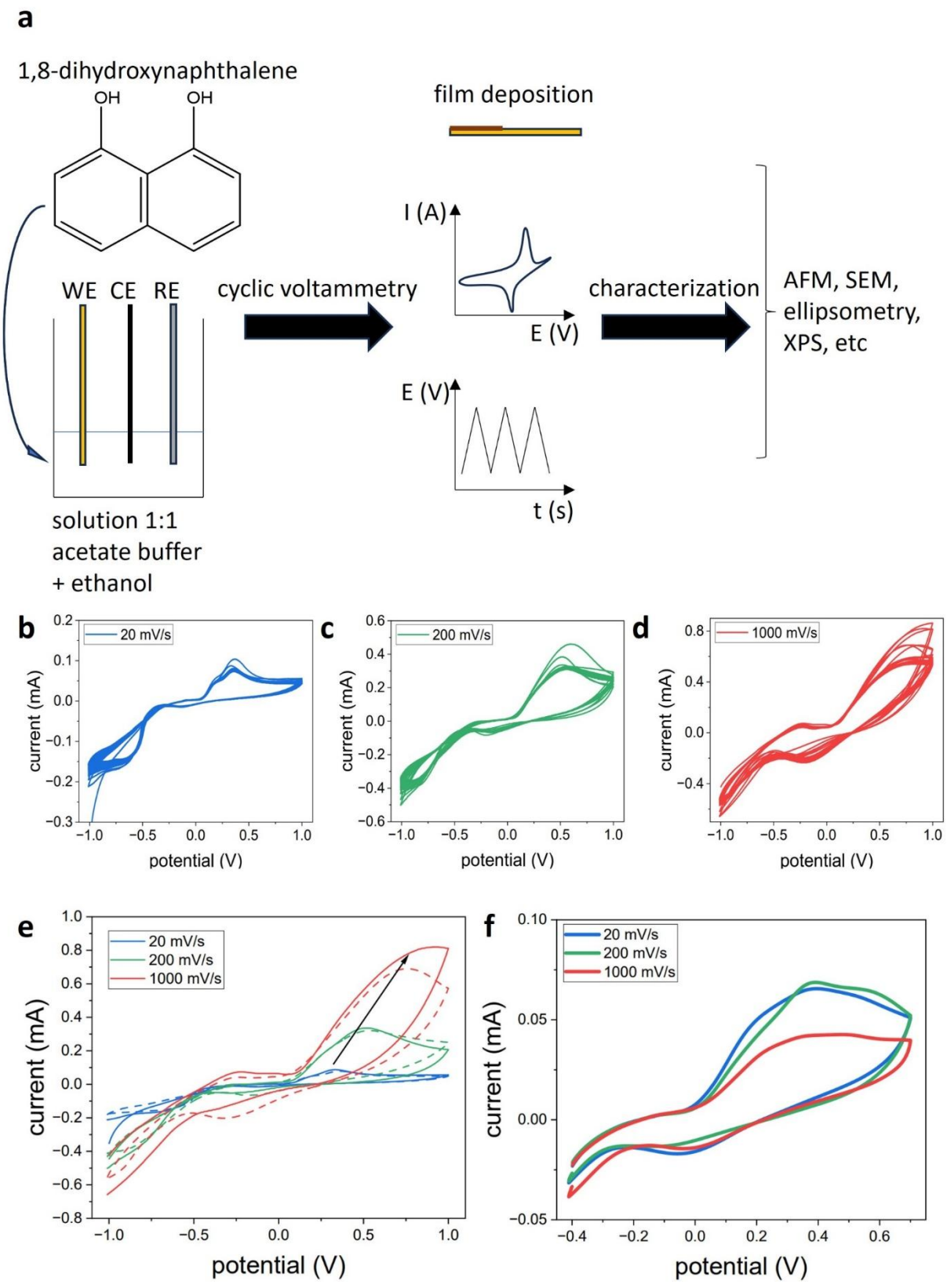

Figure 20. (a) Schéma général de l'électropolymérisation du 1,8-DHN: de la solution du précurseur jusqu'à la déposition du film et de sa caractérisation. 25 cycles CV à une vitesse de balayage de (b) 20 mV/s, (c) 200 mV/s et (d) 1000 mV/s en présence du 1,8-DHN à 1 mg/mL dans un mélange de tampon acétate de sodium et d'éthanol (1:1 v/v). Le

substrat est une electrode d'or. (e) 1er (line complète) et 5ème (ligne pointillés) cycles de CV en presence de 1,8-DHN à 1 mg/mL avec une vitesse de balayage de 20 mV/s (bleu), 200 mV/s (vert), et 1000 mV/s (rouge). (f) 1 cycle CV à 20 mV/s (bleu), 200 mV/s (vert) et 1000 mV/s (rouge) après la déposition du film en absence d'espèces rédox.

Les topographies des surfaces des films ont été étudiées par MEB, AFM et TEM et les mesures d'épaisseur ont été réalisées par MEB, AFM et ellipsométrie (Figure 26). Les films présentent des plis, davantage présents quand la vitesse de balayage est plus faible, probablement dû à des contraintes mécaniques au sein des films. Les épaisseurs varient de ~65 nm à ~440 nm après 25 cycles de dépôt. L'épaisseur peut même encore être augmentée en augmentant le temps de dépôt, ici en augmentant le nombre de cycles jusqu'à 100 où les épaisseurs peuvent dépasser le micromètre à faible vitesse de balayage. Les films sont complètement amorphes et ont des angles de contact avec des gouttes d'eau autour de 22 °C indépendamment de la vitesse de balayage.

Les films ont pu être détachés et transférés sur d'autres substrats (notamment du PDMS, mais pas sur du verre non traité). Cela a permis d'utiliser certaines techniques de caractérisation supplémentaires mais permet également un plus large éventail d'applications futures.

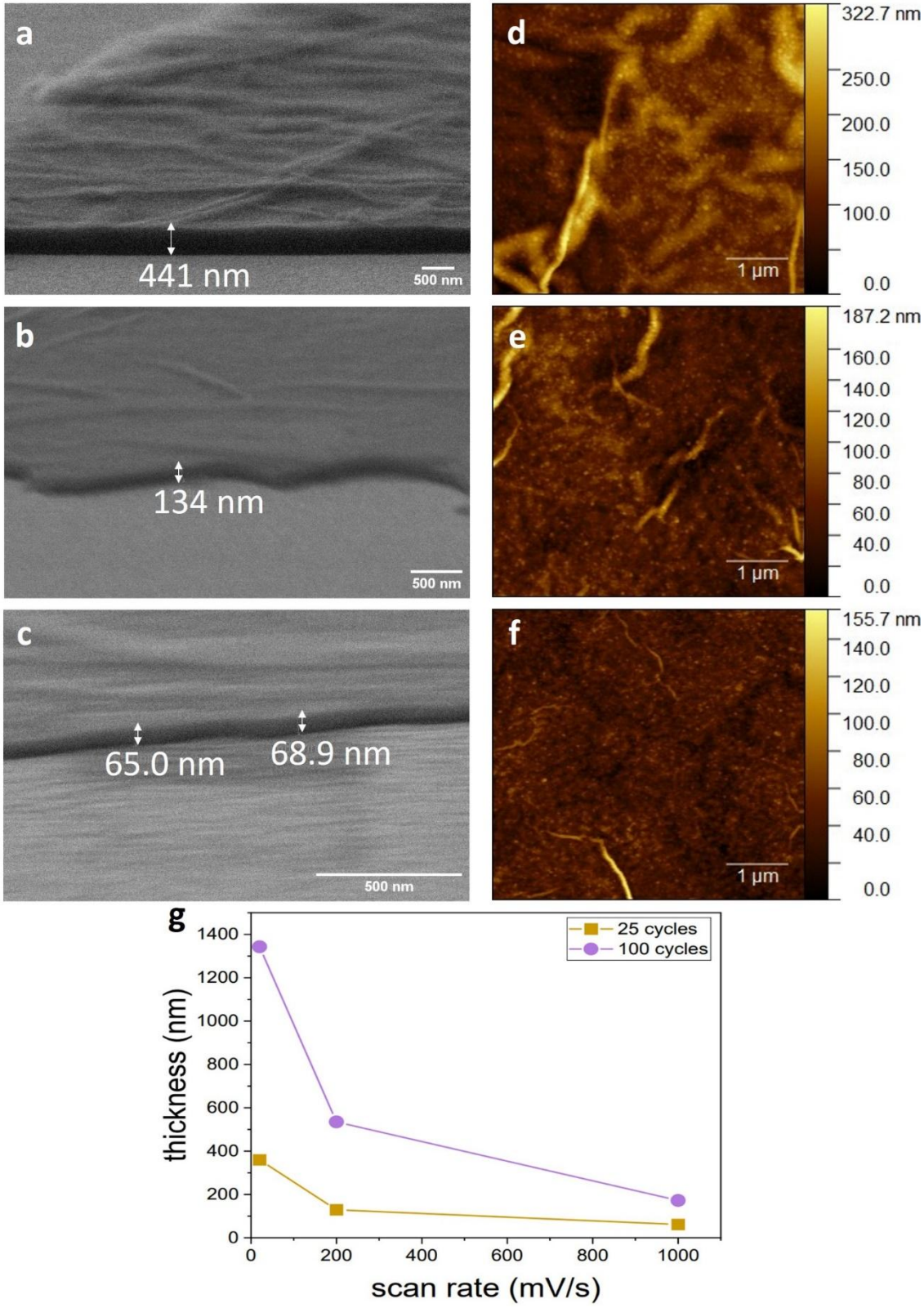

Figure 26. Images de microscope électronique à balayage des films déposés après 25 cycles de CV à (a) 20 mV/s, (b) 200 mV/s et (c) 1000 mV/s. Topographies de surface des films par AFM obtenus après 25 cycles CV à (d) 20 mV/s, (e) 200 mV/s et (f) 1000 mV/s. (g) Epaisseurs obtenues par ellipsométrie en fonction du nombre de cycles et de la vitesse de balayage.

Les mesures de caractérisation chimiques (principalement XPS et spectroscopie Raman) montrent la présence de groupements hydroxyles (fonctions alcool) et carbonyles (fonctions cétones). Le ratio C/O est inchangé par rapport au précurseur. Les taux de composition chimique semblent indépendants de la vitesse de balayage utilisée.

Un module d'élasticité d'environ 650 MPa a été mesurée, cela peut par exemple expliquer la capacité du film à être transféré sans cassure visible.

Bien que la structure exacte du polymère formé soit inconnue, et son mécanisme réactionnel également, une structure des films est proposée dans le Schéma 4.

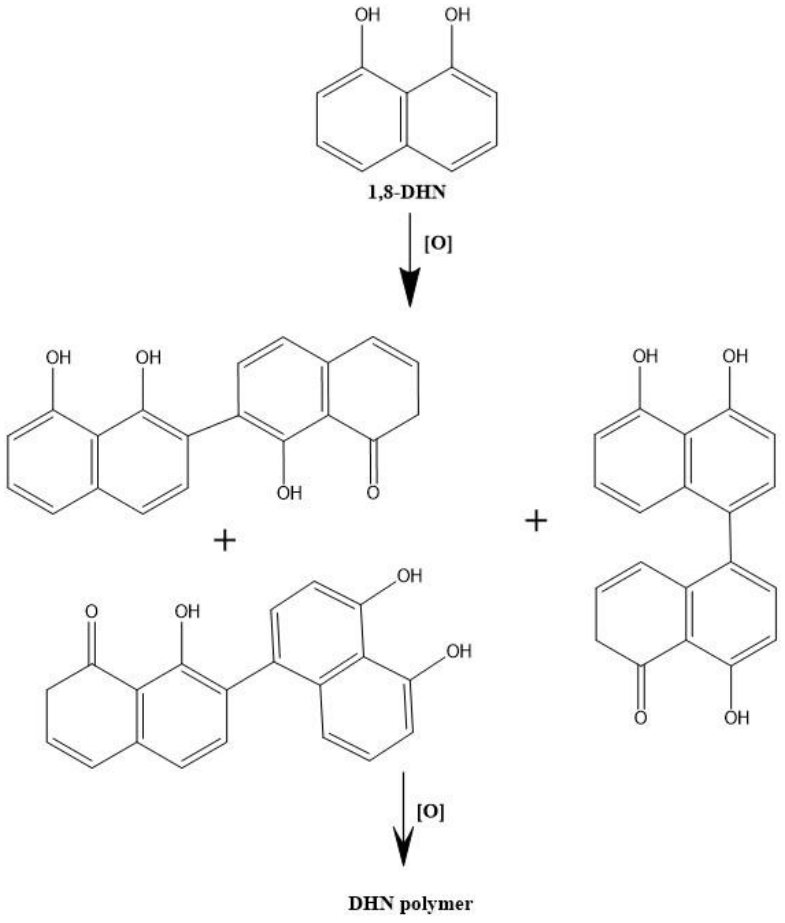

Schéma 4. Schéma réactionnel proposé pour la formation des films de DHN.

Les films de 1,8-DHN présentent une activité antioxydante tous comme ceux à partir des DHP. En revanche, ici l'épaisseur des films a une importance sur cette activité : plus le film est épais, plus l'activité antioxydante est forte. Cela suggère que les radicaux ont accès en profondeur du film et pas seulement à la surface de celui-ci.

Les films à base de DHN ont également des propriétés antibactériennes. En effet, la croissance des bactéries Pseudomonas aeruginosa (une des trois principales espèces pathogènes présentes en milieu médical) est complètement inhibée en présence du film.

Les films peuvent également être déposés sur d'autres métaux et alliages, cela a été réalisé sur un alliage à base de cobalt et de chrome (utilisé en soins dentaires). Ainsi, des applications en tant que revêtement de prothèses peuvent être envisagées. L'activité antioxydante serait un avantage supplémentaire pour réduire l'inflammation souvent déclenchée lors de l'introduction de prothèses dans le corps humain.

Enfin, des essais préliminaires pour incorporer du cuivre ont été réalisés. Malgré une stabilité peu fiable et qui reste à améliorer, les films ont montré une activité catalytique prometteuse pour la réaction de réduction électrochimique du CO_2.

4. Electrodéposition du 1,8-dihydroxynaphtalène sur le carbone vitreux

Les dépôts de 1,8-DHN ont d'abord été étudiés sur des électrodes de carbone vitreux. Les conditions sont les mêmes que celles décrites pour les dépôts sur or. Contrairement à ce qui est habituellement observé, le courant d'oxydation augmente jusqu'au 25ème cycle (et au-delà) à partir du 3ème cycle de CV (Figure 45). Cela suggère, comme sur l'or, un caractère conducteur ou poreux du film pour qu'autant de molécules du monomères restent oxydables à la surface de l'électrode sans que cette dernière soit passivée.

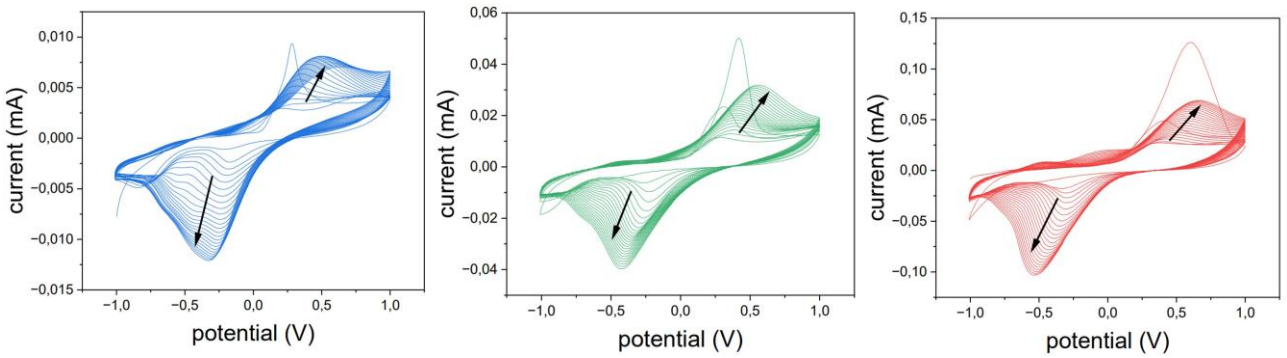

Figure 45. 25 cycles CV avec le 1,8-DHN (1 mg/mL, pH 5.75) à 20 mV/s (bleu), 200 mV/s (vert) et 1000 mV/s (rouge) sur les électrodes de carbone vitreux.

Sur le carbone vitreux, les films de 1,8-DHN ne sont pas du tout amorphes comme c'était le cas sur l'or. A 20, 200 et 1000 mV/s les films sont cristallins. A 20 mV/s, cela correspond à des domaines bien définis et organisés. En revanche quand la vitesse de balayage augmente (temps de réaction plus rapide) à 200 mV/s, ces domaines sont moins présents et moins bien organisés. A 1000 mV/s on pourrait donc s'attendre à voir cet effet se prolonger mais il a été observé que le film était très différent et complètement cristallinisé. Cela résulterait d'une vitesse de balayage trop rapide et d'un changement de mécanisme réactionnel.

Des tests préliminaires de systèmes hybrides entre les DHP et le 1,8-DHN ont été réalisés sur le carbone vitreux. L'ordre de dépôt successif a été modifié (DHN d'abord puis DHP et inversement) ainsi qu'un dépôt simultané a été effectué. Dans tous les cas les analyses EDX ont mis en évidence la présence d'azote dans les films. Cela pourrait permettre de combiner les propriétés des films de 1,8-DHN avec la présence d'azote utile en catalyse par exemple. Le remplacement des métaux de transition par de l'azote serait notamment un avantage dans le cadre de la pollution environnementale.

5. Conclusion

Des films carbonés ont été obtenus par électrodéposition de monomères polyphénoliques grâce à la voltammétrie cyclique.

La technique de voltammétrie cyclique permet une synthèse reproductible de films et un excellent contrôle de l'épaisseur du matériau obtenu. Les conditions de travail avec des solutions aqueuses, un potential appliqué relativement faible et des monomères d'origine naturelle rendent ce projet ambitieux et prometteur pour travailler en conditions de « chimie verte » pour réduire l'impact sur l'environnement.

L'électrodéposition des dihydroxypyridines a été un succès. Tout comme dans une étude précédente avec le pyrocatéchol, la déposition de matériaux de type oxyde de graphène a été obtenue sur des électrodes de carbone vitreux. L'influence de l'isomère utilisé, ainsi que l'influence de la vitesse de balayage choisie ont été démontrées.

L'électrodéposition du 1,8-dihydroxynaphtalène a été un succès à la fois sur des électrodes de travail d'or et de carbon vitreux. La vitesse ne balayage n'a pas semblé être très impactante pour la déposition de films sur l'or, tandis qu'un effet significatif a été observé lors de la déposition sur le carbone vitreux. Nous avons démontré que les films obtenus sur l'or possèdent des propriétés prometteuses pour des applications biomédicales ou en électrocatalyse par exemple, tandis que les films sur carbone vitreux nécessitent encore des caractérisations supplémentaires.

Cependant, les mécanismes de ces électrodépositions ne sont pas encore vraiment clairs Des investigations supplémentaires seront réalisées dans le futur pour améliorer la compréhension de la formation de ces films et de leurs structures chimiques exactes.

Tous les films présentent des propriétés antioxydantes. Les films basés sur le 1,8-DHN ont également des propriétés mécaniques intéressantes et une activité antibactérienne prometteuse. La presence d'azote ou de complexes de cuivre pourrait permettre des propriétés catalytiques pour l'électroréduction du CO_2. Les applications de ces matériaux incluent donc des disciplines scientifiques variées telles que la biomédecine, le stockage de l'énergie ou encore l'électrocatalyse. La capacité de ces films à être transférables sur d'autres substrats accroit également leur potentiel.

Université de Strasbourg

Kévin ZIEGLER

MAX PLANCK INSTITUTE FOR POLYMER RESEARCH

Electropolymerization of polyphenol-related biogenic monomers to design multifunctional 2D materials

Abstract

We aimed to increase the library of polyphenol-related biogenic molecules able to get electrodeposited on conductive substrates, and ideally as graphene oxide-like materials. This work presents the syntheses and a large panel of characterization measurements of films produced by cyclic voltammetry of isomers of dihydroxypyridine and the 1,8-dihydroxynaphthalene. The main results are the differences of the deposited material according to the isomer used, the scan rate or the nature of the substrate. However, we also demonstrated that all the films have antioxidant properties and the films from 1,8-dihydroxynaphthalene showed promising antibacterial properties. Their ability to be transferred to another substrate opens the way to further applications and perspectives.

Key-words: cyclic voltammetry, polyphenol, dihydroxypyridine, 1,8-dihydroxynaphthalene, antioxidant activity, antibacterial activity.

Résumé

Nous avons proposé d'augmenter la librairie de molécules polyphénoliques capables d'être électrodéposées sur une surface conductrice, et idéalement d'obtenir des matériaux de type oxyde de graphène. Ce travail présente les synthèses et un large éventail de mesures de caractérisation des films produits par voltammétrie cyclique à partir d'isomères de la dihydroxypyridine et aussi du 1,8-dihydroxynaphtalène. Les résultats principaux sont les différences observées sur les matériaux déposés en fonction de l'isomère utilisé, de la vitesse de balayage ou encore de la nature du substrat. Cependant, nous démontrons également que tous les films présentent des propriétés antioxydantes et que les films à partir du 1,8-dihydroxynaphtalène montrent également des propriétés antibactériennes prometteuses. Leur capacité à être transférés sur d'autres substrats ouvre la voie à d'autres applications et perspectives.

Mots-clés : voltammétrie cyclique, polyphénol, dihydroxypyridine, 1,8-dihydroxynaphtalène, activité antioxydante, activité antibactérienne.